Experimental Study of Synthesis Gas Combustion Chemistry and Ignition Behaviors

by

Andrew Benjamin Mansfield

A dissertation submitted in partial fulfillment
of the requirements for the degree of
Doctor of Philosophy
(Mechanical Engineering)
in the University of Michigan
2014

Doctoral Committee:

Professor Margaret S. Wooldridge, Chair
Associate Professor Claus Borgnakke
Professor James F. Driscoll
Professor Hong G. Im, King Abdullah University of Science and Technology

Dedication

This dissertation is dedicated to my mother, Annette, for her unwavering support, encouragement, and inspiration throughout this long journey.

Without her none of this would have been possible.

Thank you, Mom!

Acknowledgements

I would like to thank Professor Margaret Wooldridge for the opportunity to work in the Combustion Lab, the guidance to help me complete my dissertation work, and the support to keep me going even when the RCF was in a bad mood! Thank you to my committee for their thoughtful advice. Thank you to my lab mates for their support and friendship: Dimitris Assanis, Ethan Eagle, Mohammad Fatouraie, Darshan Karwat, Insu Lee, Steve Morris, and Scott Wagnon. I greatly appreciate the financial support from the University of Michigan, Department of Engineering and the University Turbine Systems Research program through the Department of Energy (Award number DE-FE0007465). Finally, I would like to thank my friends and family for their unyielding support and encouragement - I couldn't have done it without you!

Table of Contents

List of Figures

List of Tables

Abstract

The development of synthesis gas (syngas) fuel is of interest, as it can enable a transition from fossil to renewable energy sources while reducing the emissions associated with both. Historical research has focused on basic syngas formulations (H_2 & CO) in homogeneous environments, providing a baseline for consideration of more realistic mixtures and devices. Recent research and industrial experience for syngas fueled combustors indicate the effects of common disturbances can be dramatic and are not well-understood, with particular concern regarding the occurrence of uncontrolled inhomogeneous auto-ignition and its effect on the accuracy of common homogeneous reactor modeling.

This dissertation represents an experimental investigation of syngas combustion, aimed at comprehensively understanding the effects of specific chemical and physical disturbances at high-pressure low-temperature conditions. Experiments were conducted in the University of Michigan-Rapid Compression Facility. The auto-ignition behaviors of syngas were investigated, revealing the existence of both homogeneous and inhomogeneous characteristics depending strongly on the initial unburned thermodynamic state. The behaviors were mapped over a wide range of conditions revealing consistent patterns. It was discovered that the Sankaran Criterion, a previously proposed relationship between chemical kinetics, transport properties, and known thermal disturbances, could predict the location of inhomogeneous behavior on these maps with remarkable accuracy. This provides evidence that commonly ignored thermal disturbances can cause uncontrolled inhomogeneous auto-ignition in syngas and also provides a straightforward method to predict such behavior. As expected, inhomogeneous auto-ignition behavior was well correlated to error in homogeneous reactor modeling for higher energy content mixtures.

The effects of chemical impurities on the combustion of syngas were investigated, focusing on CH_4, a common component of syngas, and trimethylsilanol (TMS), an unstudied impurity related to those common to landfill-based syngas. The impact of CH_4 was to inhibit ignition, evidenced by auto-ignition delay time increases by up to a factor of 3. Conversely the impact of TMS was to promote ignition, causing drastic reductions in auto-ignition delay time up to 70%. These large promotion effects have significant safety implications, as pronounced early auto-ignition can lead to catastrophic failures and concentrations of similar Si containing species are expected to increase in the future.

Chapter 1
Introduction

1.1 Background and Motivation

Synthesized gas, or syngas, is a mixture composed primarily of hydrogen and carbon monoxide, which is produced via gasification of coal or other carbonaceous sources such as biomass, oil, or landfill waste. While commonly utilized as a feedstock for chemical manufacturing it is possible to use syngas directly in existing combustion devices as a fuel. In this manner syngas offers the unique and important potential to integrate diverse sources of energy into a single fuel product. Additionally, the use of syngas can lead to significant reductions in hazardous pollutant emissions through pre-combustion filtering during the gasification process and post-combustion carbon capture [1]. The development and implementation of syngas fuel systems is therefore of great interest, as it can enable a gradual transition to renewable fuel sources while simultaneously utilizing and improving the emissions associated with existing fossil fuels.

As coal is used to generate the majority of the electrical power in the United States and China, improvement of coal-based power systems is critical to the long term sustainability of the global economy, environment, and human health. The implementation of syngas fuel can meet this challenge, providing an alternative to the traditional pulverized coal-fired boiler systems commonly in use today. A new coal-based combustion scheme which uses syngas fuel, called Integrated Gasification Combined Cycle (IGCC), is currently under development. In this new plant, coal is gasified then combusted directly in a gas turbine as part of a combined

cycle power system. Compared to a pulverized coal system an IGCC plant can achieve significant reductions in emissions of SO_x, NO_x, particulate matter, and heavy metals without a significant decrease in overall plant efficiency [1]. While commercialization of this technology is still limited, there are currently 18 IGCC plants in operation worldwide producing ~ 9.2 GW of power, with an additional seven potential plants scheduled to add ~ 2.8 GW in the future [2].

Currently the gas turbine portion of the IGCC system is in development, with a focus on achieving safe and efficient combustion of syngas. A particular concern for this high-hydrogen-content (HHC) fuel are the potentially high NO_x emissions that result from increased flame temperatures [3,4]. In order to prevent NO_x formation in this system, combustion temperatures can be reduced by burning at lean, pre-mixed, and/or dilute conditions. These conditions present challenging stability, safety, and control issues however, stemming in part from uncertainties in low-temperature chemistry as well as an increased instance and influence of abnormal ignition behaviors such as flashback and early auto-ignition [4,5]. As syngas is a HHC fuel it exhibits unique and generally unstable physical and chemical characteristics, and as such, low-NO_x gas turbine combustors currently designed for air-dilute lean combustion of natural gas cannot be operated with syngas fuel [4]. It is therefore imperative to the successful implementation of syngas fuels in these and other similar systems that both the chemical kinetics of its oxidation and associated physical ignition behaviors be well understood at typical gas turbine operating conditions (P ~ 5-30 atm, T < 1100 K [6], air-dilute, fuel-to-O_2 equivalence ratio (φ) ~ 0.5 – 1.0 [4]). This knowledge will facilitate the successful design and operation of syngas fueled gas turbine combustors for use in IGCC or other similar systems.

1.1.1 Chemical kinetics of syngas oxidation

The kinetics of basic syngas (H_2 & CO only) and pure hydrogen oxidation have been well studied and modeled, see Chaos and Dryer [6] and the references contained therein. While early studies (~1970s) focused on low-pressure high-

temperature conditions, there has been a shift toward high-pressure low-temperature experimental conditions in recent decades [6]. This coincides with a desire to move toward high-pressure low-temperature combustion strategies which can reduce emissions and improve efficiency, e.g. dry-low NO_x and homogeneous charge compression ignition. As illustrated by Chaos and Dryer [6] and Chaos et al. [7] the fundamental nature of hydrogen and correspondingly syngas chemistry changes greatly as temperatures are reduced and pressure increased – predominantly in the chemical kinetics of OH formation. At high-pressure low-temperature conditions kinetic pathways for OH radical formation transition from O and H dominated pathways to slower HO_2 and H_2O_2 dominated pathways. This change reduces reactivity and introduces a pronounced pressure dependence, manifested as increased auto-ignition delay times which are highly dependent on pressure, for example [7]. Importantly, modern chemical kinetic mechanisms such as those by Li et al. [8] and Keromnes et al. [9] indeed capture chemical kinetic phenomena of basic syngas oxidation quite well for a wide range of thermodynamic conditions including at high pressures. Furthermore, these and other mechanisms have been validated quite extensively against auto-ignition, laminar flame speed, and chemical species profile data from various experimental facilities [8,9].

While basic syngas mixtures are indeed well studied, they are not fully representative of realistic syngas mixtures which are highly variable in both constituent species and concentrations [10]. Contrary to the basic formulation, diverse combinations of H_2, CO, CH_4, CO_2, N_2, and other trace species such as Si, N, and S-based compounds are known to exist in real mixtures [11–13]. This variation is detailed in Table 1-1, which illustrates typical syngas composition in real industrial applications. As indicated by Glarborg [14], even trace impurities have the potential to drastically alter the reactivity and dominant chemical kinetic pathways of the fuel oxidation process.

Table 1-1. Typical Syngas Composition [11–13,15]

Component	% Volume
H_2	25-30
CO	30-60
CO_2	5-15
H_2O	2-30
CH_4	0-5
N_2	0-4
Ar, N_2, H_2S, COS, NH_3, Ash	0-1
Trace Impurities (Fe, Cl, Si - species, Metals, etc.)	< 100 ppm

There are few experimental investigations of the effects of impurities and constituent variation on the combustion of syngas mixtures. These studies are limited to select species and focus primarily on the effects of hydrocarbon (HC) addition to basic syngas. Mathieu et al. [10] measured the effects of variations in CH_4, CO_2, H_2O, and NH_3 content on auto-ignition delay using a shocktube at ~98% Ar dilution, $\varphi = 0.5$, P = 2-32 atm, T = ~960-1860 K. The results indicated that the addition of up to 0.16% CO_2, 0.22% H_2O, or 0.02% NH_3 by total mixture volume had negligible effect at all conditions, while the addition of up to 0.08% CH_4 increased the auto-ignition delay time by up to an order of magnitude. Additionally, Mathieu et al. [16] investigated the effects of several compounds on syngas auto-ignition delay time using numerical methods, considering the addition of up to 15% CH_4, 1.7% C_2H_6, 5.3% C_2H_4, 0.7% C_2H_2, 21.8% H_2O, and 15% CO_2 by total fuel volume for mixtures at air-dilution, $\varphi = 0.5$ and 1.0, P = 1-35 atm, T = 900 – 1400K. The results of this work indicated that for all hydrocarbon (HC) species except C_2H_2 an increase in the auto-ignition delay time by a factor of two or more is expected, with most significant magnitude change for T > 1000 K. The effect of C_2H_2 addition was found to be negligible. Gersen et al. [17] measured the effects of variations in H_2, CO, and CH_4 content on auto-ignition delay times using a rapid compression machine at approximately air-dilution, $\varphi = 0.5$ and 1.0, P = ~20-80 bar, T = ~900-1100 K. The mole fraction of CH_4 in the fuel was varied from 0 to 1, for H_2 from 0 to 1, and for CH_4 from 0 to 0.5. The results showed that while the relative

concentration of CO had minimal effect, increasing the concentration of H_2 significantly decreased auto-ignition delay time and increasing the concentration of CH_4 significantly increased this time at all conditions.

In addition to these studies, the effects of impurities on the combustion of pure hydrogen have been evaluated for several compounds. As syngas combustion chemistry is dominated by hydrogen kinetic pathways [6], it is likely that effects similar to these would also be observed for syngas mixtures. Mueller et al. [18] measured the effects of NO and NO_2 addition to pure hydrogen fuel on species mole fraction profiles in a flow reactor at ~ 1% fuel dilution, φ = 1-2, P = ~0.5-14 atm, T = ~750-850 K. The experimental results, as well as those from subsequent kinetic modeling, illustrated a clear promoting effect of both NO and NO_2, with order of magnitude decreases in "characteristic reaction times" predicted for 10-1000 ppm concentrations. Mathieu et al. [19] studied the effects of up to 1600 ppm H_2S addition by total mixture volume on auto-ignition delay times in a shocktube at ~98% Ar dilution, φ = 0.5, P = 2-35 atm, T = ~960-1860 K. The findings of that study illustrated a distinct inhibiting effect, with increases in auto-ignition delay time of up to a factor of 6. Petersen et al. [20] measured the effects of up to 0.046% Silane (SiH_4) addition by total mixture volume on the auto-ignition delay times of pure hydrogen in a shocktube at ~98% Ar dilution, φ = 1.0, P = ~1 atm, T = ~1000-2250 K. The results indicate that the addition of SiH_4 at this concentration led to decreases in the auto-ignition delay time by a factor of two or more. This finding is in agreement with the previous study by McClain et al. [21] which indicated that increasing concentration of SiH_4 in an H_2 mixture significantly decreased auto-ignition delay times in a shocktube with ~ air-dilution, φ = 1.0 and 0.5, for P = ~1.5 atm and T = 800-1050K.

Overall, previous studies of the effects of impurities on syngas and hydrogen combustion are limited to a select few species and the results indicate that different species indeed yield varying ignition promoting and inhibiting effects. With these previous studies in mind there is yet a need for further investigation of the effects of impurities on syngas combustion. A number of important species remain

completely untested and for those species which have been investigated, limited experimental data, particularly for non-pure H_2 fuel, inhibits application of the results to real devices and mixtures. This is particularly important for species which promote ignition, considering that early ignition can lead to catastrophic failures. As a result, there is presently minimal ability to both predict and model chemical kinetic phenomena for realistic syngas mixtures, greatly restricting the application of this fuel in practical combustion devices.

1.1.2 Auto-ignition behaviors of syngas

While the chemical kinetics of basic syngas oxidation has been studied in detail, there have been only a few experimental investigations of the auto-ignition behavior of these fuels conducted at a narrow range of conditions (Voevodsky and Soloukhin, 1965 [22], Meyer and Oppenhiem, 1971 [23], Blumenthal et al., 1997 [24], Kalitan et al., 2007 [25], and Walton et al., 2007 [26]). Knowledge of these behaviors has great practical importance in HHC combustion systems, considering that control or avoidance of auto-ignition is key to safe and effective operation [27]. Furthermore, this knowledge is critical to the proper design and interpretation of combustion experiments which rely on this chemically driven ignition behavior, e.g. rapid compression machines, shocktubes, or flow reactors. In the auto-ignition studies listed above optical techniques were employed during auto-ignition delay time measurements in a variety of experimental facilities, which revealed diverse auto-ignition behaviors at thermodynamic conditions relevant to gas turbine operation. The observed behaviors consisted of both well-behaved homogeneous phenomena (spatially uniform reaction and/or detonation wave) and uncontrolled inhomogeneous phenomena (random localized reaction sites and deflagration). As there is no active source of ignition in these systems, e.g. a sparkplug, these results are an important indication that spontaneous and uncontrolled ignition can occur. Additionally, Chaos and Dryer [6] found that auto-ignition delay time measurements for experiments with inhomogeneous ignition behavior are up to several orders of magnitude less than typical model predictions; whereas

measurements for experiments with homogeneous ignition behavior are generally in excellent agreement with these predictions. This is a critical indication that not only is uncontrolled localized ignition taking place, but that it can lead to global auto-ignition events that occur much earlier than common model predictions. Overall these results illustrate a potentially catastrophic tendency of syngas and HHC fuels to ignite in unexpected locations or times at conditions typical of gas turbine operation.

With these important auto-ignition behaviors in mind, there is a critical lack of information regarding the conditions at which they occur and the fundamental chemical and physical processes which govern their existence and impact. Previous works do illustrate the existence these behaviors, but the conditions studied are limited and insufficient to represent the array of thermodynamic and mixture conditions in a real gas turbine system. As a result, there is presently minimal ability to predict and control the auto-ignition behaviors of syngas and other HHC fuels at conditions typical to gas turbine operation, a major barrier to their successful implementation in practical devices.

1.2 Objectives and General Approach

The primary objective of this thesis was to comprehensively advance syngas turbine design and development, through an experimental exploration and analysis of syngas combustion chemistry and auto-ignition behaviors at practical combustor conditions. An additional goal was to extend this knowledge to alternate fuel systems as appropriate, in order to facilitate the general development of low-temperature and fuel-flexible combustion strategies. The specific objectives for this thesis were:

- Investigate and broadly map the auto-ignition behaviors and auto-ignition delay times of air-dilute syngas for an extensive range of mixture and thermodynamic conditions,

- Evaluate the relationship between local and global auto-ignition phenomena, with a specific focus on the accuracy of common modeling methods,
- Explore the fundamental physical and chemical processes governing the auto-ignition behaviors and integrate these with experimental results to develop and validate methods for predicting auto-ignition behaviors in syngas,
- Investigate the effects of select impurities on syngas combustion chemistry, with a specific focus on unstudied and understudied species,
- Improve the understanding of the chemical kinetics of syngas oxidation and existing kinetic models.

These objectives were accomplished primarily through a series of experimental investigations of syngas auto-ignition behavior and auto-ignition delay times using the University of Michigan Rapid Compression Facility (UM-RCF). This facility is uniquely designed to create a quiescent volume of gas with uniform thermodynamic conditions similar to those in a gas turbine through an isentropic compression process. A detailed description of the UM-RCF and results of studies characterizing its performance can be found in Donovan et al. [28] and He et al. [29]. In these experiments, transient pressure measurements, high-speed imaging of the reactor volume, and ultra-violet (UV) laser absorption spectroscopy were employed. These tools were used to quantify the auto-ignition delay time, evaluate the occurrence and properties of auto-ignition behaviors, and to experimentally quantify the concentration of a key radical species, OH, during the ignition process for select mixtures and thermodynamic conditions. These new experimental data were combined with those from a multitude of previous works to develop comprehensive knowledge of auto-ignition times and properties as a function of initial thermodynamic state and mixture conditions. Furthermore, auto-ignition delay time and OH concentration measurements were compared to numerical predictions generated using various chemical kinetic and physical models, allowing for the identification of broader trends, enhanced analysis of the governing chemical kinetics, and an evaluation of the dominant physical behaviors.

1.3 Projects and Chapter Outline

The objectives described above were accomplished through four projects, each corresponding to a chapter in this dissertation (Chapters 3-6). Chapter 2 contains a detailed description of the experimental methods common to all projects with a focus on the University of Michigan – Rapid Compression Facility (UM-RCF). Chapter 7 contains a summary and a list of the major conclusions of this work, as well as recommendations for appropriate future work. Chapters 3-6 are described in detail below, with specific project motivations and objectives.

1.3.1 Chapter 3: High-pressure low-temperature ignition behavior of syngas mixtures

As previously mentioned, the limited experimental investigations of auto-ignition behavior by Voevodsky and Soloukhin, 1965 [22], Meyer and Oppenhiem, 1971 [23], Blumenthal et al., 1997 [24], Kalitan et al., 2007 [25], and Walton et al., 2007 [26] revealed diverse auto-ignition behaviors at thermodynamic conditions relevant to gas turbine operation. These consisted of both homogeneous (spatially uniform emission or detonation wave) and inhomogeneous (localized reaction sites and deflagration) phenomena. Importantly, Voevodsky and Soloukhin [22] and Meyer and Oppenheim [23] observed a clear and consistent transition between inhomogeneous and homogeneous auto-ignition behavior at varying initial thermodynamic conditions, i.e. the *strong ignition limit*. This is an indication that auto-ignition behaviors are generally repeatable and strongly related to the unburned condition. Voevodsky and Soloukhin [22] further illustrated that the strong ignition limit corresponds well to the second explosion limit of hydrogen at low pressures, demonstrating the importance of dominant chemical kinetic pathways in determining ignition behavior. Meyer and Oppenheim [23] expanded on the work by Voevodsky and Soloukhin [7] at low pressures, discovering that a specific value of the temperature derivative of the auto-ignition delay time (which they defined as the *thermal sensitivity* of the system) was well correlated with the strong ignition limit – thus connecting auto-ignition behavior to the dominant

chemical kinetic pathway and thermal non-uniformities in the unburned gas. This was an important indication that transitions in auto-ignition behavior can be understood and potentially predicted using thermal sensitivity.

This relationship between thermal non-uniformities and auto-ignition behavior was later investigated computationally by Sankaran et al. [30] using high fidelity direct numerical simulations of air-dilute pure H_2 at $\varphi = 0.1$. These simulations revealed that indeed various auto-ignition behaviors could be caused by distributed thermal non-uniformities. A non-dimensional criterion was then proposed, named the Sankaran Criterion in the present work, which compared thermal gradient driven propagation speed and laminar flame speed to indicate the transition between inhomogeneous and homogeneous ignition behaviors. Since a propagation speed determined by a thermal gradient is directly related to thermal sensitivity, this criterion again highlights the importance of the value of the thermal sensitivity. While providing a potentially powerful tool in the prediction of auto-ignition behavior, this criterion was not experimentally validated by Sankaran et al. or other investigators previous to the current work.

The understanding and prediction of the occurrence of various auto-ignition behaviors are important, as is the relationship between auto-ignition behaviors and the accuracy of basic homogeneous ignition modeling. As highlighted in Chaos and Dryer [6] and mentioned previously, it is apparent that auto-ignition delay time measurements for experiments with inhomogeneous ignition behavior are up to several orders of magnitude less than typical model predictions; whereas measurements for experiments with homogeneous ignition behavior are generally in excellent agreement with these predictions. With this in mind, there is currently a lack of understanding as to whether the effects inhomogeneous ignition behaviors necessarily lead to inaccuracy in basic auto-ignition delay modeling. This has profound impact on both scientific and practical applications of syngas, as both rely on accurate predictions of the auto-ignition delay times for safe and effective operation.

The objectives of this project were to comprehensively advance the understanding and prediction of the auto-ignition behaviors of air-dilute syngas for a broad range of conditions, and to also evaluate the relationship of such behaviors to the predictive accuracy of basic auto-ignition delay time modeling. These objectives were accomplished in part through an experimental investigation of syngas auto-ignition behavior and ignition delay times at lean conditions, using the UM-RCF. The results were then combined with those from the shocktube studies of Blumenthal et al. [24] and Kalitan et al. [25] to comprehensively map auto-ignition behavior as a function of initial thermodynamic state and equivalence ratio. On these maps, the strong ignition limit was identified and compared to the second explosion limits of hydrogen and predicted values of thermal sensitivity. The locations of the experimentally determined strong ignition limits were also compared to predictions made using the criterion of Sankaran et al. [30], the first application of this tool to experimental data. Lastly, the auto-ignition delay time measurements were compared to predictions made using typical zero-dimensional homogeneous reactor ignition modeling and the formaldehyde oxidation mechanism of Li et al. [8] (Li 2007 mechanism), in order to weigh the impact of auto-ignition behavior on the accuracy of auto-ignition delay time predictions.

A complete description of this project and the findings were published as, A.B. Mansfield, M.S. Wooldridge, Comb. and Flame 161 (2014) 2242–2251.

1.3.2 Chapter 4: Low-temperature ignition behavior of iso-octane

The results of the previous project indeed illustrated a remarkable ability of the Sankaran Criterion to predict the location of the strong ignition limit, i.e. the conditions where auto-ignition behavior transitions from inhomogeneous to homogeneous, using basic modeling methods. As stated previously, a goal of this body of work was to expand findings to alternative fuels in order to develop and enable low-temperature combustion strategies in general. Considering the potential value of the Sankaran Criterion to enable such strategies for fuels beyond those with HHC, the auto-ignition behavior of iso-octane and the application of the

criterion to iso-octane was investigated. As iso-octane is a well-studied primary reference fuel, it was selected as a representative of HC fuels in general. The theoretical foundation of the Sankaran criterion is not inherently fuel specific and a successful extension to non-hydrogen-based fuels was conceivable prior to the execution of this project.

While the oxidation chemistry of iso-octane has been well studied, as indicated in Mehl et al. [31] and the references therein, only Fieweger et al. [32] and Vermeer and Oppenheim [33] have directly investigated the auto-ignition behaviors of iso-octane in a controlled and quiescent experimental apparatus. Vermeer and Oppenheim [33] employed optical techniques during auto-ignition measurements in a shocktube for air-dilute stoichiometric iso-octane, which revealed diverse auto-ignition characteristics at thermodynamic and mixture conditions relevant to practical combustion devices. Similar to the results for syngas fuel, these behaviors included homogeneous (spatially uniform emission or detonation wave) and inhomogeneous (localized reaction sites and deflagration) phenomena. Vermeer and Oppenheim further observed a clear transition between these auto-ignition behaviors at varying initial thermodynamic conditions, which they again defined as the strong ignition limit. Fieweger et al. [32] expanded greatly on this work, classifying the auto-ignition behaviors of air-dilute stoichiometric iso-octane in a shocktube over a much broader range of initial temperatures, using pressure and CH emission time history characteristics. Consistent with the previous findings, Fieweger et al. [32] observed both homogeneous and inhomogeneous ignition behaviors and discovered a clearly defined strong ignition limit. The results of these studies are an important illustration that various auto-ignition behaviors are expected at conditions relevant to practical combustion devices using iso-octane, and that these generally repeatable behaviors are strongly related to initial unburned thermodynamic state. In this way previous observations of the auto-ignition behaviors of iso-octane indicate that they closely resemble the behaviors for syngas fuel, discussed in Chapter 3.

The objectives of this project were first to evaluate the hypothesis that the Sankaran Criterion could be accurately applied to iso-octane fuel, and second to investigate the effects of auto-ignition behaviors on the predictive accuracy of basic auto-ignition delay time modeling for this fuel. These objectives were accomplished in part through new experimental studies of iso-octane auto-ignition behavior and auto-ignition delay times using the University of Michigan Rapid Compression Facility (UM-RCF) and the Tsinghua University Rapid Compression Machine (TU-RCM). The auto-ignition behavior results were combined with those from the shock tube studies of Fieweger et al. [32] and Vermeer and Oppenheim [33] to map auto-ignition behavior as a function of initial thermodynamic state and equivalence ratio. Using these maps, the strong ignition limit was identified for various equivalence ratios and the location of each limit was compared to predictions made using the Sankaran Criterion. Then the auto-ignition delay time measurements for all experiments were compared to predictions made using typical zero-dimensional homogeneous reactor modeling and the iso-octane oxidation mechanism of Mehl et al. [31].

A complete description of this project and the findings were published as, A.B. Mansfield, M.S. Wooldridge, H. Di, X. He, FUEL 139 (2015) 79–86.

1.3.3 Chapter 5: The effect of impurities on syngas combustion

As discussed earlier, previous studies indicate that the addition different species indeed yields varying ignition promoting and inhibiting effects in syngas and pure hydrogen mixtures. Furthermore, limited investigation of the effects of impurities on syngas yields a corresponding limit to the application of syngas fuels in practical devices. It is of particular importance to develop an understanding of the effects of ignition promoting species, which have the potential to cause catastrophic system failure through un-predicted early auto-ignition. With this in mind, the significant promoting effect observed for SiH_4 addition to pure H_2 mixtures is particularly interesting, considering the substantial and increasing concentrations of organic Si compounds in syngas derived from waste (landfills,

waste digesters, or water treatment facilities) [13,34]. As detailed in Rasi et al. [13] and Pierce et al. [35] syngas from these sources contains both silanol {…Si-OH} and siloxane {…Si-O-Si…} species at up to 10-100 ppm concentrations. Common compounds include trimethylsilanol and decamethylcyclopentasiloxane, which make up a majority of the organic Si content within syngas from waste sources [13]. While the fouling tendencies of these and other organic Si species in combustion devices is well documented [34,35], their effect on combustion chemistry has not been investigated in any capacity. Considering the significant ignition promoting effects observed for a chemically similar compound, i.e. SiH_4, and the increasing concentrations of Si-based species in syngas, this lack of knowledge presents a significant barrier to the safe and effective implementation of this fuel.

The objective of this project was to advance the understanding of the effects of impurities on the chemical kinetics of syngas oxidation, focusing on CH_4 and trimethylsilanol (TMS) impurities at thermodynamic and mixture conditions relevant to practical device operation. This objective was accomplished through an experimental investigation of auto-ignition delay times at lean, low-temperature, high-pressure conditions, using the UM-RCF. Uniquely, high-speed imaging was utilized for each experiment, ensuring that only ideal homogeneous ignition behaviors were exhibited for the data reported here. This important diagnostic enabled testing at lower temperatures and pressures not possible in previous experimental studies by other investigators, thereby expanding knowledge of impurity effects to more practical conditions. The auto-ignition delay time and pressure time history measurements were compared to predictions made using typical zero-dimensional homogeneous reactor ignition modeling and the formaldehyde oxidation mechanism of Li et al. [8] (Li 2007 mechanism), used frequently to successfully predict syngas combustion characteristics [6,10,36]. This model was then used to interpret and analyze observed pressure time histories and impurity effects, in order to describe behavior trends and connect these with potential underlying chemical kinetic pathways.

1.3.4 Chapter 6: Experimental study of OH time histories during syngas auto-ignition

Chemical kinetic mechanisms are frequently validated against experimental measurements of bulk phenomena, i.e. auto-ignition delay time and laminar flame speed, which are representative of the global action of the chemically reacting system. Often though, these mechanisms are subsequently used across a much broader range of thermodynamic conditions to predict more specific variables such as chemical species concentrations. It is therefore highly desirable to expand the validation of these mechanisms to include comparisons with measurements of more specific parameters, e.g. OH mole fraction time histories. Such comparisons can facilitate an improvement in the chemical pathways most critical to the combustion process, thereby improving both the mechanisms accuracy across broader conditions and in predicting specific species concentrations. Based on the recent work by Burke et al. [37] to develop a revised H_2/O_2 oxidation model, there is limited OH radical concentration data during combustion for pure H_2 fuel. Furthermore, no OH radical concentration data was found in the literature for syngas fuel combustion at any conditions. All available data for H_2 is from shocktubes at high-temperature low-pressure conditions (1050 – 2700 K, 0.4 – 2 atm) for stoichiometric mixtures with very high pure Ar dilution (90+ %) [38–42]. While these data are a valuable source for chemical kinetic model development there is a need for OH concentration measurements during combustion at more engine relevant conditions and mixtures, from a wider range of facilities. As highlighted previously, the chemical kinetics of hydrogen and syngas fuel oxidation changes markedly at the high-pressure low-temperature conditions often desired in modern engine applications.

The objective of this project was to provide valuable real-time OH concentration data corresponding to the auto-ignition process for syngas fuel and to use this data to validate and improve commonly used chemical kinetic mechanisms for syngas oxidation. This was accomplished through an experimental investigation of auto-ignition delay times at engine relevant conditions, using the UM-RCF. Laser spectroscopy was applied, allowing for real-time measurement of the OH

radical concentration for each experiment. Importantly, high-speed imaging was also utilized for each experiment, ensuring that only homogeneous ignition behaviors were exhibited for the data reported here. The auto-ignition delay time, pressure time history, and OH mole fraction time history measurements were compared to predictions made using typical zero-dimensional homogeneous reactor ignition modeling and the commonly used syngas oxidation mechanisms of Li et al. [8] and Keromnes et al. [9], importantly considering known uncertainties in reaction rates.

REFERENCES

[1] US Department of Energy. Gasifipedia - Syngas Processing, http://www.netl.doe.gov/research/coal/energy-systems/gasification/syngas-processing 2014.

[2] US Department of Energy. Gasification Plant Database, http://www.netl.doe.gov/research/coal/energy-systems/gasification/gasification-plant-databases 2014.

[3] US Department of Energy. Advanced Turbine Research Program, http://www.netl.doe.gov/research/coal/energy-systems/turbines/advanced-research 2014.

[4] Lieuwen T, McDonell V, Santavicca D, Sattelmayer T. Burner Development and Operability Issues Associated with Steady Flowing Syngas Fired Combustors. Combust Sci Technol 2008;180:1169–92.

[5] Richards G., McMillian M., Gemmen R., Rogers W., Cully S. Issues for low-emission, fuel-flexible power systems. Prog Energy Combust Sci 2001;27:141–69.

[6] Chaos M, Dryer FL. Syngas Combustion Kinetics and Applications. Combust Sci Technol 2008;180:1053–96.

[7] Lieuwen T, Yang V, Yetter R. Gas Synthesis Combustion: Fundamentals and Applications. CRC; 2009.

[8] Li J, Zhao Z, Kazakov A, Chaos M, Dryer FL, Scire JJ. Mechanism for CO, CH2O, and CH3OH Combustion. Int J Chem Kinet 2007.

[9] Kéromnès A, Metcalfe WK, Heufer K a., Donohoe N, Das AK, Sung C-J, et al. An experimental and detailed chemical kinetic modeling study of hydrogen and syngas mixture oxidation at elevated pressures. Combust Flame 2013;160:995–1011.

[10] Mathieu O, Kopp MM, Petersen EL. Shock-tube study of the ignition of multi-component syngas mixtures with and without ammonia impurities. Proc Combust Inst 2012;34:3211–8.

[11] CL Miller, DC Cicero MA. Hydrogen From Coal Program: Research, development, and demonstration plan for the period 2007 through 2016. 2007.

[12] Ciferno J, Marano J. Benchmarking biomass gasification technologies for fuels, chemicals and hydrogen production. 2002.

[13] Rasi S, Lehtinen J, Rintala J. Determination of organic silicon compounds in biogas from wastewater treatments plants, landfills, and co-digestion plants. Renew Energy 2010;35:2666–73.

[14] Glarborg P. Hidden interactions—Trace species governing combustion and emissions. Proc Combust Inst 2007;31:77–98.

[15] Jones R, Shilling N. IGCC gas turbines for refinery applications. GE Power Syst Schenectady, NY 2003.

[16] Mathieu O, Petersen EL, Heufer A, Donohoe N, Metcalfe W, Curran HJ, et al. Numerical Study on the Effect of Real Syngas Compositions on Ignition Delay Times and Laminar Flame Speeds at Gas Turbine Conditions. J Eng Gas Turbines Power 2013;136:011502.

[17] Gersen S, Darmeveil H, Levinsky H. The effects of CO addition on the autoignition of H2, CH4 and CH4/H2 fuels at high pressure in an RCM. Combust Flame 2012:2–5.

[18] Mueller M, Yetter R, Dryer F. Flow reactor studies and kinetic modeling of the H2/O2/NOx and CO/H2O/O2/NOx reactions. Int J Chem Kinet 1999;31:705–24.

[19] Mathieu O, Deguillaume F, Petersen EL. Effects of H2S addition on hydrogen ignition behind reflected shock waves: Experiments and modeling. Combust Flame 2013;161:23–36.

[20] Petersen E, Kalitan D, Rickard MA. Reflected Shock Ignition of SiH4/H2/O2/Ar andSiH4/CH4/O2/Ar Mixtures. J Propuls Power 2004;20:665–74.

[21] McLain A, Jachimowski C, Rogers R. Ignition of SiH4-H2-02-N2 behind reflected shock waves 1983.

[22] Voevodsky V, Soloukhin R. On the mechanism and explosion limits of hydrogen-oxygen chain self-ignition in shock waves. Symp Combust 1965:279–83.

[23] Meyer JW, Oppenheim a. K. On the shock-induced ignition of explosive gases. Symp Combust 1971;13:1153–64.

[24] Blumenthal R, Fieweger K, Komp K. Self-ignition of H2-air mixtures at high pressure and low temperature. Proc. 20th ISSW, World Sci., 1996, p. 935–40.

[25] Kalitan DM, Mertens JD, Crofton MW, Petersen EL. Ignition and Oxidation of Lean CO / H 2 Fuel Blends in Air. J Propuls Power 2007;23:1291–303.

[26] Walton SM, He X, Zigler BT, Wooldridge MS. An experimental investigation of the ignition properties of hydrogen and carbon monoxide mixtures for syngas turbine applications. Proc Combust Inst 2007;31:3147–54.

[27] Lieuwen T, McDonell V, Petersen E, Santavicca D. Fuel Flexibility Influences on Premixed Combustor Blowout, Flashback, Autoignition, and Stability. J Eng Gas Turbines Power 2008;130:011506.

[28] Donovan MT, He X, Zigler BT, Palmer TR, Wooldridge MS, Atreya A. Demonstration of a free-piston rapid compression facility for the study of high temperature combustion phenomena. Combust Flame 2004;137:351–65.

[29] He X, Zigler BT, Walton SM, Wooldridge MS, Atreya a. A rapid compression facility study of OH time histories during iso-octane ignition. Combust Flame 2006;145:552–70.

[30] Sankaran R, Im HG, Hawkes ER, Chen JH. The effects of non-uniform temperature distribution on the ignition of a lean homogeneous hydrogen–air mixture. Proc Combust Inst 2005;30:875–82.

[31] Mehl M, Pitz WJ, Westbrook CK, Curran HJ. Kinetic modeling of gasoline surrogate components and mixtures under engine conditions. Proc Combust Inst 2011;33:193–200.

[32] Fieweger K, Blumenthal R, Adomeit G. Shock-tube investigations on the self-ignition of hydrocarbon-air mixtures at high pressures. Symp Combust 1994;25:1579–85.

[33] Vermeer DJ, Oppenheim AK. Auto-Ignition of Hydrocarbons Behind Reflected Shock Waves. Combust Flame 1972;18:327–36.

[34] Wheless E, Pierce J. Siloxanes in landfill and digester gas update. Proc 27th SWANA Landfill Gas Symp San Antonio, TX 2004.

[35] Pierce J. Siloxane Quantification, Removal, and Impact on Landfill Gas Utilization Facilities. 8th Annu. LMOP Conf. Proj. Expo, 2005.

[36] Mansfield AB, Wooldridge MS. High-pressure low-temperature ignition behavior of syngas mixtures. Combust Flame 2014;161:2242–51.

[37] Burke MP, Chaos M, Ju Y, Dryer FL, Klippenstein SJ. Comprehensive H2/O2 kinetic model for high-pressure combustion. Int J Chem Kinet 2012;44:444–74.

[38] Masten D, Hanson RK, Bowman CT. Shock tube study of the reaction H + O2 = OH + O using OH laser absorption. J Phys Chem 1990;94:7119–28.

[39] Herbon JT, Hanson RK, Golden DM, Bowman CT. A shock tube study of the enthalpy of formation of OH. Proc Combust Inst 2002;29:1201–8.

[40] Vasu S, Davidson D, Hanson R. Shock tube study of syngas ignition in rich CO2 mixtures and determination of the rate of H+ O2+ CO2= HO2+ CO2. Energy & Fuels 2011:990–7.

[41] Hong Z, Cook RD, Davidson DF, Hanson RK. A shock tube study of OH + H2O2 --> H2O + HO2 and H2O2 + M = 2OH + M using laser absorption of H2O and OH. J Phys Chem A 2010;114:5718–27.

[42] Hong Z, Lam K-Y, Sur R, Wang S, Davidson DF, Hanson RK. On the rate constants of OH+HO2 and HO2+HO2: A comprehensive study of H2O2 thermal decomposition using multi-species laser absorption. Proc Combust Inst 2013;34:565–71.

Chapter 2
Experimental and Computational Methods

In this chapter the experimental and computational methods common to all projects are described. These are based primarily on experiments in the UM-RCF with computational predictions made using the CHEMKIN software suite [1]. Additional systems and methods specific to each project are described in more detail in each chapter, respectively.

2.1 University of Michigan – Rapid Compression Facility

The UM-RCF is uniquely designed to create a gas volume with uniform thermodynamic conditions through an isentropic compression process [2]. A detailed description of the UM-RCF and results of studies characterizing its performance can be found in Donovan et al. [2] and He et al. [3]. Briefly, the apparatus consists of a long cylinder, the Driven Section, in which a gas mixture is rapidly compressed by the motion of a free piston (Sabot). Prior to compression, the Driven Section is evacuated with a pump and then filled with a specific test gas mixture. Upon firing, the Sabot travels the length of the Driven Section compressing the test gas mixture into the Test Section – a small cylindrical volume located at the end of the Driven Section (~ 50 mm length and 50 mm diameter). As the Sabot reaches its final position near the Test Section, the Sabot achieves an annular interference fit, thereby sealing the test gas mixture in the Test Section. At this point, the Test Section is filled with a uniform and isentropically compressed test gas mixture at the desired initial thermodynamic condition. This is achieved in large part because cool boundary layer gases from the Driven section are trapped in an external volume formed by the geometry of the Sabot [2,4].

For each project, the Test Section was instrumented with a piezoelectric transducer (6125B Kistler, Amherst, NY) and charge amplifier (5010 Kistler, Amherst, NY) for pressure measurements, and a transparent polycarbonate end-wall to permit high-speed imaging of the ignition process. During each experiment the pressure time history was recorded using the pressure transducer at 100 kHz sampling frequency. The uncertainty in the pressure measurements is estimated as ≤ 1% (~ 0.1 atm) considering both the signal-to-noise ratio in the post-ignition pressure time history data and the non-linearity limits defined by Kistler during the calibration process. High-speed color imaging was recorded using a digital video camera (V711-8G-MAG-C, Vision Research, Phantom) with a Navitar 50mm lens (F0.95), a Hoya 62 mm lens (+2 zoom), and a Hoya 62 mm UV(0) filter. Video sequences were recorded at 25,000 frames/second with a CMOS array resolution of 512 x 512 pixels, resulting in an exposure time of 39.3 μs.

All test gas mixtures were made using a dedicated stainless steel tank and the mixture composition was determined by measurement of the relative partial pressures of the components. After filling, the tank was continuously stirred by an internal mechanism and was left to mix for at least one hour before use. Error in the mixture composition is assumed to be negligible and have negligible effect on the ignition results, considering ~80-95% (mole basis) of the mixture is comprised of N_2 and O_2.

2.2 Typical pressure time history measurement

For each experiment in the UM-RCF, a pressure time history was recorded allowing for the determination of an auto-ignition delay time. A typical pressure time history during a homogeneous auto-ignition experiment for the present work can be seen in Fig. 2-1. Trends in the pressure data illustrate a pressure increase during the compression stroke until the Sabot is seated at the end-of-compression event, followed by a slight decrease in pressure due to heat transfer from the test gas volume into the cool Test Section walls, followed by a large and rapid increase in pressure during the ignition event. For each experiment, the raw pressure time

history was first filtered with a 75-point smoothing algorithm to reduce noise, then the time and pressure values were noted at three distinct events: end-of-compression (EOC), minimum pressure (P_{min}), and maximum pressure (P_{max}), denoted in Fig. 2-1.

The method for assigning an auto-ignition delay time to each experiment varied between projects and is described individually in the proceeding chapters; generally speaking it is the time between the EOC and the ignition event.

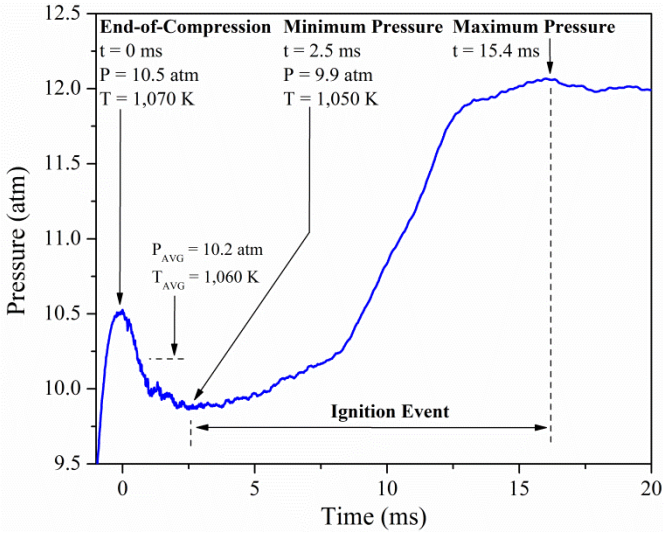

Fig. 2-1. Typical experimental pressure time history from the UM-RCF at experimental conditions of P = 10.2 atm, T = 1,060 K, pure syngas fuel (H_2, CO only), φ = 0.1, H_2:CO molar ratio = 0.7, ~ Air-dilute with N_2 and Ar.

2.2 Assignment of Thermodynamic State

For each experiment a thermodynamic state was assigned, representing the isobaric/isothermal condition at which the experiment was conducted. While the pressure within the Test Section was directly measured throughout each experiment, it was necessary to calculate the bulk temperature using thermodynamic relations. Experimentally verified by Donovan et al. [2], the initial compression stroke in the UM-RCF is well represented as isentropic compression. Furthermore, assuming that the gas volume contained in the Test Section is composed of an "adiabatic core" and a "boundary layer region", as defined in Lee and Hochgreb [5], the pressure decrease after the EOC event can be modeled as

isentropic expansion. With these well supported assumptions in place, the initial uncompressed thermodynamic conditions were used in conjunction with isentropic state relations to calculate the temperature throughout the experiment. Propagation of the pressure measurement uncertainty of ≤ 1% through the isentropic state relations yields an uncertainty of ≤ 0.4% in the temperature (~5 K). This is in very good agreement with expected thermal variations in the UM-RCF, experimentally determined by Donovan et al. [2] to be less than ~10 K by direct thermocouple measurement.

Regarding the assignment of a specific thermodynamic state to each experiment, the EOC state (P,T) or a derived average state were assigned, depending on which best represented the experiment. In most cases, there was no appreciable decrease in temperature between the EOC event and the ignition event (i.e.< 10 K change from P_{EOC} to P_{min}), and so the EOC thermodynamic state was assigned to the experimental result. However, for the cases with significant decreases in temperature (i.e. > 10 K) in that time period, an average thermodynamic state was assigned. The average pressure was defined mathematically as the arithmetic mean of all pressure measurements between EOC and P_{min}. The average temperature was calculated thereafter assuming an isentropic expansion from the thermodynamic state at the EOC event to the average pressure. Assignment of an average state in this manner captures the effects of heat transfer to the cool Test Section walls while retaining critical clarity in both reporting and interpreting the experimental results, thus greatly improving the archival value of the results as compared to using the EOC conditions. Similar methods of assigning an average or "effective state" to experiments exhibiting some non-adiabatic behavior have been successfully applied in numerous past experiments using the UM-RCF [2,6]. Moreover, the use of average conditions allows straightforward interpretation of the data using isobaric and isothermal reporting techniques such as the P-T diagrams and Arrhenius diagrams presented later in this work.

Other methods to represent the effects of heat transfer on similar rapid compression experiments exist, but focus on adjustments in auto-ignition modeling rather than assignment of an adjusted thermodynamic state as done here. These alternative methods are discussed in detail in the proceeding section.

2.3 Computational Methods

Auto-ignition delay time predictions were made in the present work using the constant volume adiabatic zero-dimensional homogeneous reactor model in the CHEMKIN software suite [1] with various chemical kinetic mechanisms. Using this model corresponding predictions of auto-ignition delay time or other parameters were calculated for each auto-ignition experiment using the assigned thermodynamic state and mixture composition. Importantly for each prediction, quantified uncertainty bounds of the model predictions were calculated using the known uncertainty in the "A-factor" of the Arrhenius reaction rates for the most sensitive reactions, selected using OH sensitivity analysis in the CHEMKIN software suite. The selected reactions and rate coefficients used in each project are listed in each chapter individually.

As mentioned above, there are alternatives to the method of assigning an average thermodynamic state to each experiment and subsequently modeling each experiment as a constant volume adiabatic system. These methods commonly assign the EOC state to each experiment and then integrate a non-reactive pressure time history or a derived "volume trace" into the modeling process, as done in Gersen et al. [7], Mittal et al. [8], and Würmel et al. [9], in an attempt to account for heat transfer effects in the experiment. While incorporation of a volume trace in the modeling is indeed a more time-dependent treatment of heat transfer effects, the merit of implementing such detail is small and is may be significantly outweighed by the often overlooked drawbacks. Foremost, if this empirical method is used without appropriate documentation, the archival value of the data is significantly reduced. Without any record of the heat loss profiles, appropriate comparisons cannot be made between experimental facilities or model predictions,

and any quantitative understanding of the effects of heat transfer in the experiments is lost. A standard for reporting rapid compression machine heat losses using these empirical corrections has yet to be established or a criterion for when it is appropriate to take such steps to represent heat losses (clearly not all experiments need such attempts, only systems and conditions with high heat transfer rates). As noted above, a criterion of a maximum temperature change of 10 K was applied in this body of work. Further, comparison of the volume trace and the effective state methods for syngas fuel, detailed in Mansfield and Wooldridge [10] revealed no significant difference between auto-ignition delay time predictions (< 15%) using the average state or volume trace method, which was particularly irrelevant when the uncertainty in the chemical kinetic mechanism was appropriately considered. Thus, the assignment of an average state allows for both improved archival clarity and equivalent accuracy as compared to the volume trace method.

The present discussion of state assignment and modeling techniques was published as, A.B. Mansfield & M.S. Wooldridge. Combust Flame 161 (2014) 2242–51.

REFERENCES

[1] Reaction Design. CHEMKIN 10101 2010.

[2] Donovan MT, He X, Zigler BT, Palmer TR, Wooldridge MS, Atreya A. Demonstration of a free-piston rapid compression facility for the study of high temperature combustion phenomena. Combust Flame 2004;137:351–65.

[3] He X, Zigler BT, Walton SM, Wooldridge MS, Atreya a. A rapid compression facility study of OH time histories during iso-octane ignition. Combust Flame 2006;145:552–70.

[4] Walton S, He X, Zigler B, Wooldridge M, Atreya a. An experimental investigation of iso-octane ignition phenomena. Combust Flame 2007;150:246–62.

[5] Lee D, Hochgreb S. Hydrogen Autoignition at Pressures above the second explosion limit. Int J Chem Kinet 1998;30:385–406.

[6] Walton SM, He X, Zigler BT, Wooldridge MS. An experimental investigation of the ignition properties of hydrogen and carbon monoxide mixtures for syngas turbine applications. Proc Combust Inst 2007;31:3147–54.

[7] Gersen S, Anikin N, Mokhov a, Levinsky H. Ignition properties of methane/hydrogen mixtures in a rapid compression machine. Int J Hydrogen Energy 2008;33:1957–64.

[8] Mittal G, Sung C-J, Yetter R a. Autoignition of H2/CO at elevated pressures in a rapid compression machine. Int J Chem Kinet 2006;38:516–29.

[9] Würmel J, Silke EJ, Curran HJ, Ó Conaire MS, Simmie JM. The effect of diluent gases on ignition delay times in the shock tube and in the rapid compression machine. Combust Flame 2007;151:289–302.

[10] Mansfield AB, Wooldridge MS. High-pressure low-temperature ignition behavior of syngas mixtures. Combust Flame 2014;161:2242–51.

Chapter 3

High-pressure low-temperature ignition behavior of syngas mixtures

In order to comprehensively improve the understanding and prediction of the auto-ignition behaviors of syngas and also to evaluate the relationship of such behaviors to the predictive accuracy of basic auto-ignition delay time modeling, auto-ignition behavior and auto-ignition delay times at lean conditions were investigated using the UM-RCF. The results were then combined with those from previous studies to comprehensively map auto-ignition behavior and evaluate methods for predicting transitions in auto-ignition behavior. Furthermore, auto-ignition delay time measurements were compared to predictions made using a common syngas chemical kinetic mechanism, in order to weigh the impact of auto-ignition behavior on the accuracy of auto-ignition delay time predictions.

This chapter has been published as, A.B. Mansfield, M.S. Wooldridge, Comb. and Flame 161 (2014) 2242–2251.

1. METHODS

1.1 Experimental

Ignition experiments were conducted for realistic but simple syngas mixtures for two values of equivalence ratio (φ = 0.1 and 0.5), designed to represent lean syngas mixtures used in the power industry [1]. Both mixtures contained only H_2 and CO as fuel, with a molar ratio of H_2:CO = 0.7, and were approximately air-dilute with N_2, i.e. molar O_2 to inert gas ratio of 1:3.76. In some cases small amounts of the N_2 diluent gas were replaced by Ar and/or CO_2 to modify the test temperature. Ignition experiments were conducted at approximately 3, 5, 10, and 15 atm for the broadest range of temperatures allowable in the UM-RCF for these

mixtures (~ 950-1150 K, based on experimental test times). The composition of the gas mixture and the thermodynamic state corresponding to each auto-ignition delay time measurement are given in the Supplemental Material section.

1.2 Computational

Auto-ignition ignition delay time predictions were made using the constant volume adiabatic zero-dimensional homogeneous reactor model in the CHEMKIN software suite [2] with the Li 2007 chemical kinetic mechanism. This mechanism was used only, given its previous success in predicting syngas ignition behavior [3,4] and the minor differences in predictions seen between other H_2 and CO reaction mechanisms in other studies [5]. Using this ignition model a corresponding auto-ignition delay time prediction was calculated for each ignition experiment considered in the present work using the exact initial thermodynamic condition and mixture composition, including those conducted in the UM-RCF and those from Blumenthal et al. [6] and Kalitan et al. [7]. For each prediction, quantified uncertainty bounds of the model predictions were calculated using the known uncertainty in the "A-factor" of the Arrhenius reaction rates for the two most sensitive reactions, $H + O_2 = H + OH$ (R1) & $H + O_2 (+M) = HO_2 (+M)$ (R9), selected using OH sensitivity analysis in the CHEMKIN software suite. The rate coefficients used for this reaction are listed in the Supplemental Material section. Iso-contours of constant predicted auto-ignition delay time and thermal sensitivity were also calculated using this model for a broad range of initial thermodynamic conditions, though a constant pressure boundary condition was applied and only the nominal A-factors in the kinetic model were used when calculating thermal sensitivity.

2. RESULTS AND DISCUSSION

For each experiment in the UM-RCF, a pressure time history and a high-speed imaging video were recorded, allowing for the determination of an auto-

ignition delay time and direct observation and classification of the auto-ignition behavior. A typical pressure time history during an ignition experiment for the present work can be seen in Fig. 3-1. Trends in the pressure data illustrate a pressure increase during the compression stroke until the Sabot is seated at the end-of-compression event, followed by a slight decrease in pressure due to heat transfer from the test gas volume into the cool Test Section walls, followed by a large and rapid increase in pressure during the ignition event. For each experiment, the time and pressure value was noted at three distinct events: end-of-compression (EOC), minimum pressure (P_{min}), and maximum pressure (P_{max}), denoted in Fig. 3-1. After filtering the pressure time history with a 75-point smoothing algorithm to reduce signal noise, the pressure and time value for each event was defined mathematically as a local maximum or minimum respectively. The nominal ignition event was defined as occurring at the average time of P_{min} and P_{max} with symmetric uncertainty bounds assigned to span the time from P_{min} to P_{max}. The nominal auto-ignition delay time was defined as the time from EOC to the ignition event, with symmetric uncertainty bounds defined by the uncertainty bounds of the ignition event time. Overall, this definition is quite general and biases the auto-ignition delay times slightly to faster times compared to conventional definitions based on the maximum rate of pressure rise. However, this approach ensures the analysis can be applied to all experiments regardless of ignition behavior, which was critical given the wide range of conditions considered in this work yielding variable pressure time history characteristics. Additionally, the uncertainty limits assigned in this study ensure that the conventional definition of auto-ignition delay time based on the maximum rate of pressure rise is captured within the bounds of the reported measurements. For each experiment a thermodynamic state was assigned, representing the isobaric/isothermal condition at which the experimental was conducted, as described in Chapter 2.

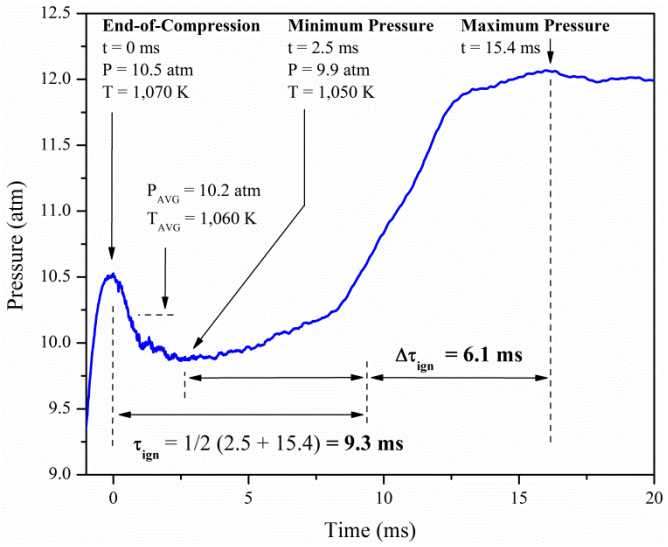

Fig. 3-1. Typical experimental pressure time history at experimental conditions of P = 10.2 atm, T = 1,060 K, φ = 0.1; where, τ_{ign} is the auto-ignition delay time and $\Delta\tau_{ign}$is the symmetric uncertainty of the auto-ignition delay time.

Typical high-speed imaging results of chemilluminescence during syngas auto-ignition in the UM-RCF are shown in Fig. 3-2a & 3-2b, illustrating both homogeneous and inhomogeneous auto-ignition phenomena respectively. As seen in the figure, homogeneous ignition is indicated by spatially uniform chemilluminescence emission; whereas, inhomogeneous ignition is indicated by local emission features forming flame-like structures which propagate and merge. In some experiments, inhomogeneous phenomena were followed by homogeneous ignition of the unburned gas volume. Based on the observed chemilluminescence behavior, each experiment was classified as exhibiting one of three ignition behaviors, strong, weak, or mixed, described in detail in Table 3-1. In general, the imaging closely resembled previous high-speed imaging results for syngas ignition seen in Walton et al. [8]. In several low-pressure experiments no chemilluminescence was observed, likely due to low energy content and/or low-densities, and the ignition behavior was classified as strong by default.

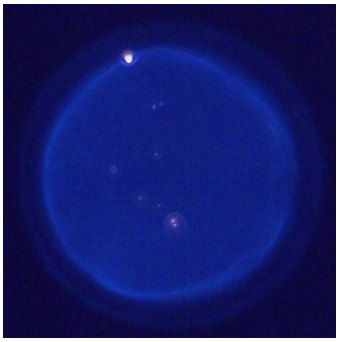

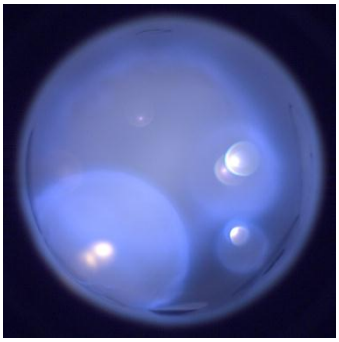

Fig. 3-2a. (left) Single frame from high-speed imaging of homogeneous ignition behavior, illustrating uniform chemilluminescence for experimental conditions P = 3.3 atm, T = 1043 K, φ = 0.1.

Fig. 3-2b. (right) Single frame from high-speed imaging of inhomogeneous ignition behavior, illustrating non-uniform chemilluminescence with various localized flame-like structures, for experimental conditions P = 9.2 atm, T = 1019 K, φ = 0.5.

Table 3-1. Classification of ignition behavior based on high-speed imaging results

Ignition Classification	Imaging Characteristics	Auto- Ignition Phenomena
Strong	Spatially uniform only	Homogeneous
Weak	Flame-like structures only	Inhomogeneous
Mixed	Flame-like structures then spatially uniform in unburned gas volume	Inhomogeneous, then homogeneous in unburned gas volume

In order to compare ignition behaviors from the UM-RCF to those observed in Blumenthal et al. [6] and Kalitan et al. [7], it was necessary to re-classify the behavior in these other studies according to the three categories in Table 1. In Blumenthal et al. experiments were originally classified as "Strong", "DDT" (Deflagration to Detonation Transition), or "no DDT" which were defined as strong, mixed, and weak ignition in the present work respectively. In Kalitan et al. experiments were classified as exhibiting "early OH emission" or not, which were defined as mixed and strong ignition in the present work respectively.

2.1 Auto-Ignition Behavior

Fig. 3-3 presents the observed ignition behavior as a function of initial thermodynamic state for mixtures with φ = 0.1. A range of behaviors is evidenced,

with strong ignition generally at temperatures above ~1000 K transitioning to mixed and/or no ignition as the temperature decreases. The data show the ignition behavior is strongly related to initial thermodynamic state and is repeatable, with generally clear boundaries between different regions. The boundary between mixed and strong ignition behaviors at lower pressures (2-5 atm) is the strong ignition limit and is marked as a hashed area. A strong ignition limit is not evident at higher pressures (10-15 atm) though, where no mixed ignition is observed at any temperature.

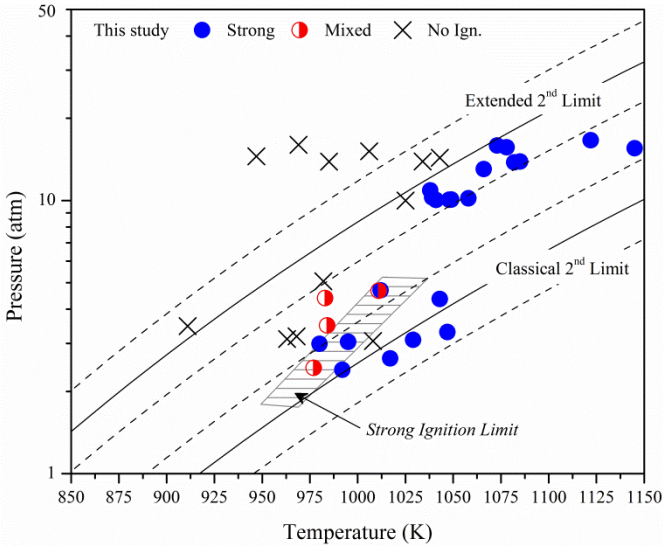

Fig. 3-3. Ignition behavior as a function of thermodynamic state for mixtures with φ = 0.1. The Strong Ignition Limit is shown as a hashed area. H_2/O_2 explosion limits are shown as solid lines with upper and lower bounds shown as dashed lines, representing uncertainty in the rate coefficient of reactions R1 and R9.

Fig. 3-4 presents the observed ignition behavior as a function of thermodynamic state for mixtures with φ = 0.5, including results from Blumenthal et al. [6] and Kalitan et al. [7]. Again, a range of behaviors was observed, with strong ignition generally at the highest temperatures transitioning to mixed, then weak, then no ignition as the temperature decreases. There is excellent agreement between the results in the present work and those from Blumenthal et al. [6] and Kalitan et al. [7]. This finding suggests that the ignition behavior of syngas is not highly sensitive to the molar ratio of H_2:CO at these conditions and that the

behavior trends are not strongly device dependent. Overall the data show the ignition behavior is strongly related to initial thermodynamic state and is repeatable, with generally clear boundaries between different regions. The boundary between mixed and strong ignition is the strong ignition limit, which exhibits a clear dependence on pressure and is marked as a hashed area. The onset of mixed ignition at higher pressures as the equivalence ratio is increased from 0.1 to 0.5 is an indication that the energy content of the mixture is related to the auto-ignition behavior, in agreement with previous findings that connected inhomogeneous ignition phenomena and "high energy density mixtures" [4]. This relation is not evident at lower pressures, however, where the strong ignition limit seems largely unaffected by changes in the equivalence ratio.

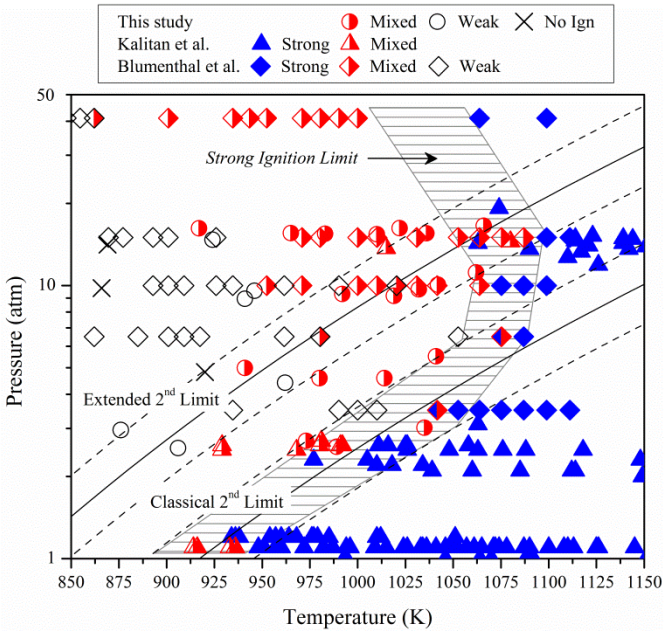

Fig. 3-4. Ignition behavior as a function of thermodynamic state for mixtures with φ = 0.5. Results are from the present work, Kalitan et al. [7], and Blumenthal et al. [6]. The Strong Ignition Limit is shown as a hashed area. H_2/O_2 explosion limits are shown as solid lines with upper and lower bounds shown as dashed lines, representing uncertainty in the rate coefficient of reactions R1 and R9.

With the strong ignition limit experimentally determined for φ = 0.1 and 0.5, it was possible to develop a more complete understanding of the transition in auto-ignition behavior. This was accomplished through a comparison of the strong

ignition limit in each case to: (1) the second explosion limits of hydrogen, as suggested by Voevodsky and Soloukhin [9], (2) values of thermal sensitivity, as proposed by Meyer and Oppenheim [10], and (3) predicted locations of the strong ignition limit, as proposed by Sankaran et al. [11].

2.1.1 H_2/O_2 Second Explosion Limits

The explosion limits are thermodynamic states which mark a transition between regions of dominant H_2/O_2 chemistry. While Voevodsky and Soloukhin [9] considered only the classical second explosion limit in their analysis, in the present work the extended second explosion limit was also included. A detailed description of these two limits is given in Zheng and Law [12]. Briefly, the classical second limit represents the competition between the dominant chain-branching pathway (R1), and the dominant chain-terminating pathway (R9). The limit is the thermodynamic state at which the reaction rates of these two reactions are equal and no net radicals (O, OH) are produced. The extended second limit represents a similar balance between radical generation and termination, though it includes HO_2 chemical pathways significant only at pressures greater than ~ 1 atm, i.e. the second limit represents the competition between the chain-branching reactions ((R1), $HO_2 + H = OH + OH$ (R11)), the chain-propagating reaction (R9), and the chain-terminating reaction ($HO_2 + H = H_2 + O_2$ (R10)). The extended second limit is the thermodynamic state at which no net radicals (H, O, OH, HO_2) are produced. Note that this formulation for the extended second limit is simplified, as done in Zheng and Law [12], assuming that HO_2 is consumed only by H. The thermodynamic states corresponding to the classical and extended second limits were calculated using formulations from Zheng and Law [12] where,

Classical Second Limit: $[M] = {}^{2k_1}/_{k_9}$ [mole/m^3] (3-1)

Extended Second Limit: $[M] = {}^{2k_1}/_{k_9} * \frac{k_{10}}{k_{10}+k_{11}}$ (3-2)

$$[M] = {}^{P}/_{\bar{R}T} \quad (3\text{-}3)$$

Where, $\bar{R}$ = universal gas constant , P = pressure, T = temperature.

The thermodynamic location of the second explosion limits were calculated using the nominal reaction rate values of the Li 2007 mechanism. Uncertainty bounds were assigned using the known uncertainty of the reaction rate of R1 & R9, consistent with the computational work described previously.

The calculated classical and extended second explosion limits are included in the maps of ignition behavior in Fig. 3-3 and 3-4. As illustrated in Fig. 3-3 for φ = 0.1, the classical explosion limit correlates with the strong ignition limit at low pressures (2-5 atm) and the extended explosion limit correlates well with the transition from strong to no ignition at high pressures (10-15 atm). As illustrated in Fig. 3-4 for φ = 0.5, the classical explosion limit correlates well with the strong ignition limit at low pressures (1-5 atm); however, at higher pressures the strong ignition limit is not well described by either the classical or extended explosion limit with progressively worse deviation as pressure increases beyond 5 atm. It is therefore apparent that the classical H_2/O_2 second explosion limit is a good predictor of the location of the strong ignition limit for pressures less than ~ 5 atm for a range of equivalence ratios; however, the accuracy of such prediction falls off rapidly as pressure increases beyond this value even if the extended second limit is considered. This finding at lower pressures is in excellent agreement with Voevodsky and Soloukhin [9], and suggests that at low pressures the dominant H_2/O_2 chemical pathway is highly correlated to the auto-ignition behavior, whereas at higher pressures other factors must be considered. As discussed in Chaos et al. [13] and the references contained therein, competing chemical kinetic and transport time-scales near the extended second explosion limit at higher pressures are expected

and it is likely that consideration of transport phenomena is indeed necessary at higher pressures.

2.1.2 Thermal Sensitivity

As previously discussed, Meyer and Oppenheim [10] built on the work by Voevodsky and Soloukhin [9] and devised a method to more deliberately consider the relationship between gas-dynamic effects and the strong ignition limit, based on the assumption that numerous thermal non-uniformities exist within the reacting volume. It was postulated that these non-uniformities will lead to localized reaction centers (inhomogeneous behavior) in regions with higher thermal sensitivity and longer auto-ignition delay times, where chemical kinetic and transport time-scales are similar. It was indeed demonstrated in their study for an air-dilute pure H_2 mixture at $\varphi = 1.0$ that a limiting value of the thermal sensitivity of approximately -2 μs/K exists which corresponds well to the strong ignition limit at pressures below 3 atm; where regions with higher thermal sensitivity exhibit inhomogeneous auto-ignition and regions with lower thermal sensitivity exhibit homogeneous auto-ignition.

In a similar fashion, thermal sensitivity values were calculated in the present work and iso-contours of these values were compared to the experimentally determined strong ignition limit for each equivalence ratio. Figs. 3-5 and 3-6 present the ignition behavior for $\varphi = 0.1$ and $\varphi = 0.5$, respectively, as a function of initial thermodynamic state with iso-contours of predicted auto-ignition delay time and thermal sensitivity included for comparison. For $\varphi = 0.1$ there is a close correlation between the iso-contour of thermal sensitivity $\approx$ - 0.7 ms/K and the strong ignition limit. Correspondingly for $\varphi = 0.5$ there is a close correlation between the iso-contour of thermal sensitivity $\approx$ - 0.04 ms/K and the strong ignition limit. These two values are therefore considered the critical values of thermal sensitivity for each equivalence ratio and their existence supports the notion of a critical thermal sensitivity previously made by Meyer and Oppenheim [8]. Important to note is the excellent agreement between the critical iso-contour of

thermal sensitivity and the strong ignition limit at high pressures for φ = 0.5, a marked improvement over the predictions using the H_2/O_2 second explosion limits. Similar to the findings by Meyer and Oppenheim [10], for both equivalence ratios regions with thermal sensitivity in excess of the critical iso-contours exhibited mixed or weak behavior; whereas, regions with lower sensitivity exhibited only strong behavior. These findings are strong evidence that the value of thermal sensitivity is indeed an important factor in determining auto-ignition behavior across many mixture and thermodynamic conditions relevant to gas turbine operation. It follows that the assumptions originally made by Meyer and Oppenheim [10] are supported in the present work as well, that thermal non-uniformities and subsequent localized reaction centers are a dominant cause of inhomogeneous ignition behavior.

From the perspective of predicting auto-ignition behavior, using thermal sensitivity is a step forward from using the explosion limits in that high pressure behaviors can be captured. However, in order to determine the critical value of thermal sensitivity of a given mixture it is still necessary to find the strong ignition limit experimentally for at least a few pressure values. These experiments may be avoided for mixtures and conditions sufficiently similar to those studied in the present work. For example, critical values can be estimated for different equivalence ratios by interpolating between the results of the current work (φ = 0.1 and 0.5) and in Meyer and Oppenheim (φ = 1.0). Furthermore, it is not clear how these thermal sensitivity limits extend to less ideal combustion devices, which can contain higher magnitudes of thermal non-uniformities and turbulence. Overall, while a priori prediction of the strong ignition limit is not possible using thermal sensitivity, establishing the connection between thermal sensitivity and the strong ignition limit at a minimum reduces the number of experiments necessary to define the strong ignition limit for a system.

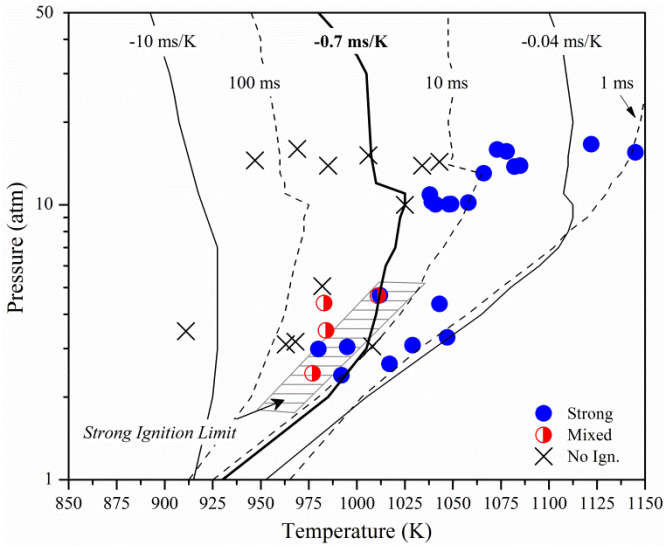

Fig. 3-5. Ignition behavior as a function of thermodynamic state for mixtures with φ = 0.1. The Strong Ignition Limit is shown as a hashed area. Calculated iso-contours of thermal sensitivity are shown as solid lines and calculated iso-contours of auto-ignition delay time are shown as dotted lines. The iso-contour of critical thermal sensitivity, - 0.7 ms/K, is the bold solid line.

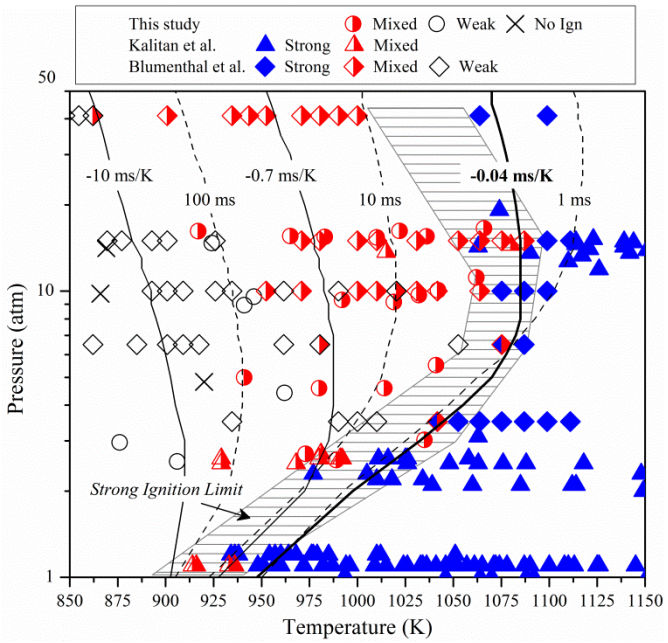

Fig. 3-6. Ignition behavior as a function of thermodynamic state for mixtures with φ = 0.5. The Strong Ignition Limit is shown as a hashed area. Results are from the present work, Kalitan et al. [7], and Blumenthal et al. [6]. Calculated iso-contours of thermal sensitivity are shown as solid lines and calculated iso-contours of auto-ignition delay time are shown as dotted lines. The iso-contour of critical thermal sensitivity, - 0.04 ms/K, is the bold solid line.

2.1.3 Sankaran Criterion

As previously mentioned, the effect of distributed thermal non-uniformities on auto-ignition behavior in pure H_2 mixtures was investigated in detail by Sankaran et al. [11] using high fidelity direct numerical simulation methods. In that work auto-ignition behavior was investigated for air-dilute H_2 at $\varphi = 0.1$ in a small constant pressure reactor (4.1mm x 4.1mm), with a distribution of thermal gradients and a constant turbulence flow field. Two distinct ignition behaviors emanating from thermal hot spots were subsequently observed: *spontaneous propagation* – where a reaction front propagates at a speed (u_p) equal to the inverse of the gradient of the auto-ignition delay time $(d\tau/dx)^{-1}$, and *deflagration* - where a reaction front propagates at the laminar flame speed (s_u^0). Sankaran et al. [11] postulated that a non-dimensional transition parameter, ß, exists which indicates the relative dominance of the two ignition behaviors,

$$\beta = \frac{s_u^0}{u_p} = \frac{s_u^0}{\left(\frac{d\tau}{dx}\right)^{-1}} \tag{3-4}$$

where, if ß < 1 a homogeneous explosion (strong ignition) will occur, and if ß > 1 then an inhomogeneous deflagration front (mixed or weak ignition) will occur. If the gradient of the auto-ignition delay time is decomposed into a product of the thermal gradient (dT/dx) and thermal sensitivity (dτ/dT), as was done by Walton et al. [14], then the importance of thermal sensitivity is illustrated in the following criterion (which we define as the Sankaran Criterion),

$$\frac{d\tau}{dT} < \left(\frac{dT}{dx} s_u^0\right)^{-1} \tag{3-5}$$

where, strong ignition will occur if the inequality is true, and mixed or weak ignition will occur if the inequality is false.

In the current work, the Sankaran Criterion was used predict the thermodynamic location of the strong ignition limit by evaluating the inequality across the range of initial temperature and pressure values for each equivalence ratio and a range of initial thermal gradients (3, 5, 10, 20 K/mm). Typical thermal gradients in similar experimental devices are expected to be on the order of 5 K/mm based on findings from Walton et al. [14] and Strozzi et al. [15]. Additional thermal gradient values were included to illustrate the sensitivity of the predicted limits to this parameter and expand the predictions to higher thermal gradients which may be more representative of practical combustion devices. Laminar flame speeds were calculated using the "Premixed Laminar Flame-Speed Calculation" module in the CHEMKIN software suite [2] with the Li 2007 kinetic model [11]. At temperatures above ~ 1025 K it was necessary to extrapolate laminar flame speeds from lower temperatures, which was done using an exponential fit with correlation coefficients above 0.997. For simplicity, the nominal A-factors and transport parameters provided in the Li 2007 mechanism were used for the calculations. Thermal sensitivity values determined for the iso-contours presented earlier were used for this analysis as well. All calculations were completed with the same syngas mixture used in the experimental work (air-dilute with molar ratio H_2:CO = 0.7).

Figs. 3-7 and 3-8 present the ignition behavior for φ = 0.1 and φ = 0.5, respectively, as a function of initial thermodynamic state with iso-contours of predicted auto-ignition delay time and predicted strong ignition limits for various thermal gradient magnitudes. For φ = 0.1 there is excellent correlation between the experimental and the predicted strong ignition limit for 5 K/mm. Quite remarkably, the predicted limit moves to drastically lower temperatures as pressure is increased beyond 3 atm, correctly predicting the absence of a strong ignition limit at higher pressures mentioned earlier. This shift to lower temperatures corresponds to a significant decrease in laminar flame speeds as pressure increases beyond 3 atm and is not captured by the critical thermal sensitivity iso-contour. For φ = 0.5, there is also remarkable correlation between the experimental and the predicted strong ignition limit for 5 K/mm for the entire pressure range considered. The prediction is

somewhat less representative of the experimental data closer to 1 atm, predicting a strong ignition limit ~ 50 K higher than what was measured, but that is most likely within the uncertainty of the prediction. As opposed to the results for φ = 0.1, there is general agreement between the predicted strong limit and the critical thermal sensitivity iso-contour for all pressures, which is the result of a much more gradual decrease in laminar flame speeds as pressure is increased for φ = 0.5.

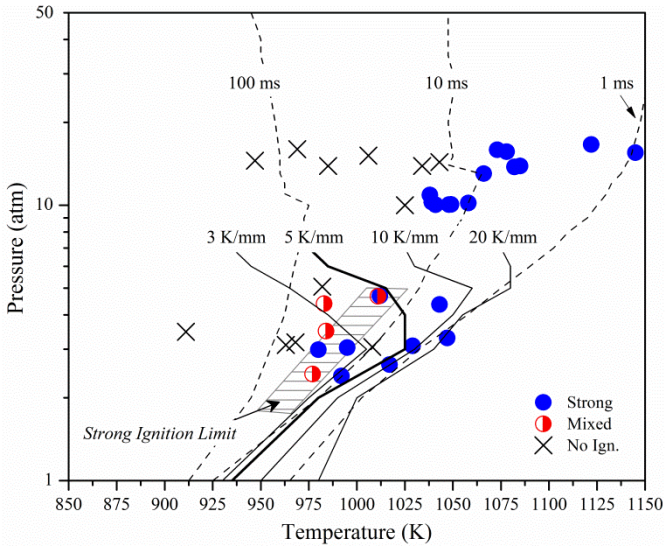

Fig. 3-7. Ignition behavior as a function of thermodynamic state for mixtures with φ = 0.1. The Strong Ignition Limit is shown as a hashed area. Predicted locations of the strong ignition limit are shown as solid lines and calculated iso-contours of auto-ignition delay time are shown as dotted lines. The most accurate predicted strong ignition limit, for a 5 K/mm gradient, is the bold solid line.

Concerning the results for various thermal gradients, there is minimal difference between strong ignition limit predictions at pressures below ~ 3 atm for φ = 0.1 and ~ 7 atm for φ = 0.5. In both cases, at higher pressures the predicted strong ignition limit shifts to higher temperatures as the thermal gradient is increased. The shift to higher temperatures occurs with decreasing magnitude as the thermal gradient magnitude is increased, suggesting that the strong ignition limit may asymptote as thermal gradients increase to much higher values. It is noteworthy that the thermal gradient of 5 K/mm yielded the most accurate

predictions, in excellent agreement with the expected gradient magnitudes in the experimental UM RCF and shock tube equipment.

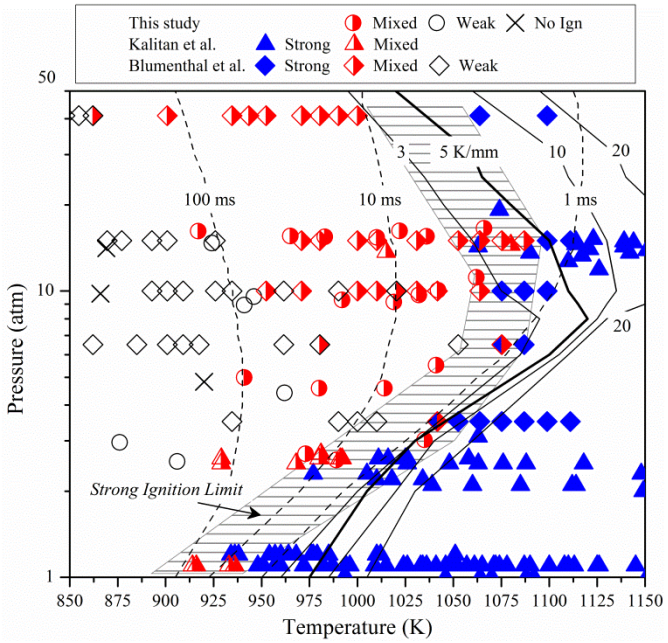

Fig.3-8. Ignition behavior as a function of thermodynamic state for mixtures with φ = 0.5. The Strong Ignition Limit is shown as a hashed area. Predicted locations of the strong ignition limit are shown as solid lines and calculated iso-contours of auto-ignition delay time are shown as dotted lines. The most accurate predicted strong ignition limit, for a 5 K/mm gradient, is the bold solid line.

Overall, these results indicate that the Sankaran Criterion is indeed an excellent tool for a priori prediction of the strong ignition limit, with no experimentation necessary for its application. It is accurate and easy to use, requiring only basic computational modeling and the magnitude of characteristic thermal gradients in the system. Beyond the predictive capability, it also provides a straightforward method for extending experimental results to other mixtures, conditions, and devices; a key attribute for combustor designers. The validation of this simple non-dimensional criterion is important, as this criterion quantitatively describes the roles of chemical kinetics, thermo-physical properties, and device dependent thermal characteristics on auto-ignition behavior. In this way, it is not an alternative to the explosion limit and thermal sensitivity methods investigated previously by Voevodsky and Soloukhin [9] and Meyer and Oppenheim [10], but

instead is an important integration of these methods with transport phenomena. This criterion not only provides a practical tool for combustor designers and experimentalists, it also sheds light on the fundamental nature of thermally driven auto-ignition behaviors in pre-mixed combustion systems.

Considering the success of this criterion it is apparent that localized thermal gradients are the dominant driver of inhomogeneous ignition behavior in this work and the studies by Blumenthal et al. [8] and Kalitan et al. [9]. Non-uniformities will be present in any experimental or practical combustion system and could come from a number of sources such as heat transfer, mixing, or the presence of minute reactive or non-reactive particles like those observed in Elsworth et al. [16] and considered in Chaos and Dryer [4]. Previously, Chaos and Dryer [4] and Blumenthal et al. [6] predicted that hot spots of 150-200 K would be necessary to cause inhomogeneous auto-ignition. The present work highlights the importance of considering not only the absolute temperature of hot spots but also the corresponding thermal gradients, as those on the order of merely 3-5 K/mm were found to drive inhomogeneous ignition behaviors in the current work.

Varying levels of turbulence will likely impact the accuracy of the Sankaran Criterion, through an influence on the development of thermal gradients (highlighted in the study by Sankaran et al. [11]), chemical kinetics (highlighted in the study by Ihme [17]), and flame speeds (highlighted in the study by Daniele et al. [18]). While both the UM-RCF and the shocktubes considered in this study are assumed to be nominally quiescent, significantly higher levels of turbulence are expected in practical devices. An investigation of turbulence effects is outside the scope of the present work; however, current computational efforts are underway to expand the work of Sankaran et al. [11] and Bansal and Im [19] to more directly probe the issues of turbulence-chemistry interactions.

2.2 Auto-ignition delay time

As previously discussed, while there are well documented inaccuracies of zero-dimensional homogeneous reactor modeling in predicting auto-ignition delay

time in systems with inhomogeneous ignition behavior [4], there is currently a lack of understanding as to whether the occurrence of inhomogeneous ignition necessarily leads to this inaccuracy. Illustrated in Fig. 3-9 are the measured and predicted auto-ignition delay times as a function of inverse temperature for mixtures with $\varphi = 0.1$ over a range of pressures. Recall that the error bars on the experimental data represent the limits of the definition of the auto-ignition delay time and the error bars on the simulation results represent the effects of the uncertainty limits of R1 and R9. The results indicate excellent agreement between the measured and predicted values, across all thermodynamic conditions investigated and for both ignition behaviors exhibited (strong and mixed). It is therefore apparent that the presence of inhomogeneous ignition phenomena does not significantly affect the predictive accuracy of the zero-dimensional homogeneous reactor model using the Li 2007 mechanism at these conditions. This is likely related to the low energy content of the mixture, limiting the quantity of energy released during local ignition events and/or reducing flame speeds. The results support this notion, given that while high-speed imaging indicates the presence of local ignition events almost immediately after EOC in most cases, inspection of the lower bound of the measured auto-ignition delay time indicates that the first signs of pressure increase occur only just before the auto-ignition event. Important to note is the rather large uncertainty in the predicted auto-ignition delay times for 3 atm, highlighting that consideration of uncertainty in the reaction mechanism is critical when comparing modeling and experimental data.

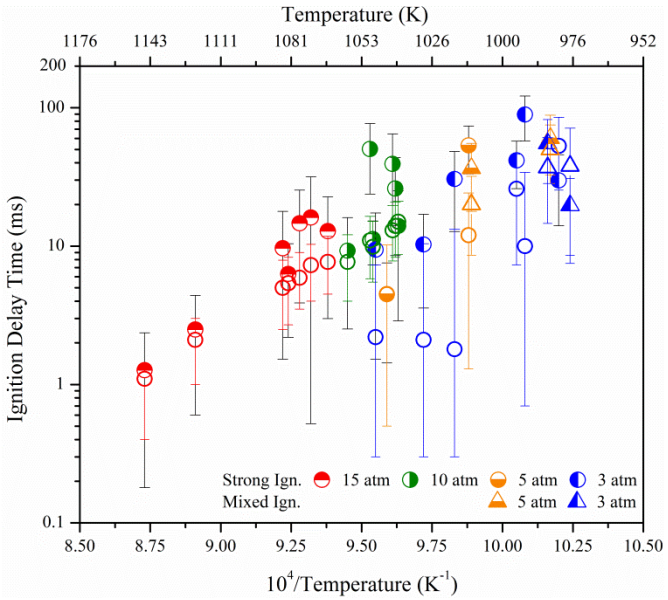

Fig. 3-9. Measured and predicted auto-ignition delay time as a function of inverse temperature for mixtures with φ = 0.1. Half-filled symbols are experimental measurements and open symbols are the predictions corresponding to each measurement. Uncertainty bounds of the predictions are the effect of the uncertainty in the rate coefficient of reactions R1 and R9; whereas, uncertainty bounds of the measurements are the limits of the definition of the auto-ignition delay time.

Illustrated in Fig. 3-10 are the measured and predicted auto-ignition delay times as a function of inverse temperature for mixtures with φ = 0.5 over a range of pressures. Unlike the earlier results, these data indicate poor agreement between the measured and predicted auto-ignition delay times, with rapidly increasing error as temperatures decrease below ~1000 K. Note also the limited effect of the uncertainty of the reaction mechanism on the predicted values at most of the simulation conditions. The results therefore illustrate that the presence of inhomogeneous ignition phenomena does indeed significantly decrease the predictive accuracy of the zero-dimensional homogeneous reactor model using the Li 2007 mechanism at these conditions. It is assumed here that the discrepancy is not the result of poor performance of this kinetic mechanism at these conditions, given the multitude of previous successful applications [3,4] and the agreement illustrated in the present work for φ = 0.1. This predictive inaccuracy is instead likely related to the higher energy content of the mixture, leading to larger energy release during local ignition events and/or increased flame speeds. It is clear that

nearly all the predicted auto-ignition delay times greatly exceed the measured values, consistent with previous findings highlighted in Chaos and Dryer [4]. These results are expected considering that energy release during inhomogeneous ignition events would cause a temperature increase of the unburned gas mixture, thus accelerating the auto-ignition process. With this in mind, the increasing error trend as temperature decreases can be explained by noting that as auto-ignition delay time increases localized energy release will exist for an increasingly longer time, thus allowing for an increasingly pronounced effect on the unburned gases. Overall the results of the present work illustrate an important finding, that the equivalence ratio or energy content of the mixture is directly related to the predictive accuracy of zero-dimensional homogeneous reactor modeling of auto-ignition delay times in systems with inhomogeneous auto-ignition behaviors.

Unique for $\varphi = 0.5$ is the existence of weak ignition behavior at the lowest temperature conditions, seen as star markers in Fig. 3-10. Auto-ignition delay time predictions should not be expected to have good agreement with measurements in cases with weak ignition behavior, given that no homogeneous auto-ignition event is observed. These data were still included here to illustrate a potential pitfall in interpreting pressure time history data for low-temperature auto-ignition experiments where inhomogeneous ignition is possible. Had the ignition behavior not been directly observed by imaging and classified appropriately as weak (flame propagation with no observed auto-ignition of the unburned gas), it is quite likely that these data would have been incorrectly categorized as homogeneous auto-ignition events, resulting in potentially unnecessary and inaccurate modification of physical or chemical representations of the combustion system. Diagnostics of ignition behavior are therefore vitally important in any ignition study of syngas or other high-hydrogen content fuels at temperatures below ~ 1000 K.

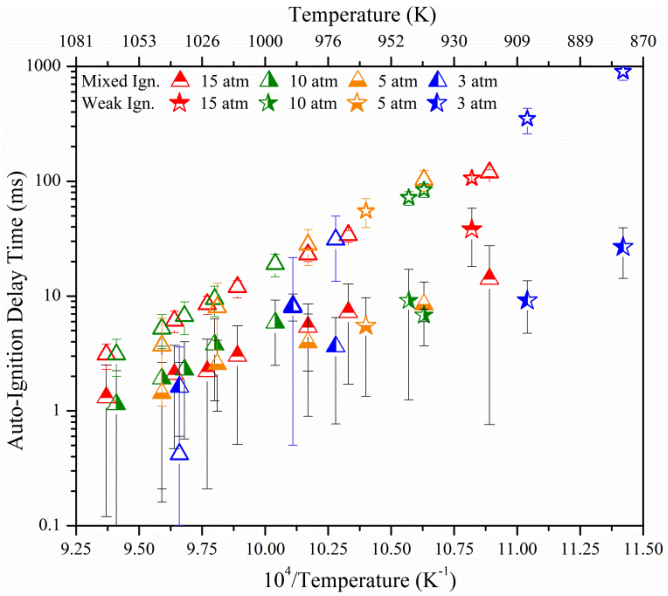

Fig. 3-10. Measured and predicted auto-ignition delay time as a function of inverse temperature for mixtures with φ = 0.5. Half-filled symbols are experimental measurements and open symbols are the predictions corresponding to each measurement. Uncertainty bounds of the predictions are the effect of the uncertainty in the rate coefficient of reactions R1 and R9; whereas, uncertainty bounds of the measurements are the limits of the definition of the auto-ignition delay time.

3. CONCLUSIONS

This work represents the first attempt to integrate results from diverse experimental platforms to describe common auto-ignition behaviors in high-hydrogen content fuels, and further to provide a quantitative basis for predicting and interpreting data of other ignition studies, beyond syngas and the conditions studied here. Studies such as these are vital for enabling low-temperature combustion strategies, such as Dry Low-NO_x. The comprehensive results of the present work clearly illustrate the existence of both homogeneous and inhomogeneous auto-ignition behaviors for lean air-dilute syngas and pure H_2 mixtures at thermodynamic conditions relevant to gas turbine engines and other combustion systems. Analysis of patterns in the ignition behaviors revealed a dependence on temperature, pressure, and equivalence ratio with distinct thermodynamic regions in which the ignition behavior was consistent and repeatable. The strong ignition limit was identified for each equivalence ratio,

marking the transition between homogeneous and inhomogeneous ignition behaviors.

The locations of the experimentally determined strong ignition limits were compared to the second explosion limits of hydrogen, iso-contours of thermal sensitivity, and predicted strong ignition limits using the Sankaran Criterion. These three approaches represent the historical progression of strong ignition limit prediction and analysis methods. The second explosion limits of hydrogen were found to correlate with the strong ignition limits only at pressures below 5 atm, indicating the importance of dominant chemical kinetic pathways in determining auto-ignition behavior at low pressures and the necessity to consider additional factors higher pressures. Iso-contours of a critical thermal sensitivity described the strong ignition limit well; where any region (i.e. state and mixture conditions) with a sensitivity value in excess of the critical limit exhibited inhomogeneous ignition phenomena and any region with a lower value exhibited homogeneous ignition phenomena. The critical values were equivalence ratio dependent and were found to be approximately - 0.7 ms/K for $\varphi = 0.1$ and - 0.04 ms/K for $\varphi = 0.5$. It follows that thermal non-uniformities and subsequent localized reaction centers are a dominant cause of inhomogeneous ignition behavior in the present work. Predictions of the strong ignition limit by the Sankaran Criterion, which compares laminar flame speed to a thermal gradient driven front propagation speed, were found to have excellent agreement with the experimentally determined strong ignition limit for both equivalence ratios for an assumed thermal gradient of 5 K/mm. The experimental validation of this criterion, the first of its kind, indicates that it can indeed be used for a priori prediction of the strong ignition limit. As this criterion quantitatively describes the roles of chemical kinetics, thermo-physical properties, and device dependent thermal characteristics in determining auto-ignition behavior it also provides unique and critical insight into thermally driven auto-ignition behaviors. Overall both the Sankaran Criterion and the ignition behavior maps created in the present work provide important, new, and unique

tools that can be used in the design of combustion devices using high-hydrogen content fuels like syngas.

In order to investigate the relationship between auto-ignition behavior and the accuracy of zero-dimensional homogeneous reactor modeling in predicting auto-ignition delay time, measured and predicted ignition delay times were compared. The results indicate the presence of inhomogeneous ignition phenomena does not significantly affect the predictive accuracy of the zero-dimensional homogeneous reactor model using the Li 2007 mechanism for $\varphi = 0.1$; whereas, the presence of inhomogeneous ignition phenomena does significantly affect the predictive accuracy for $\varphi = 0.5$. This is an important indication that while inhomogeneous ignition phenomena are not avoidable by reducing equivalence ratio, the subsequent effects on the accuracy of typical auto-ignition modeling may be reduced or eliminated. This inaccuracy for $\varphi = 0.5$ is likely related to the higher energy content of the mixture, leading to larger energy release during local ignition events and/or increased flame speeds which can cause a significant violation of the isothermal/isobaric assumptions of the homogeneous reactor model. The importance of properly observing and classifying ignition behaviors was also highlighted, as ignition at the lowest temperatures exhibited no homogeneous auto-ignition, only flame propagation, and the pressure time histories could be confused as consistent with homogeneous auto-ignition behavior if imaging diagnostics had not been applied.

REFERENCES

[1] Jones R, Shilling N. IGCC gas turbines for refinery applications. GE Power Syst Schenectady, NY 2003.

[2] Reaction Design. CHEMKIN 10101 2010.

[3] Li J, Zhao Z, Kazakov A, Chaos M, Dryer FL, Scire JJ. Mechanism for CO, CH2O, and CH3OH Combustion. Int J Chem Kinet 2007.

[4] Chaos M, Dryer FL. Syngas Combustion Kinetics and Applications. Combust Sci Technol 2008;180:1053–96.

[5] Petersen EL, Kalitan DM, Barrett AB, Reehal SC, Mertens JD, Beerer DJ, et al. New syngas/air ignition data at lower temperature and elevated pressure and comparison to current kinetics models. Combust Flame 2007;149:244–7.

[6] Blumenthal R, Fieweger K, Komp K. Self-ignition of H2-air mixtures at high pressure and low temperature. Proc. 20th ISSW, World Sci., 1996, p. 935–40.

[7] Kalitan DM, Mertens JD, Crofton MW, Petersen EL. Ignition and Oxidation of Lean CO / H 2 Fuel Blends in Air. J Propuls Power 2007;23:1291–303.

[8] Walton SM, He X, Zigler BT, Wooldridge MS. An experimental investigation of the ignition properties of hydrogen and carbon monoxide mixtures for syngas turbine applications. Proc Combust Inst 2007;31:3147–54.

[9] Voevodsky V, Soloukhin R. On the mechanism and explosion limits of hydrogen-oxygen chain self-ignition in shock waves. Symp Combust 1965:279–83.

[10] Meyer JW, Oppenheim a. K. On the shock-induced ignition of explosive gases. Symp Combust 1971;13:1153–64.

[11] Sankaran R, Im HG, Hawkes ER, Chen JH. The effects of non-uniform temperature distribution on the ignition of a lean homogeneous hydrogen–air mixture. Proc Combust Inst 2005;30:875–82.

[12] Zheng X., Law C. Ignition of premixed hydrogen/air by heated counterflow under reduced and elevated pressures. Combust Flame 2004;136:168–79.

[13] Lieuwen T, Yang V, Yetter R. Gas Synthesis Combustion: Fundamentals and Applications. CRC; 2009.

[14] Walton S, He X, Zigler B, Wooldridge M, Atreya a. An experimental investigation of iso-octane ignition phenomena. Combust Flame 2007;150:246–62.

[15] Strozzi C, Sotton J, Mura A, Bellenoue M. Characterization of a two-dimensional temperature field within a rapid compression machine using a toluene planar laser-induced fluorescence imaging technique. Meas Sci Technol 2009;20:125403.

[16] Elsworth J, Haskell W, Read I. Non-uniform ignition processes in rapid-compression machines. Combust Flame 1969;13:437–8.

[17] Ihme M. On the role of turbulence and compositional fluctuations in rapid compression machines: Autoignition of syngas mixtures. Combust Flame 2012.

[18] Daniele S, Jansohn P, Mantzaras J, Boulouchos K. Turbulent flame speed for syngas at gas turbine relevant conditions. Proc Combust Inst 2011;33:2937–44.

[19] Bansal G, Im HG. Autoignition and front propagation in low temperature combustion engine environments. Combust Flame 2011;158:2105–12.

SUPPLEMENTAL MATERIAL

Table 3-A. Summary of experimental conditions and results for mixtures with φ = 0.1

Test gas composition [a] (% Vol.)					EOC Thermo. State [b]		Assigned Thermo. State [c]		Ign. Beha -vior [d]	Auto-ignition delay time [e] (ms)				
H_2	CO	O_2	N_2	CO_2	*P* (atm)	*T* (K)	*P* (atm)	*T* (K)		τ_{ign}	$\Delta\tau_{ign}$	τ_{pred}	$\delta\tau_{pred}$ -	$\delta\tau_{pred}$ +
1.7	2.5	20.8	68.3	0	17.1	1131	16.6	1122	S	2.5	1.9	2.1	0.9	1.1
1.7	2.5	20.8	68.3	0	15.5	1145	-	-	S	1.3	1.1	1.1	0.3	0.7
1.7	2.5	20.8	68.1	2.0	14.6	1097	13.8	1082	S	6.3	4.1	5.4	2.9	2.7
1.7	2.5	20.8	68.1	2.0	14.3	1094	13.9	1085	S	9.7	8.1	5.0	2.9	2.5
1.7	2.5	20.8	68.1	2.0	13.4	1073	13.0	1066	S	12.9	9.9	7.7	4.1	3.2
1.7	2.4	20.8	70.4	0	15.7	1078	-	-	S	14.6	10.8	5.9	3.1	2.4
1.7	2.5	20.9	74.2	0	15.9	1073	-	-	S	16.1	15.6	7.3	3.0	3.3
1.7	2.5	20.8	62.6	12.4	14.5	947	-	-	NI	-	-	-	-	-
1.7	2.5	20.9	62.5	12.4	16.0	969	-	-	NI	-	-	-	-	-
1.7	2.4	20.8	70.0	5.2	13.9	985	-	-	NI	-	-	-	-	-
1.7	2.4	20.8	70.0	5.2	15.1	1006	-	-	NI	-	-	-	-	-
1.7	2.4	20.8	74.8	0.3	14.3	1043	-	-	NI	-	-	-	-	-
1.7	2.4	20.8	74.8	0.3	13.9	1034	-	-	NI	-	-	-	-	-
1.7	2.4	20.8	73.0	2.0	10.6	1064	10.1	1049	S	50.3	26.5	11.0	5.4	5.2
1.7	2.4	20.8	70.4	0	10.2	1053	10.1	1048	S	11.2	3.9	9.9	5.2	4.4
1.7	2.5	20.9	74.2	0	10.5	1067	10.2	1058	S	9.3	6.8	7.7	4.4	3.7
1.7	2.5	20.9	73.2	1.7	10.4	1039	10.0	1041	S	39.3	25.3	13.0	6.6	5.2
1.7	2.5	20.9	73.2	1.7	10.4	1044	10.3	1039	S	26.1	17.6	14.0	6.8	5.7
1.7	2.5	20.9	73.2	1.7	10.9	1039	-	-	S	14.0	11.1	15.0	6.1	6.3
1.7	2.4	20.9	71.5	3.4	10.0	1025	-	-	NI	-	-	-	-	-
1.7	2.4	20.8	70.4	4.7	4.8	1066	4.4	1043	S	4.5	3.1	4.5	5.7	4.0
1.7	2.5	20.9	73.3	1.7	5.1	1032	4.7	1012	S	53.5	20.3	12.0	12.2	10.7
1.7	2.5	20.9	73.3	1.7	4.8	1019	4.7	1011	M	36.5	18.7	20.0	11.9	11.4
1.7	2.4	20.9	71.5	3.4	4.6	996	4.4	983	M	60.4	27.8	50.0	25.0	21.7
1.7	2.4	20.8	65.8	9.3	5.1	982	-	-	NI	-	-	-	-	-
1.7	2.6	20.8	74.8	0	3.4	1053	3.1	1029	S	10.3	6.7	2.1	8.3	1.8
1.7	2.4	20.8	74.8	0.3	2.7	1022	2.4	992	S	89.4	31.9	10.0	24.1	9.3
1.7	2.4	20.8	67.9	3.9	3.3	1047	-	-	S	9.4	7.9	2.2	5.1	1.9
1.7	2.4	20.8	69.9	5.2	3.4	1022	3.0	995	S	41.7	15.7	26.0	20.1	18.7
1.7	2.4	20.8	65.9	9.2	3.1	992	3.0	980	S	28.9	15.9	53.0	32.4	27.6
1.7	2.4	20.8	74.8	0.3	2.9	1045	2.6	1017	S	30.5	17.8	1.8	11.4	1.5
1.7	2.4	20.8	67.9	3.9	2.9	1023	2.4	977	M	20.0	11.1	38.0	33.0	30.5
1.7	2.4	20.8	70.4	0	3.6	995	3.5	984	M	55.3	26.9	37.0	23.9	22.4
1.7	2.4	20.8	50.3	24.7	3.5	911	-	-	NI	-	-	-	-	-
1.7	2.5	20.7	62.8	12.3	3.2	968	-	-	NI	-	-	-	-	-
1.7	2.5	20.7	62.8	12.3	3.1	963	-	-	NI	-	-	-	-	-
1.7	2.4	20.8	69.9	5.1	3.1	1008	-	-	NI	-	-	-	-	-

[a] Balance Ar.

[b] Pressure uncertainty ~ 0.1 atm and temperature uncertainty ~ 5 K

[c] If reported then average thermodynamic state, otherwise EOC state was assigned

[d] S = Strong, M = Mixed, W = Weak, NI = No ignition observed.

[e] τ_{ign} = measured, $\Delta\tau_{ign}$ = symmetric uncertainty bounds of measurement, τ_{pred} = predicted, $\delta\tau_{pred}$ - / $\delta\tau_{pred}$ + = lower/upper uncertainty bound of prediction

Table 3-B. Summary of experimental conditions and results for mixtures with φ = 0.5

Test gas composition [a] (% Vol.)					EOC Thermo. State [b]		Assigned Thermo. State [c]		Ign. Beha-vior [d]	Auto-ignition delay time [e] (ms)				
H_2	CO	O_2	N_2	CO_2	*P* (atm)	*T* (K)	*P* (atm)	*T* (K)		τ_{ign}	$\Delta\tau_{ign}$	τ_{pred}	$\delta\tau_{pred}$ -	$\delta\tau_{pred}$ +
5.1	7.3	12.5	71.4	3.4	15.6	1037	-	-	M	2.1	1.6	6.1	1.3	1.3
5.1	7.3	12.5	71.4	3.4	16.6	1067	-	-	M	1.3	1.2	3.1	0.7	0.8
5.1	7.3	12.6	67.5	7.4	16.3	1024	-	-	M	2.2	2.0	8.5	1.5	1.6
5.1	7.3	12.6	67.5	7.4	15.5	1011	-	-	M	3.0	2.5	12.0	1.6	2.4
5.1	7.3	12.5	63.0	12.0	15.9	989	15.5	983	M	5.4	3.2	23.0	3.2	3.0
5.1	7.4	12.5	60.0	15.0	15.8	968	-	-	M	7.2	5.5	34.0	3.2	4.5
5.1	7.4	12.5	52.9	22.1	16.2	918	-	-	M	14.1	13.3	119.0	6.5	9.1
5.1	7.4	12.5	55.8	19.2	15.2	932	14.7	924	W	38.0[f]	20.1	106.0	7.3	9.0
5.1	7.3	12.5	46.1	28.9	14.1	869	-	-	NI	-	-	-	-	-
5.1	7.3	12.5	75.0	0	11.2	1063	-	-	M	1.1	1.1	3.1	1.1	1.1
5.1	7.3	12.7	73.8	1.1	9.2	1020	-	-	M	3.8	2.6	9.4	2.8	2.8
5.1	7.3	12.7	73.8	1.1	10.1	1043	-	-	M	1.9	1.8	5.2	1.7	1.7
5.1	7.3	12.6	73.8	1.2	9.7	1033	-	-	M	2.3	1.7	6.7	2.2	2.1
5.1	7.3	12.6	67.6	7.4	9.4	996	-	-	M	5.9	3.4	19.0	4.0	4.3
5.1	7.4	12.5	68.0	15.0	9.6	946	-	-	W	9.1	7.9	72.0	8.9	10.6
5.1	7.4	12.5	60.0	15.0	8.9	941	-	-	W	7.7	6.8	84.0	11.0	12.0
5.1	7.3	12.6	46.1	28.9	9.8	866	-	-	NI	-	-	-	-	-
5.1	7.3	12.7	73.8	1.1	5.5	1043	-	-	M	1.4	1.2	3.7	2.7	2.6
5.1	7.2	12.6	71.4	3.4	4.7	1019	-	-	M	2.6	1.6	8.0	4.9	4.6
5.1	7.3	12.6	66.8	8.2	4.6	983	-	-	M	3.9	3.0	28.0	9.9	9.6
5.1	7.3	12.6	58.4	16.6	5.1	947	5.0	941	M	8.4	4.8	103.0	20.3	21.6
5.1	7.3	12.6	63.1	11.9	4.5	969	4.4	962	W	5.5	4.2	55.0	15.3	15.6
5.1	7.3	12.6	55.9	19.1	4.8	920	-	-	NI	-	-	-	-	-
5.0	7.3	12.6	75.0	0	2.6	998	2.6	989	M	8.2	2.2	8.0	13.6	7.5
5.2	7.2	12.7	74.8	0	3.2	1048	3.0	1035	M	1.6	1.0	0.4	3.2	0.3
5.1	7.2	12.6	66.9	8.1	2.8	982	2.7	973	M	3.6	2.9	31.0	18.5	17.6
5.1	7.2	12.6	50.5	24.6	3.5	907	3.0	876	W	26.8	12.5	900.0	136.0	144.0
5.1	7.2	12.6	58.5	16.5	2.9	933	2.5	906	W	9.2	4.4	350.0	81.0	91.7

[a] Balance Ar.

[b] Pressure uncertainty ~ 0.1 atm and temperature uncertainty ~ 5 K

[c] If reported then average thermodynamic state, otherwise EOC state was assigned

[d] S = Strong, M = Mixed, W = Weak, NI = No ignition observed.

[e] τ_{ign} = measured, $\Delta\tau_{ign}$ = symmetric uncertainty bounds of measurement, τ_{pred} = predicted, $\delta\tau_{pred}$ - / $\delta\tau_{pred}$ + = lower/upper uncertainty bound of prediction

[f] For cases with Weak ignition, represents time of ignition event since no auto-ignition was observed.

Table 3-C. Reaction rate parameters with uncertainty

#	Reaction [a]	A_{min}	A_0	A_{max}	n	E_a
1	$H + O_2 = OH + O$ [b]	$2.789(10)^{15}$	$3.5458(10)^{15}$	$4.508(10)^{15}$	-0.4	$16.6(10)^3$
2	$H + O_2 (+M) = HO_2 (+M)$, k_∞ [c]	$1.11(10)^{12}$	$1.48(10)^{12}$	$1.85(10)^{12}$	0.6	0.0
2	$H + O_2 (+M) = HO_2 (+M)$, k_o [d]	$6.31(10)^{20}$	$6.37(10)^{20}$	$7.00(10)^{20}$	-1.72	$5.25(10)^2$

Units are cm^3, s, cal, K; $k = AT^n \exp\left(-\frac{E_a}{RT}\right)$

[a] Nominal parameters from J. Li, Z. Zhao, A. Kazakov, M. Chaos, F.L. Dryer, and J.J. Scire, Int. J. Chem. Kinet. 39 (2007) 109-136.

[b] A-factor uncertainty from J.P. Hessler, J. Phys. Chem. A 102 (1998) 4517- 4526.

[c] A-factor uncertainty from C.J. Cobos, H. Hippler, J. Troe, J. Phys. Chem. 89 (1985) 342-349.

[d] A-factor uncertainty approximated as ±10%, from J.V. Michael, M.C. Su, J.W. Sutherland, J.J. Carroll, A.F. Wagner, J. Phys. Chem. A 106 (2002) 5297-5313.

Chapter 4
Low-temperature ignition behavior of iso-octane

Given the success of the Sankaran Criterion in predicting auto-ignition behavior of syngas the primary objective of this project was to evaluate the effectiveness of this criterion applied to iso-octane fuel. An additional objective was to evaluate the effect of auto-ignition behavior on the accuracy of basic auto-ignition delay time modeling. These were accomplished through experimental studies of iso-octane auto-ignition behavior and auto-ignition delay times using the UM-RCF and the Tsinghua University Rapid Compression Machine (TU-RCM). The auto-ignition behavior results were combined with those from previous studies to map auto-ignition behavior evaluate the success of the Sankaran Criterion in predicting transitions in behavior. Furthermore, the auto-ignition delay time measurements for all experiments were compared to predictions made using a typical iso-octane oxidation mechanism to evaluate the impact of auto-ignition behavior on their accuracy.

This chapter has been published as, A.B. Mansfield, M.S. Wooldridge, H. Di, X. He, FUEL 139 (2015) 79–86.

1. METHODS

1.1 Experimental Methods

Ignition experiments were conducted using mixtures of iso-octane/air with molar fuel-to-O_2 equivalence ratios of φ = 0.25 and 1.0, at air levels of dilution, i.e. molar O_2-to-diluent gas ratio of 1:3.76. In the UM-RCF N_2 was the primary diluent, with small volumes of Ar and/or CO_2 added to modify the test temperature; in the TU-RCM Ar was the primary diluent, with small volumes of N_2 added to modify the

test temperature. In the UM-RCF, ignition experiments for φ = 0.25 were conducted between 3-20 atm for temperatures ~900-1125 K and experiments for φ = 1.0 were conducted at ~8 and 18 atm for temperatures ~830-975 K. In the TU-RCM, ignition experiments were conducted between at φ = 0.25 for 5-30 atm and temperatures ~740-1050 K. The reactant composition and initial state conditions for each auto-ignition experiment are provided in the Supplemental Material.

A detailed description of the TU-RCM can be found in Di et al. [1]. Briefly, the TU-RCM consists of a Driven Section in which a gas mixture is rapidly compressed by a piston. Prior to compression, the test volume is evacuated with a pump and then filled with a specific test gas mixture. Upon firing, high pressure air drives the piston into the Driven Section compressing the test gas mixture into the Test Section. As the piston reaches its final position hydraulic oil pressure dampens the motion. At this point, the Test Section is filled with a uniform and isentropically compressed test gas mixture at the desired initial thermodynamic condition. For the current study, the TU-RCM test section was instrumented with a piezoelectric pressure transducer (Kistler 6052CU20, Amherst, NY) combined with a charger amplifier (Kistler 5018A1000, Amherst, NY) for pressure measurements. The data were recorded at 100 kHz using a data acquisition system (National Instruments cDAQ-9178 chassis coupled with analog input model cDAQ-9223). The uncertainty in the pressure measurements is estimated as ≤ 1%. High-speed color imaging was recorded using a high speed camera (Phantom V7.3, Vision Research, CMOS array, 128 x 128 pixels) with a 105 mm lens (Sigma, F2.3). Video sequences were recorded at 10,000 frames/second with an exposure time of 98 μs. All test gas mixtures were made using a dedicated stainless steel tank and the mixture composition was determined by measurement of the relative partial pressures of the components.

1.2 Computational Methods

Auto-ignition delay time predictions were made using the constant volume adiabatic zero-dimensional reactor model in the CHEMKIN software suite [2] with the Mehl 2011 mechanism [3]. Using this ignition model, a corresponding auto-ignition delay time prediction was calculated for each ignition experiment conducted in the UM-RCF and TU-RCM, using the specific unburned thermodynamic condition and mixture composition of each experiment. Uncertainty bounds were calculated for the model predictions, reflecting the uncertainties in the pre-exponential "A-factor" of the Arrhenius reaction rates for the three most important reactions ($H + O_2 = OH + O$ (R1), H_2O_2 (+M) = OH + OH (+M) (R16), and I-C_8H_{18} = Y-C_7H_{15} + CH_3 (R3214)), determined via OH sensitivity analysis using the CHEMKIN software suite. The precise values of the rate coefficients used for these reactions are listed in the Supplemental Material. Iso-contours of constant predicted auto-ignition delay times were also calculated for a broad range of initial thermodynamic conditions, using the nominal A-factors for simplicity.

Predicted locations of the strong ignition limit were calculated using the Sankaran Criterion as done previously in Chapter 3 for syngas fuel (Mansfield and Wooldridge [4]) using 5, 10, 20 K/mm assumed thermal gradient values. Thermal sensitivity values were calculated in this study using the same zero-dimensional reactor model and the Mehl 2011 mechanism used for predicting ignition delay times; although a constant pressure boundary condition was applied, consistent with previous studies by Vermeer and Oppenheim [5], Meyer and Oppenheim [6], and Mansfield and Wooldridge [4]. It is assumed that the formation and early existence of localized flame-like structures, the primary concern of predictions in the present work, occur in a nominally constant pressure environment. Laminar flame speed values were calculated using the correlations developed by Middleton et al. [7] for premixed iso-octane. The flame speed correlation was validated in that study by comparison with a wide range of experimental and computational works at initial temperatures between 298-1000 K. As a consequence, predictions of the

location of the strong ignition limit in the present work were intentionally limited to initial temperatures less than ~ 1100 K. Valid laminar flame speed data at higher temperatures would allow the predictions in the present work to be extended to higher temperatures.

2. RESULTS AND DISCUSSION

For each experiment in the UM-RCF and TU-RCM, a pressure time history and a high-speed imaging video were recorded, allowing for the determination of an auto-ignition delay time and direct observation and classification of the auto-ignition behavior. Figure 4-1 presents a typical pressure time history and corresponding still frames from the high-speed video of a UM-RCF experiment exhibiting homogeneous ignition. Trends in the time history data illustrate a pressure increase during the compression stroke until the Sabot is seated at the end-of-compression (EOC), followed by a slight decrease in pressure due to heat transfer from the test gas volume into the cool Test Section walls, followed by a large and rapid increase in pressure during the ignition event. As seen in the frames from the high-speed video, the spatial uniformity of the chemilluminescence is a clear indication the ignition occurs homogeneously in the Test Section. Figure 4-2 presents a typical pressure time history with corresponding still frames from the high-speed video of a UM-RCF experiment exhibiting inhomogeneous ignition. The characteristics of the pressure time history are not remarkably different than those for homogeneous ignition in Fig. 4-1, though it is clear that the heat addition and corresponding pressure increase occurs over nearly twice the time. As seen in the high-speed imaging sequence there are two localized flame-like structures which propagate and consume some of the test-gas mixture prior to homogeneous ignition of the remainder of the test gas volume. This sequence of ignition behaviors occurred in every experiment which exhibited inhomogeneous ignition. Inspection of the imaging results for all experiments exhibiting inhomogeneous ignition revealed that local flame-like structures initiate in widely varying locations within the UM-RCF Test Section, indicating that the behavior is likely related to a

distribution of disturbances not a single ignition source. Figure 4-3 presents a typical pressure time history with corresponding still frames from the high-speed video of a TU-RCM experiment exhibiting homogeneous ignition. The characteristics of the pressure time history and the high-speed imaging are quite similar to homogeneous ignition data of Fig. 4-1 indicating similar homogeneous behaviors are observed in both experimental facilities. No experiments in the TU-RCM exhibited inhomogeneous ignition behaviors for the conditions and compositions studied.

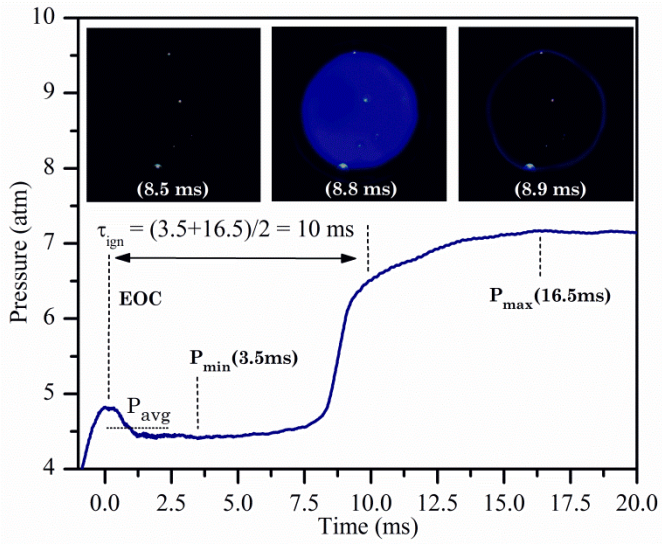

Figure 4-1. Typical experimental result for pressure time history in the UM-RCF during homogeneous ignition, for initial conditions P_{avg} = 4.5 atm, T_{avg} = 1035 K, φ = 0.25; where τ_{ign} is the auto-ignition delay time. Three frames from the corresponding high-speed imaging illustrate uniform chemilluminescence during auto-ignition.

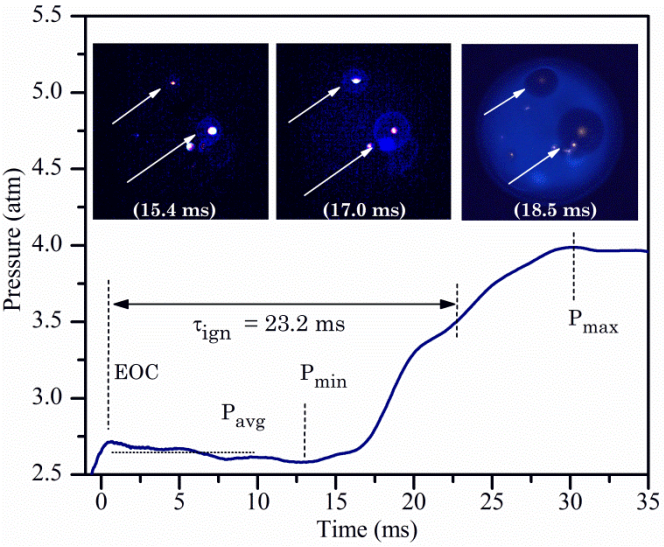

Figure 4-2. Typical experimental result for pressure time history in the UM-RCF during inhomogeneous ignition, for initial conditions P_{avg} = 2.7 atm, T_{avg} = 1016 K, φ = 0.25. Three frames from the corresponding high-speed imaging illustrate the formation and propagation of localized flame-like fronts prior to the subsequent auto-ignition of the unburned charge.

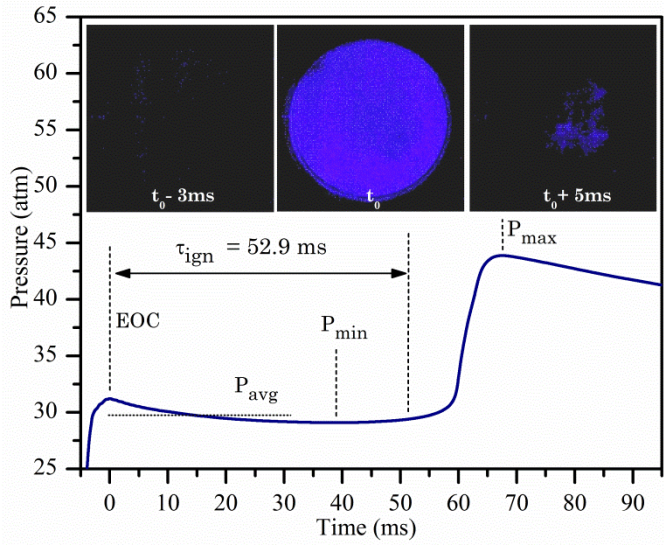

Figure 4-3. Typical experimental result for pressure time history in the TU-RCM during homogeneous ignition, for initial conditions P_{avg} = 29.7 atm, T_{avg} = 784 K, φ = 0.25. Three frames from the corresponding high-speed imaging illustrate uniform chemilluminescence during auto-ignition. The time, t_0, corresponds approximately to the auto-ignition delay event (~ 62 ms).

For each experiment, the time and pressure data were noted at three distinct events: EOC, minimum pressure (P_{min}), and maximum pressure (P_{max}), denoted in Figs. 4-1 through 4-3. According to the same method as described in Chapter 3,

after filtering the pressure time history with a 75-point smoothing algorithm, the nominal auto-ignition delay time was defined as the time difference between the EOC and the average of P_{max} and P_{min}, with the uncertainty of the reported ignition delay time defined as one-half the time difference between P_{max} and P_{min}.

While the pressure of the Test Section was measured directly, the temperatures for each experiment were calculated using thermodynamic relations. Based on previous findings [8,9] both the compression process and the subsequent expansion of the adiabatic core region due to minor heat transfer can be modeled as isentropic processes. With this well supported assumption in place, the initial thermodynamic conditions were used with isentropic state relations to calculate the temperature at EOC and at P_{min}. Propagation of the pressure measurement uncertainty through the isentropic state relations yields an uncertainty of $\leq 0.4\%$ in the assigned temperatures (~5 K). For each experiment a thermodynamic state was assigned, representing the isobaric/isothermal condition at which the experiment was conducted, as described in Chapter 2.

In order to compare the auto-ignition behaviors observed in the current work with those from the previous shocktube studies (Fieweger et al. [10] and Vermeer and Oppenheim [5]) it was necessary to systematically categorize the behaviors. Two ignition classifications were defined for the present work: (1) *Strong Ignition*, where only homogeneous ignition occurs, and (2) *Mixed Ignition*, where local ignition and flame propagation occurs and is followed by homogeneous ignition of the unburned gas volume. In the present work new experiments exhibiting homogeneous ignition behavior only (shown in Fig. 4-1) were classified as strong and those exhibiting initial inhomogeneous behavior (shown in Fig. 4-2) were classified as mixed. Fieweger et al. [10] and Vermeer and Oppenheim [5] categorized experiments as exhibiting strong or mild ignition, where strong ignition was described as the appearance of an essentially instantaneous shock, induced by an explosion, and mild ignition was described as the appearance of numerous localized flames gradually developing into an explosion and shock. Therefore, experiments classified as exhibiting strong ignition in those Shocktube studies were

also classified as strong in the present work, and those classified as mild were re-classified as mixed in the present work.

2.1 Auto-ignition behavior

Fig. 4-4 presents the observed ignition behavior as a function of thermodynamic state for mixtures with φ = 0.25. A range of behaviors is evident, with strong ignition at all conditions except the lowest pressures (3-5 atm) where there is a transition from strong to mixed to no ignition as temperature decreases from ~ 1100 K to 950 K. There is excellent agreement between experimental results from the UM-RCF and those from the TU-RCM at the higher pressure conditions, suggesting that behaviors are device independent. Overall the data show the ignition behaviors are well grouped and strongly related to the initial thermodynamic state, with a clearly defined strong ignition limit at lower pressures, marked as a hashed area in Fig. 4-4. The transition to no ignition at the lowest temperatures for P = 3 and 5 atm was not expected, as the predicted auto-ignition delay times in this region are well within the normal limits of the UM-RCF (~75 ms); however, reduced pressure rise rates during mixed ignition, previously highlighted in Fig. 4-2, likely lead to more significant heat transfer effects at these conditions and could result in unexpected quenching of the test gas mixture. Also presented in Fig. 4-4 is the location of the predicted strong ignition limit for three thermal gradients, illustrating excellent correlation between the location of the experimentally observed strong ignition limit and the prediction which uses a 10 K/mm thermal gradient magnitude. This is an indication that the Sankaran Criterion can accurately predict the strong ignition limit for iso-octane at these conditions. Interestingly, the most accurate prediction corresponds to an assumed thermal gradient magnitude in close agreement with the experimental findings of Donovan et al. [8] and Strozzi et al. [11].

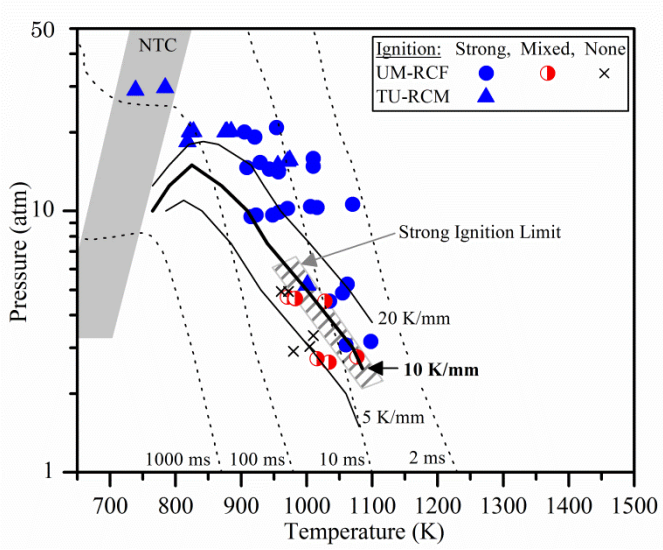

Figure 4-4. Ignition behavior as a function of initial thermodynamic state for mixtures with φ = 0.25. The strong ignition limit identified by the experimental data is shown as the hashed area, and the NTC region identified by model predictions is shown as the gray area. Iso-contours of predicted auto-ignition delay time are shown as dotted lines, and predicted locations of the strong ignition limit are shown as solid lines. The most accurate prediction of the strong ignition limit, for a 10 K/mm gradient, is the bold solid line.

The experimental results indicate the propensity for strong ignition behavior greatly increases near the negative temperature coefficient (NTC) region (as predicted using the Mehl 2011 mechanism), highlighted in gray in Fig. 4-4. Remarkably, the Sankaran Criterion correctly forecasts the leftward curvature in the strong ignition limit as the NTC region is approached. Within the NTC region, an inverse relationship between temperature and auto-ignition delay time is predicted by the Mehl 2011 mechanism, i.e. the auto-ignition delay time increases with increasing temperature. Therefore, as temperature is lowered and the NTC region is crossed from the high-temperature side, the magnitude of the thermal sensitivity rapidly decreases and the sign of the thermal sensitivity changes from negative to positive. As indicated by the Sankaran Criterion, Eq. 3-4, a reduction in thermal sensitivity magnitude indeed corresponds to an increased likeliness for strong ignition behavior. Therefore, increased propensity for strong ignition behaviors near the NTC region is likely due to a corresponding decrease in the magnitude of the thermal sensitivity.

Fig. 4-5 presents the observed ignition behavior as a function of thermodynamic state for mixtures with φ = 1.0. A range of behaviors is evident, with strong ignition generally occurring at higher temperatures and a highly pressure dependent transition to mixed ignition occurring as temperature is decreased. There is excellent agreement between the experimental results from the UM-RCF, TU-RCM, and those from Fieweger et al. [10], where the latter results span a larger range of pressures and temperatures. As the results from Vermeer and Oppenheim [5] are at much higher temperatures and lower pressures than the other three data sets, it was not possible to directly compare their results to the others; however, the same trend of strong ignition at higher temperatures and mixed ignition at lower temperatures is evident. Overall the data show the ignition behaviors are consistent between devices, well grouped, and strongly related to the initial thermodynamic state, with a clearly defined strong ignition limit spanning 1000-650 K for P > 10 atm and ~1400 K for P < 5 atm. The measured strong ignition limit is marked as the two hashed areas in Fig. 4-5. Regarding the effect of equivalence ratio on the location of the strong ignition limit, there is a shift toward higher temperatures as φ is increased from 0.25 to 1.0, in agreement with the trend observed in hydrogen based fuels by Mansfield and Wooldridge [4]. As discussed in that work, this is likely related to the energy content of the mixture and the relative amount of energy released during local ignition events.

Also presented in Fig. 4-5 is the location of the predicted strong ignition limit for three thermal gradients, illustrating excellent correlation between the measured strong ignition limit and the predicted location for 5 K/mm at P > 10 atm. This correlation is a clear indication that the Sankaran Criterion can accurately predict the location of the strong ignition limit for iso-octane at higher equivalence ratio conditions. As the calculation of a predicted strong ignition limit for initial temperatures above 1100 K was not reasonable using the flame speed correlation from Middleton et al. [12], predictions could not be compared to the measured limit

around ~1400 K; however, the trajectory of the predictions is consistent with the measured strong ignition limit at high temperatures.

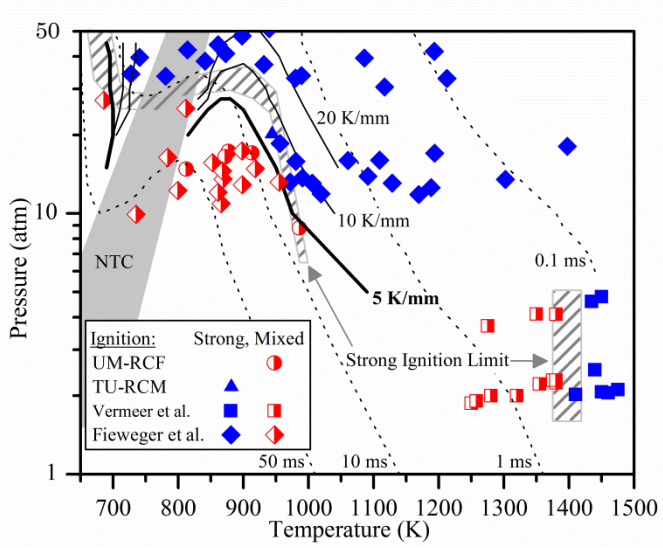

Figure 4-5. Ignition behavior as a function of initial thermodynamic state for mixtures with φ = 1.0. The strong ignition limit identified by the experimental data is shown as the hashed areas and the NTC region identified by model predictions is shown as the gray area. Results are from the present work, Vermeer and Oppenheim [5], and Fieweger et al. [10]. Iso-contours of predicted auto-ignition delay time are shown as dotted lines, and predicted locations of the strong ignition limit are shown as solid lines. The most accurate prediction of the strong ignition limit, for a 5 K/mm gradient, is the bold solid line.

Quite remarkably, for φ = 1.0 the predicted strong ignition limit for a 5 K/mm thermal gradient accurately predicts the location of the experimentally observed strong ignition limit on both the high and low temperature sides of the NTC region. Consistent with the results for lower φ, the strong ignition limits curve toward lower pressures at temperatures near the NTC region from both low and high temperature directions. This is again due to the rapid reduction in the magnitude of thermal sensitivity near the NTC region. Strong ignition limit predictions were not calculated for points within the NTC region as the inverted sign of the thermal sensitivity values contradicts the physical foundation of the Sankaran Criterion. The basis of this criterion assumes the existence of a spontaneous propagation and/or laminar flame moving from high-temperature to low-temperature down a thermal gradient centered at a thermal hot spot. It is presently unclear if and how

flame and/or propagation front motion would be affected if the thermal sensitivity were positive, meaning the lower temperature regions would ignite earlier. However, as evidenced by the results in Fig. 4-5 the trend of the strong ignition limit is not significantly changed as the NTC region is traversed. This suggests that the underlying mechanism governing ignition behavior is also not significantly changed in this region, though more detailed experimentation in this region would be necessary to validate such an assertion.

Overall, these results illustrate that the Sankaran Criterion is indeed an excellent tool for *a priori* prediction of the strong ignition limit for iso-octane fuels across a broad range of thermodynamic and mixture conditions. As highlighted previously for syngas in Chapter 3 (Mansfield and Wooldridge [4]) this is an important and useful tool, which not only provides a practical and simple approach to predicting complex ignition behaviors, but it also describes the roles of chemical kinetics, thermo-physical properties, and device dependent thermal characteristics in governing these behaviors. Importantly, in conjunction with the previous findings for syngas fuels [4], the results of the present work are a strong indication that the Sankaran Criterion can be applied to a broad range of fuels – beyond the important hydrocarbon primary reference fuel iso-octane and fuels with high hydrogen content. Furthermore, the similarity in thermal gradient values which result in the most accurate predictions for both fuels and a range of equivalence ratios suggests that an assumption of a 5-10 K/mm gradient can be reasonably applied for a broad range of fuel types and mixture compositions.

The quantitative nature of the Sankaran Criterion is particularly important to the extension of this criterion to more practical combustion systems like internal combustion engines, which will experience much larger magnitudes of thermal gradients (up to ~ 50 K/mm, approximated using experimental data from Einecke et al. [12]) as well as mixture inhomogeneities and turbulence. As indicated in Figs. 4-4 & 4-5, increasing the value of thermal gradient shifts the predicted location of the strong ignition limit toward higher pressures. Considering the approximate magnitude of thermal gradients in real engine systems, mixed ignition behaviors

are likely to occur at pressures up to and exceeding 50 atm for T ≤ ~1100K, conditions particularly important to modern boosted low-temperature engine operation. As such, it is possible that "pre-ignition" and "super-knock" behaviors at high-pressure low-temperature conditions, like those described by Kalghatgi et al. [13], are related to the inhomogeneous ignition behaviors observed in the present work.

Regarding the influence of mixture inhomogeneity and turbulence in practical combustion systems, these factors are expected to influence the accuracy and utility of the Sankaran Criterion in predicting ignition behaviors. Although quantifying these effects is outside the scope of the current study, these topics are valuable directions for future work. A computational investigation of the influence of turbulence and mixture inhomogeneities on the success of the Sankaran Criterion is currently underway by Pal and Im [14] for syngas fuels, expanding on the previous computational work by Sankaran et al. [15] and Bansal and Im [16]. Additional experimental studies are also important to further bridge the results of the current work to engine development.

2.2 Auto-ignition delay time

Fig. 4-6a & b present the measured and predicted auto-ignition delay times as a function of inverse temperature for mixtures with φ = 0.25 at various pressures. Recall that the error bars on the experimental data represent the limits of the definition of the auto-ignition delay time and the error bars on the predictions represent the effects of known uncertainty in reactions R1, R16, and R3214. The results indicate excellent agreement between the measurements and predictions across the complete range of temperature and pressure conditions for both observed ignition behaviors (strong and mixed). Furthermore, excellent agreement is evidenced between the results from the UM-RCF those from the TU-RCM. It is therefore clear that the accuracy of auto-ignition delay time predictions made using the typical zero-dimensional model described above and the Mehl 2011 mechanism are not significantly affected by inhomogeneous ignition behavior at these

conditions for φ = 0.25. This is an indication that the energy released during the inhomogeneous ignition process does not significantly influence the subsequent homogeneous auto-ignition.

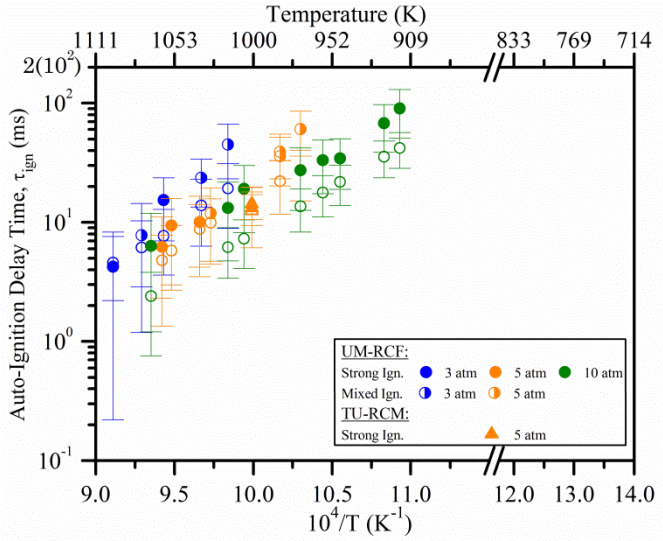

Figure 4-6a. Measured and predicted auto-ignition delay time as a function of inverse temperature for mixtures with φ = 0.25, for P = 3, 5, and 10 atm. Solid markers represent experimental measurements and hollow markers represent corresponding model predictions. Uncertainty bounds of the predictions are the effects of the uncertainties in the rate coefficients of reactions R1, R16, R3214; whereas, uncertainty bounds of the measurements are the limits of the definition of the auto-ignition delay time.

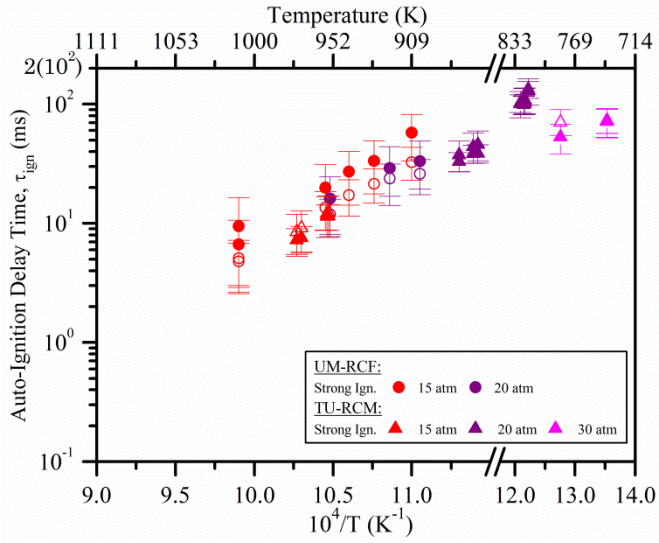

Figure 4-6b. Measured and predicted auto-ignition delay time as a function of inverse temperature for mixtures with φ = 0.25, for P = 15, 20, and 30 atm. Solid markers represent experimental measurements and hollow markers represent corresponding model predictions. Uncertainty bounds of the predictions are the effects of the uncertainties in the rate coefficients of reactions R1, R16, R3214; whereas, uncertainty bounds of the measurements are the limits of the definition of the auto-ignition delay time.

Fig. 4-7 presents the measured and predicted auto-ignition delay times as a function of inverse temperature for mixtures with φ = 1.0 at various pressures. Overall the results indicate excellent agreement between all measurements and predictions for temperatures greater than 1000 K at all pressures; however, the agreement varies at temperatures less than this value. There is generally good agreement between the experimental results from the UM-RCF and those from Fieweger et al. [10] and Vermeer and Oppenheim [5], though the only significant overlap in initial conditions is for 15 atm. Regarding the results from Vermeer and Oppenheim [5] there is excellent agreement between the measurements and predictions for the experiments which exhibited strong ignition and good agreement for those which exhibited mixed ignition. While the nominal auto-ignition delay time measurements appear to be slightly less than the nominal predictions when mixed ignition behavior occurs, the uncertainty bounds in all cases have significant overlap indicating that the model is still accurate at these conditions. Regarding the results from Fieweger et al. [10] at 15 atm, there is excellent agreement between the measurements and predictions for the experiments which exhibited

strong ignition (at temperatures above ~1000 K); however, after the onset of mixed ignition at lower temperatures the measurements are consistently lower than predictions with increasing discrepancy as the temperature is decreased. The results from the UM-RCF at 15 atm are in agreement with these findings, where the measurements are systematically lower than predicted times. This is consistent with behaviors seen previously for syngas and hydrogen fuels [4,17], which were linked to energy release during inhomogeneous ignition coupled with increasingly longer auto-ignition delay times. Regarding the results from Fieweger et al. [10] at 35 atm, all of which exhibited strong ignition, there is excellent agreement between the measurements and predictions for temperatures 1000-1250 and 725 – 750K; while at temperatures between these ranges the measurements are up to an order of magnitude faster than predictions. As illustrated in Fig. 4-5 the NTC region lies between ~750 and 1000 K at this pressure, which suggests that this discrepancy is related to error in the Mehl 2011 mechanism and/or the CHEMKIN zero-dimensional reactor model in predicting auto-ignition delay times in the NTC region. This level of discrepancy is generally consistent with the benchmarking results of Mehl et al. [3] for the NTC region at high pressures, though limited experimental data was reported for those conditions.

Overall these results are an indication that the effect of ignition behavior on the predictive accuracy of auto-ignition delay times made using zero-dimensional modeling is strongly dependent on the equivalence ratio, where inhomogeneous behaviors have little impact for mixtures with $\varphi = 0.25$ and can cause significant reductions in delay times for $\varphi = 1.0$. This dependence on equivalence ratio is in excellent agreement with previous findings by Mansfield and Wooldridge [4], who found similar behavior for syngas fuel and related such behavior to the amount of energy released during inhomogeneous ignition. Furthermore, the results of Vermeer and Oppenheim [5] at high temperatures indicate the effect of inhomogeneous ignition behavior on predictive accuracy is also dependent on the magnitude of the auto-ignition delay time itself, in that very short auto-ignition

delay times (< 1 ms) lead to a negligible effect of inhomogeneous behaviors even at high φ.

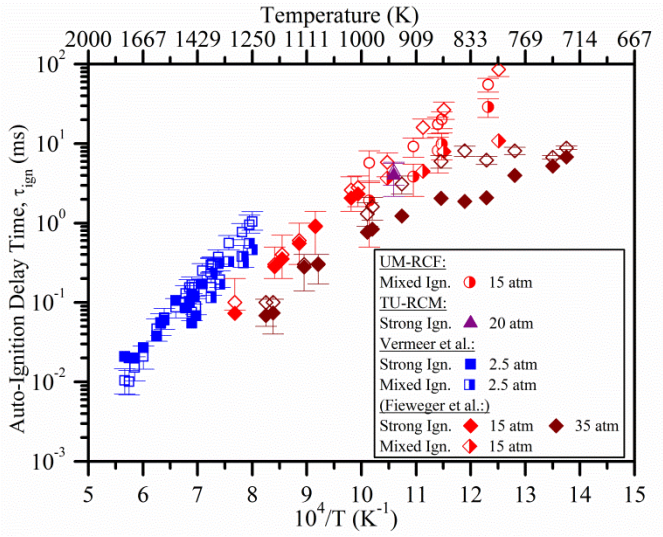

Figure 4-7. Measured and predicted auto-ignition delay time as a function of inverse temperature, for mixtures with φ = 1.0. Results are from the present work, Fieweger et al. [10], and Vermeer and Oppenheim [5]. Solid markers represent experimental measurements and hollow markers represent corresponding model predictions. Uncertainty bounds of the predictions are the effects of the uncertainties in the rate coefficients of reactions R1, R16, R3214; whereas, uncertainty bounds of the measurements are the limits of the definition of the auto-ignition delay time.

3. CONCLUSIONS

This work represents an important integration of results from diverse experimental platforms to describe common ignition behaviors of iso-octane, and further to provide a quantitative basis for predicting and interpreting data of ignition studies beyond the fuel and conditions studied here. Studies such as this are vital towards fundamental understanding of low-temperature combustion systems where prediction and control of chemically driven ignition phenomena is key to safety and performance. Importantly, the insights and tools developed in this work are relevant not only to systems which rely solely on chemically controlled ignition but also those which can be impacted by uncontrolled auto-ignition during an active ignition process, e.g. knock, pre-ignition, and super-knock in spark ignited internal combustion engine systems.

The comprehensive results of the present work clearly illustrate the existence of both inhomogeneous and homogeneous auto-ignition behaviors for stoichiometric

and lean air-dilute iso-octane mixtures at thermodynamic conditions relevant to engines and other combustion systems. Analysis of patterns in the ignition behaviors revealed a dependence on temperature, pressure, and equivalence ratio with distinct thermodynamic regions in which the ignition behavior is consistent and repeatable. The strong ignition limit was identified for each equivalence ratio, indicating a transition in ignition behavior from homogeneous to inhomogeneous. The location of this limit was found to shift to higher temperatures as the equivalence ratio was increased, with the most significant change at pressures greater than 10 atm. Interestingly, proximity to the NTC region increased the propensity for homogeneous ignition, likely resulting from a decrease in thermal sensitivity of the auto-ignition delay time.

The location of the strong ignition limit for each equivalence ratio was predicted with remarkable accuracy using the Sankaran Criterion, which is a comparison of the laminar flame speed to the thermal gradient driven spontaneous propagation speed. For $\varphi = 0.25$ the prediction was most accurate for an assumed thermal gradient of 10 K/mm, whereas for $\varphi = 1.0$ this value was 5 K/mm. In conjunction with the previous findings for syngas fuels by Mansfield and Wooldridge [4], this is a strong indication that the Sankaran Criterion can be used to predict ignition behavior for a broad range of hydrocarbons and hydrogen based fuels. This validation of the Sankaran Criterion for a hydrocarbon fuel importantly broadens the use of this tool and is an indication that ignition processes in hydrocarbon and high hydrogen content fuels are fundamentally similar. Furthermore, the quantitative nature of this criterion uniquely describes the roles of chemical kinetics, transport phenomena, and thermal characteristics in determining auto-ignition behavior, allowing for a deeper understanding of these phenomena and facilitating a thoughtful extension to more complex systems which include turbulence and mixture inhomogeneity.

Auto-ignition delay time measurements were compared to zero-dimensional model predictions for all experiments considered in the present work, revealing the accuracy of predictions was strongly dependent on equivalence ratio and ignition

behavior. The results indicate that the presence of inhomogeneous ignition behavior does not significantly affect the accuracy of auto-ignition delay time predictions for mixtures with φ = 0.25; whereas, for mixtures with φ = 1.0 the presence of inhomogeneous ignition behavior can significantly reduce the accuracy of predictions at the conditions studied here. This inaccuracy at higher φ is likely the result of increased energy release during the inhomogeneous event, causing a significant shift in the thermodynamic state of the yet unburned gas mixture and a subsequent violation of the isobaric/isothermal assumptions in the zero-dimensional model. These results are an important indication that while inhomogeneous ignition behavior may still be present at lean conditions, the subsequent effect on the auto-ignition delay time may be reduced or eliminated. Furthermore, it is evident that ignition behavior must be appropriately classified in any future experimental work for near stoichiometric mixtures of iso-octane at temperatures below ~ 1000 K to ensure proper interpretation of the results.

REFERENCES

[1] Di H, He X, Zhang P, Wang Z, Wooldridge MS, Law CK, et al. Effects of buffer gas composition on low temperature ignition of iso-octane and n-heptane. Combust Flame 2014.

[2] Reaction Design. CHEMKIN 10101 2010.

[3] Mehl M, Pitz WJ, Westbrook CK, Curran HJ. Kinetic modeling of gasoline surrogate components and mixtures under engine conditions. Proc Combust Inst 2011;33:193–200.

[4] Mansfield AB, Wooldridge MS. High-pressure low-temperature ignition behavior of syngas mixtures. Combust Flame 2014;161:2242–51.

[5] Vermeer DJ, Oppenheim AK. Auto-Ignition of Hydrocarbons Behind Reflected Shock Waves. Combust Flame 1972;18:327–36.

[6] Meyer JW, Oppenheim a. K. On the shock-induced ignition of explosive gases. Symp Combust 1971;13:1153–64.

[7] Middleton RJ, Martz JB, Lavoie G a., Babajimopoulos A, Assanis DN. A computational study and correlation of premixed isooctane air laminar reaction fronts diluted with EGR. Combust Flame 2012;159:3146–57.

[8] Donovan MT, He X, Zigler BT, Palmer TR, Wooldridge MS, Atreya A. Demonstration of a free-piston rapid compression facility for the study of high temperature combustion phenomena. Combust Flame 2004;137:351–65.

[9] Lee D, Hochgreb S. Hydrogen Autoignition at Pressures above the second explosion limit. Int J Chem Kinet 1998;30:385–406.

[10] Fieweger K, Blumenthal R, Adomeit G. Shock-tube investigations on the self-ignition of hydrocarbon-air mixtures at high pressures. Symp Combust 1994;25:1579–85.

[11] Strozzi C, Sotton J, Mura A, Bellenoue M. Characterization of a two-dimensional temperature field within a rapid compression machine using a toluene planar laser-induced fluorescence imaging technique. Meas Sci Technol 2009;20:125403.

[12] Einecke S, Schulz C, Sick V. Measurement of temperature, fuel concentration and equivalence ratio fields using tracer LIF in IC engine combustion. Appl Phys B 2014;71:717–23.

[13] Kalghatgi GT, Bradley D. Pre-ignition and “super-knock” in turbo-charged spark-ignition engines. Int J Engine Res 2012;13:399–414.

[14] Pal P, Mansfield AB, Wooldridge MS, Im HG. Characteristics of Syngas Auto-ignition at High Pressure and Low Temperature Conditions with Thermal Inhomogeneities. 12th Int. Conf. Combust. Energy Util., vol. 00, 2014, p. 1–4.

[15] Sankaran R, Im HG, Hawkes ER, Chen JH. The effects of non-uniform temperature distribution on the ignition of a lean homogeneous hydrogen–air mixture. Proc Combust Inst 2005;30:875–82.

[16] Bansal G, Im HG. Autoignition and front propagation in low temperature combustion engine environments. Combust Flame 2011;158:2105–12.

[17] Chaos M, Dryer FL. Syngas Combustion Kinetics and Applications. Combust Sci Technol 2008;180:1053–96.

SUPPLEMENTAL MATERIAL

Table 4-A. Summary of experimental conditions and results for mixtures with φ = 1.0, UM-RCF

Test gas composition[a] (% Vol.)				*Thermo. State*[b]		Ignition Behavior[c]	Auto-ignition delay time [d] (ms)				
iC_8H_{18}	O_2	N_2	Ar	*P* (atm)	*T* (K)		τ_{ign}	$\Delta\tau_{ign}$	τ_{pred}	$\delta\tau_{pred+}$	$\delta\tau_{pred-}$
1.64	20.7	44.2	33.5	8.8	986	M	1.9	1.4	5.7	2.4	2.5
1.67	20.7	67.7	9.94	17.1	913	M	3.8	1.7	9.2	2.5	2.5
1.67	20.7	77.6	0	17.3	877	M	8.2	3.9	17.5	4.2	4.2
1.67	20.7	77.6	0	16.5	872	M	9.9	3.7	20.2	4.8	4.8
1.67	20.7	67.7	0	14.8	812	M	28.9	7.5	55.0	10.9	10.4

[a] Balance CO_2

[b] Assigned thermodynamic state, with pressure uncertainty ~ 0.1 atm and temperature uncertainty ~ 5 K

[c] S = Strong, M = Mixed, W = Weak, NI = No ignition

[d] τ_{ign} = measured, $\Delta\tau_{ign}$ = symmetric uncertainty bounds of measurement, τ_{pred} = predicted, $\delta\tau_{pred-}$ / $\delta\tau_{pred-}$ = lower/upper uncertainty of prediction

Table 4-B. Summary of experimental conditions and results for mixtures with φ = 1.0, TU-RCM

Test gas composition (% Vol.)				*Thermo. State*[a]		Ignition Behavior[b]	Auto-ignition delay time [c] (ms)				
iC_8H_{18}	O_2	N_2	Ar	*P* (atm)	*T* (K)		τ_{ign}	$\Delta\tau_{ign}$	τ_{pred}	$\delta\tau_{pred+}$	$\delta\tau_{pred-}$
1.65	20.7	0	77.7	20.2	944	S	4.0	1.8	4.4	1.2	1.4

[a] Assigned thermodynamic state, with pressure uncertainty ~ 0.1 atm and temperature uncertainty ~ 5 K.

[b] S = Strong, M = Mixed, W = Weak, NI = No ignition

[c] τ_{ign} = measured, $\Delta\tau_{ign}$ = symmetric uncertainty bounds of measurement, τ_{pred} = predicted, $\delta\tau_{pred-}$ / $\delta\tau_{pred-}$ = lower/upper uncertainty of prediction

Table 4-C. Summary of experimental conditions and results for mixtures with φ = 0.25, UM-RCF

Test gas composition [a] (% Vol.)				*Thermo. State*[b]		Ignition Behavior [c]	Auto-ignition delay time [d] (ms)				
iC$_8$H$_{18}$	O$_2$	N$_2$	Ar	*P* (atm)	*T* (K)		τ_{ign}	$\Delta\tau_{ign}$	τ_{pred}	$\delta\tau_{pred+}$	$\delta\tau_{pred-}$
0.42	21.1	68.7	0	19.2	921	S	29.1	14.9	23.8	7.6	7.0
0.42	21.1	71.3	0	20.9	954	S	16.2	8.4	11.9	4.0	3.8
0.42	21.1	64.1	0	20.1	905	S	33.2	15.9	26.1	8.1	6.7
0.42	21.1	75.8	0	14.8	1010	S	6.6	4.0	5.1	2.1	2.1
0.42	21.1	76.8	0	15.9	1010	S	9.5	6.9	4.8	2.0	1.9
0.42	21.1	72.0	0	14.5	943	S	27.2	12.9	17.2	6.0	5.7
0.42	21.1	67.8	0	15.3	929	S	33.5	15.8	21.4	7.2	6.7
0.42	21.1	74.5	0	14.1	957	S	19.9	11.2	13.5	4.9	4.7
0.42	21.2	64.1	0	14.7	909	S	57.7	24.4	32.7	10.6	9.7
0.42	21.1	65.2	13.3	10.6	1070	S	6.3	5.6	2.4	1.4	1.2
0.42	21.1	75.8	2.7	10.3	1016	S	13.2	8.5	6.2	2.8	2.8
0.42	21.1	76.8	0	10.4	1006	S	19.1	10.9	7.3	3.2	3.2
0.42	21.1	74.5	0	10.3	972	S	27.3	14.7	13.6	5.4	5.3
0.42	21.1	73.7	0	9.9	958	S	33.1	15.8	17.8	6.8	6.7
0.42	21.1	72.0	0	9.7	948	S	34.5	15.6	21.9	8.2	8.0
0.42	21.1	67.8	0	9.5	915	S	90.2	39.4	42.1	14.6	13.7
0.42	21.1	68.7	0	9.7	923	S	67.9	29.3	35.5	12.5	11.8
0.41	21.1	63.3	15.2	4.5	1035	S	10.0	6.5	8.8	5.2	4.6
0.42	21.1	63.2	15.2	5.3	1062	S	6.2	4.9	4.8	3.0	2.5
0.42	21.1	63.2	15.2	4.9	1055	S	9.4	6.4	5.8	3.6	3.1
0.41	21.1	76.8	0	4.7	971	M	60.7	24.7	27.5	12.8	12.4
0.42	21.1	65.2	13.3	4.5	1028	M	11.9	7.4	9.9	5.8	5.2
0.42	21.1	75.8	2.7	4.6	983	M	35.9	15.7	22.1	10.9	10.4
0.42	21.1	75.8	2.7	4.6	983	M	39.0	15.8	22.1	10.8	10.4
0.42	21.1	74.5	0	4.9	972	NI	-	-	-	-	-
0.42	21.1	73.7	0	4.9	961	NI	-	-	-	-	-
0.41	21.1	56.0	22.4	3.2	1098	S	4.3	4.0	4.6	3.0	2.4
0.41	21.1	63.3	15.1	3.1	1060	S	15.3	8.4	7.7	5.1	4.1
0.41	21.1	56.1	22.4	2.8	1077	M	7.8	6.6	6.2	4.2	3.3
0.41	21.1	63.4	15.1	2.6	1034	M	23.7	10.2	13.9	9.1	7.6
0.41	21.1	67.4	11.0	2.7	1016	M	45.0	21.8	19.2	8.9	11.9
0.41	21.1	75.8	2.7	2.9	980	NI	-	-	-	-	-
0.41	21.1	75.8	2.7	3.3	1010	NI	-	-	-	-	-
0.41	21.1	75.8	2.7	3.0	1005	NI	-	-	-	-	-

[a] Balance CO_2

[b] Assigned thermodynamic state, with pressure uncertainty ~ 0.1 atm and temperature uncertainty ~ 5 K.

[c] S = Strong, M = Mixed, W = Weak, NI = No ignition

[d] τ_{ign} = measured, $\Delta\tau_{ign}$ = symmetric uncertainty bounds of measurement, τ_{pred} = predicted, $\delta\tau_{pred-}$ / $\delta\tau_{pred-}$ = lower/upper uncertainty of prediction

Table 4-D. Summary of experimental conditions and results for mixtures with φ = 0.25, TU-RCM

Test gas composition (% Vol.)				*Thermo. State*[a]		Ignition Behavior[b]	Auto-ignition delay time [c] (ms)				
iC_8H_{18}	O_2	N_2	Ar	*P* (atm)	*T* (K)		τ_{ign}	$\Delta\tau_{ign}$	τ_{pred}	$\delta\tau_{pred+}$	$\delta\tau_{pred-}$
0.42	20.9	55	23.7	29.7	784	S	52.9	14.7	70.3	19.7	15.8
0.42	20.9	55	23.7	29.1	739	S	71.1	19.2	72.6	19.1	16.0
0.42	20.9	55	23.7	29.0	739	S	71.8	19.2	72.9	19.3	16.0
0.42	20.9	0	78.7	18.5	818	S	134	22	129	34.6	30.1
0.42	20.9	0	78.7	20.1	827	S	102	17	101	27.0	23.8
0.42	20.9	0	78.7	20.1	822	S	102	19	108	28.6	25.1
0.42	20.9	0	78.7	20.1	823	S	98.8	17.2	106	28.4	24.9
0.42	20.9	0	78.7	20.1	823	S	99.6	17.4	107	28.4	24.9
0.42	20.9	0	78.7	20.2	885	S	33.1	6.0	37.6	11.3	10.5
0.42	20.9	25.7	53.1	20.1	878	S	38.3	6.6	44.0	13.1	11.9
0.42	20.9	25.7	53.1	20.1	876	S	38.7	6.7	45.8	13.6	12.4
0.42	20.9	0	78.7	15.0	956	S	11.5	2.8	12.2	4.7	4.6
0.42	20.9	0	78.7	15.0	956	S	11.4	2.8	12.0	4.7	4.4
0.42	20.9	25.7	53.1	15.7	974	S	7.2	1.8	8.5	3.4	3.2
0.42	20.9	25.7	53.1	15.5	971	S	7.6	1.8	9.1	3.6	3.5
0.42	20.9	0	78.7	5.2	1001	S	14.3	3.7	12.5	7.1	6.4
0.42	20.9	0	78.7	5.2	1001	S	13.2	3.8	12.6	7.1	6.5

[a] Assigned thermodynamic state, with pressure uncertainty ~ 0.1 atm and temperature uncertainty ~ 5 K.

[b] S = Strong, M = Mixed, W = Weak, NI = No ignition

[c] τ_{ign} = measured, $\Delta\tau_{ign}$ = symmetric uncertainty bounds of measurement, τ_{pred} = predicted, $\delta\tau_{pred-}$ / $\delta\tau_{pred-}$ = lower/upper uncertainty of prediction

Table 4-E. Reaction Rate Parameters with uncertainty

#	Reaction	A_{min}	A_0 [e]	A_{max}	n	E_a
1	$H + O_2 = OH + O$ [a]	$2.789(10)^{15}$	$3.5458(10)^{15}$	$4.508(10)^{15}$	-0.4	$16.6(10)^3$
16	$H_2O_2(+M) = OH + OH, k_0$ [b]	$1.86(10)^{14}$	$2.95(10)^{14}$	$4.68(10)^{14}$	0	$48.4(10)^3$
16	$H_2O_2(+M) = OH + OH, k_\infty$ [c]	$7.59(10)^{16}$	$1.20(10)^{17}$	$1.90(10)^{17}$	0	$45.5(10)^3$
3214	$I\text{-}C_8H_{18} = Y\text{-}C_7H_{15} + CH_3$ [d]	$3.27(10)^{26}$	$1.635\ (10)^{27}$	$8.175(10)^{27}$	-2.8	$83.9(10)^3$

Units are cm^3, s, cal, K; $k = AT^n \exp\left(-\frac{Ea}{RT}\right)$

Pre-exponential "A-factor" uncertainty sources:

[a] Hessler J. Calculation of Reactive Cross Sections and Microcanonical Rates from Kinetics and Thermochemical Data. J Phys Chem A 1998;102:4517-4526.

[b] Brower L, Cobos C, Troe J, Dubal H, and Crim H. Specific rate constants k(E,J) and product state distributions in simple bond fission reactions. II. Application to HOOH = OH+OH. J Chem Phys 1987;86 : 6171-6182.

[c] Baulch D, Cobos C, Cox R, Esser C, Frank P, Just T, Kerr J, Pilling M, Troe J, Walker R, Warnatz J. Evaluated Kinetic Data for Combustion Modeling. J Phys Chem Ref. Data 1992;21:411-429

[d] Not available, assumed multiplicative uncertainty factor of 5.

[e] Nominal parameters from Mehl et al. 2011 kinetic mechanism [3]

Chapter 5
The effect of impurities on syngas combustion

The objective of this project was to advance the understanding of the effects of impurities on the chemical kinetics of syngas oxidation, focusing on CH_4 and trimethylsilanol (TMS) impurities at thermodynamic and mixture conditions relevant to practical device operation. This was accomplished through an experimental investigation of auto-ignition delay times of syngas with various mixture compositions using the UM-RCF. Uniquely, high-speed imaging was utilized for each experiment, enabling testing at lower temperatures and pressures not possible in previous experimental studies by other investigators. The auto-ignition delay time and pressure time history measurements were compared to predictions made using a typical syngas oxidation mechanism, in order to connect observations with potential underlying chemical kinetic pathways and elucidate behavior trends.

1. METHODS

1.1 Experimental Methods

Ignition experiments were conducted for realistic syngas mixtures with fuel to oxygen equivalence ratio of $\varphi = 0.1$ and were air-dilute with N_2, i.e. molar O_2 to inert gas ratio of 1:3.76. In some cases, small amounts of the N_2 diluent gas were replaced by Ar and/or CO_2 to modify the test temperature. Four fuel mixtures were used, (1) pure syngas: 30% H_2, 70% CO (fuel volume), (2) syngas with CH_4: 27% H_2, 67% CO, 6% CH_4, (3) pure syngas with 10 ppm TMS, and (4) pure syngas with 100 ppm TMS. Mixtures were designed to represent lean syngas mixtures used in the power industry while spanning typical CH_4 concentrations [1,2] and typical TMS

impurity concentrations observed by Rasi et al. [3] (~ 5 ppm). Considering the upward trend in organic Si species in waste-based syngas reported by Rasi et al. [3], the mixture containing 100 ppm TMS was selected to represent potential future concentrations. Ignition experiments were conducted at 5 and 15 atm for the broadest range of temperatures allowable in the UM-RCF for these mixtures (~ 1010-1110 K, based on experimental test times and associated uncertainties). While it was desirable to increase the equivalence ratio beyond the value chosen here, $\varphi = 0.1$, it was not possible to achieve homogeneous ignition behavior at the thermodynamic conditions of interest for higher values of φ. Please see Chapter 3 (Mansfield and Wooldridge [4]) for a discussion of the state and syngas mixture conditions associated with homogeneous versus inhomogeneous ignition. A detailed tabulation of the gas mixture composition and thermodynamic state corresponding to each auto-ignition delay time measurement is given in the Supplemental Material section.

1.2 Computational Methods

Auto-ignition ignition delay time and pressure time history predictions were made using the constant volume adiabatic zero-dimensional homogeneous reactor model in the CHEMKIN software suite [5] with the Li 2007 chemical kinetic mechanism. This mechanism was used given previous success in predicting syngas ignition behavior [6,7], [4] and because it includes CH_4 oxidation chemistry. Using this auto-ignition model, a corresponding auto-ignition delay time prediction was calculated for each ignition experiment in this study using the initial thermodynamic condition and mixture composition of the experiments. The auto-ignition delay time from the model predictions was defined as the time from the start of the calculation to the time when dT(t)/dt was maximized. In most cases two inflection points were predicted in the temperature time history, indicating two "steps" of energy release during ignition. The occurrence of two-step auto-ignition corresponds well to the experimental observations and is discussed in detail below. Important to note is that TMS is not included in the Li 2007 mechanism and the

authors are aware of no oxidation model which includes this species and associated combustion products. Therefore auto-ignition delay time predictions are presented only for experiments which used the pure syngas or syngas with CH_4 mixtures. For each prediction, quantified uncertainty bounds were calculated using the known uncertainty in the "A-factor" of the Arrhenius reaction rates for the four most sensitive reactions, $CO + O_2 = CO_2 + O$ (R21), $HO_2 + H = H_2 + O_2$ (R10), $H + O_2 = H + OH$ (R1) and $H + O_2 (+M) = HO_2 (+M)$ (R9). These were identified using OH sensitivity analysis conducted in the CHEMKIN software suite for the pure syngas mixture at P = 15 atm, and T = 1066 K. The results of the sensitivity analysis and the rate coefficients used are listed in Supplemental Material.

2. RESULTS

For each experiment in the UM-RCF, a pressure time history and a high-speed imaging video were recorded, allowing for the determination of auto-ignition delay times and direct observation of the auto-ignition behavior. A typical pressure time history during an ignition experiment for initial pressures of 15 and 5 atm can be seen in Figs. 5-1 and 5-2, respectively. Similar trends are observed for both experiments. The pressure initially increases during the compression stroke until the Sabot is seated at the end-of-compression (EOC) event, followed by a slight decrease in pressure due to heat transfer from the test gas volume into the cool Test Section walls, followed by a large and rapid increase in pressure during the ignition. For each experiment, the time and pressure was noted at the three distinct events: end-of-compression, minimum pressure (P_{min}), and maximum pressure (P_{max}), highlighted in Fig. 5-1. After filtering the pressure time history with a 75-point smoothing algorithm to reduce signal noise, the pressure and time value for each event was defined mathematically as a local maximum or minimum respectively. The pressure data (P(t)) between P_{min} and P_{max} was then filtered a second time with a 100-point smoothing algorithm to further reduce signal noise, and the numerical derivative of the pressure time history (dP(t)/dt) was calculated using a center differencing scheme. For each auto-ignition experiment a thermodynamic state was

assigned representing the unburned iso-thermal iso-baric condition at which the experiment was conducted, as described in Chapter 2.

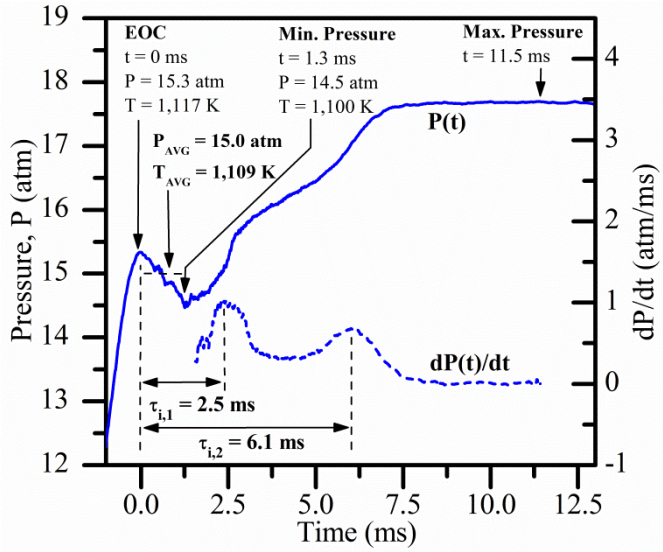

Fig.5-1. Typical pressure time history, P(t), and time derivative of the pressure time history, dP(t)/dt, for experimental conditions exhibiting two-step ignition behavior; P = 15.0 atm, T = 1,109 K, φ = 0.1 for a pure syngas mixture. $\tau_{i,1}$ and $\tau_{i,2}$ are the first and second auto-ignition delay times respectively.

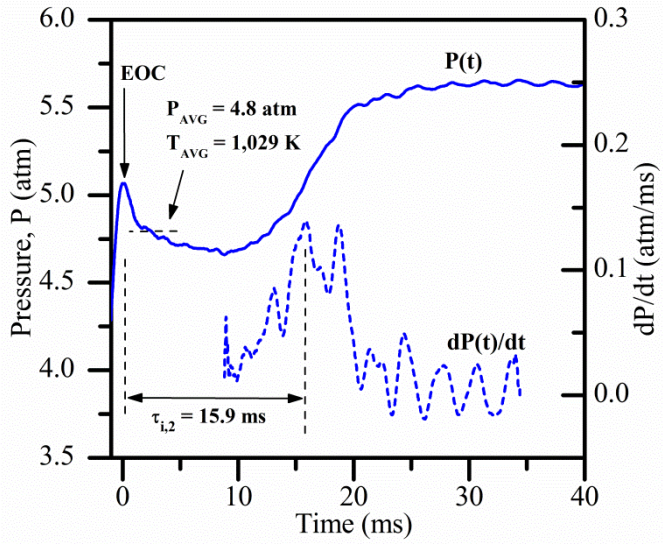

Fig.5-2. Typical pressure time history, P(t), and time derivative of the pressure time history, dP(t)/dt, for experimental conditions exhibiting one-step ignition behavior; P = 4.8 atm, T = 1,029K, φ = 0.1 for pure syngas mixture. $\tau_{i,2}$ is the auto-ignition delay time.

For experiments with an initial pressure of 15 atm, seen in Fig. 5-1, trends in the dP/dt time history exhibited two peaks for all mixtures; one corresponding to

each "step" of pressure rise during the ignition event. As evidenced, each step represents a region of rapid pressure rise and the two steps observed are separated by region with a reduced rate of pressure. Two ignition delay times were therefore determined for each experiment that exhibited these features ($\tau_{i,1}$ and $\tau_{i,2}$) as the time from EOC to each peak in the dP/dt time history. The definitions are illustrated in Fig. 5-1. For experiments with an initial pressure of 5 atm, as presented in Fig. 5-2, a single peak in dP/dt was observed for all mixtures and correspondingly one ignition delay time, $\tau_{i,2,}$ was determined from each of these experiments. The most significant source of uncertainty associated with these auto-ignition delay time measurements is from the selection of the smoothing algorithm in the data filtering process. Uncertainty for each measurement was quantified by varying the number of points included in the initial filtering algorithm by ± 50% and defining bounds for each measurement which spanned the resulting range of auto-ignition delay times calculated. In the vast majority of cases the uncertainty in the measured auto-ignition delay time was < 1%; though, in a few select cases 20-35% uncertainty was observed, likely the result of a convolution of the auto-ignition event with an artifact in the pressure time history. Uncertainty bounds in the assigned temperature values were also calculated in this manner, as variation in the smoothing algorithm parameters affects the selection of key pressure values (EOC, P_{min}, P_{max}) used to calculate the temperature. While in most cases the temperature uncertainty was less than the previously defined value of ~ 5 K, in certain cases the uncertainty exceeded this value. A tabulated list of all experimental results, including calculated uncertainty bounds for the auto-ignition delay time measurements and assigned temperatures, is provided in the Supplemental Material section.

A frame from the typical high-speed imaging results of chemilluminescence during syngas auto-ignition is shown in Fig. 5-3. As seen, homogeneous ignition is indicated by the spatial uniformity of the chemilluminescence emission. For each experiment the high-speed imaging results were reviewed to confirm that only homogeneous ignition occurred. This ensured that all characteristics of the

pressure time history correspond to global phenomena (chemical kinetics and heat transfer), which are well represented by a zero-dimensional homogeneous reactor model. As illustrated in detail in Chapters 3 & 4 (Mansfield and Wooldridge [4,8]), the effects of localized ignition phenomena can significantly impact the accurate interpretation of pressure time history results for syngas fuel and so avoiding these behaviors was critical in the present work.

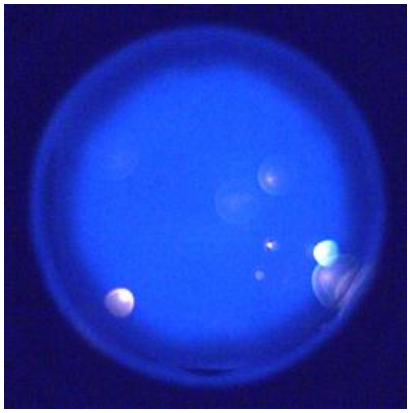

Fig.5-3. Single frame from high-speed imaging of typical ignition behavior within Test Section, illustrating homogeneous chemilluminescence, for the pure syngas mixture at experimental conditions P = 4.6atm, T = 1052 K, φ = 0.1.

2.1 Auto-ignition delay times at 5 and 15 atm

Fig. 5-4a & b illustrate the auto-ignition delay time measurement results for the second ($\tau_{i,2}$) and first ($\tau_{i,1}$) steps of the ignition at 15 atm. Overall the results for both steps illustrate excellent repeatability and consistent trends throughout the temperature range evaluated. The data demonstrate TMS can be added to the syngas mixtures in a controlled and consistent manner in the present experimental system, an important verification considering that this compound has not been tested in any known previous combustion experiment. The effects of CH_4 and TMS impurity addition are in trend wise agreement between the first and second auto-ignition delay times, generally with CH_4 inhibiting and TMS promoting ignition, though the magnitude of the impact is more pronounced for $\tau_{i,2}$. The observed inhibiting effects for the syngas with CH_4 mixture are in close agreement with

previous findings by Gersen et al. [9] and Mathieu et al. [10] who also observed this outcome.

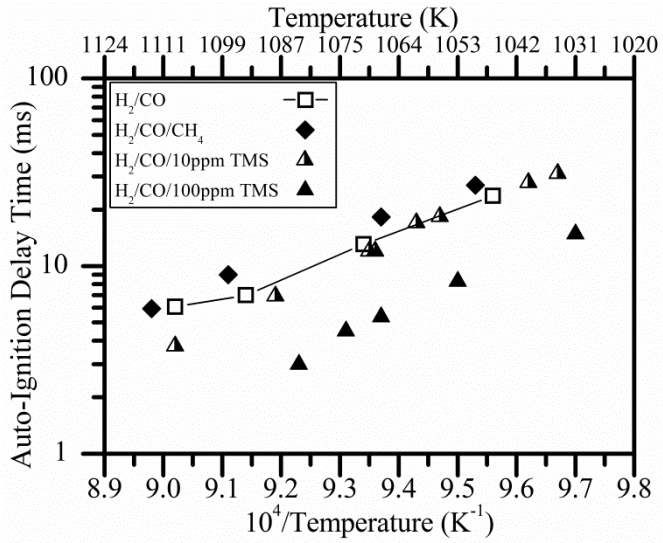

Fig.5-4a. Measured auto-ignition delay time of the second step of ignition ($\tau_{i,2}$) as a function of inverse temperature for P = 15 atm. The solid line is provided for visual reference to the pure syngas data. Uncertainty bounds of the auto-ignition measurements and temperatures are the limits of the post-processing algorithm filtering parameters, and are not visible on this scale.

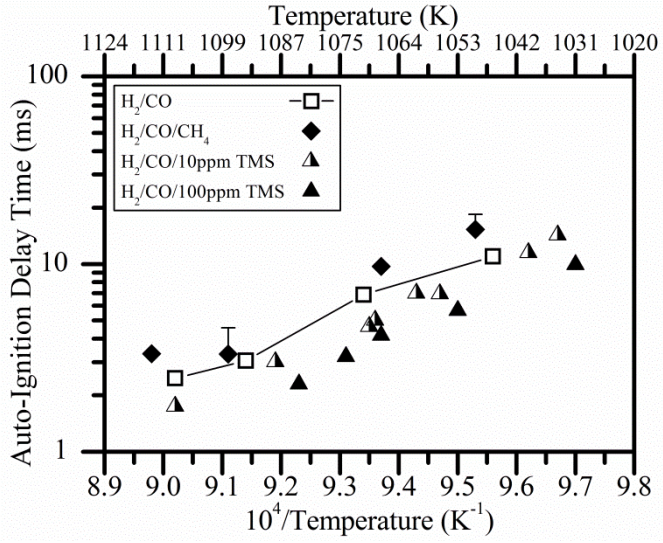

Fig.5-4b. Measured auto-ignition delay time of the first step of ignition ($\tau_{i,1}$) as a function of inverse temperature for P = 15 atm. Uncertainty bounds of the auto-ignition measurements and temperatures are the limits of the post-processing algorithm filtering parameters. The solid line is provided for visual reference to the pure syngas data.

Regarding the results for $\tau_{i,2}$ shown in Fig. 5-4a, it is apparent that the addition of CH_4 consistently increases the auto-ignition delay time relative to the pure syngas mixtures by ~ 40%. Conversely, the addition of TMS causes a decrease in the auto-ignition delay times, with magnitude dependent on both the concentration and the initial temperature. For 10 ppm TMS addition, significant effects are only observed at T > 1060 K, at which point the auto-ignition delay time is reduced by ~ 30%. For 100 ppm TMS addition, there is a drastic impact on the measurements, with consistent 50-70% decrease in the auto-ignition delay time across all temperatures. Regarding the results for $\tau_{i,1}$ shown in Fig. 5-4b, it is apparent that the addition of CH_4 consistently increases the auto-ignition delay time measurement by 40-50%. Again, the addition of TMS results in a reduction in measured auto-ignition delay times; where 10 ppm addition leads to a consistent 10-30% reduction, and 100 ppm leads to a consistent 45-50% reduction. As the effect of 10 ppm and 100 ppm TMS addition was similar for $\tau_{i,1}$, but drastically different for $\tau_{i,2}$, this suggests that the second step of the ignition process is more sensitive to this impurity. Conversely, the difference between $\tau_{i,1}$ and $\tau_{i,2}$ remains approximately constant at ~ 5 ms for both pure syngas and syngas with CH_4 across all conditions.

Fig. 5-5 illustrates the auto-ignition delay time measurement results ($\tau_{i,2}$) for 5 atm initial pressure. Again, the results indicate excellent repeatability and consistent trends throughout the temperature range. Recall that the uncertainty bounds of the temperature assignments are the limits of the post-processing filtering algorithm parameters. The effects of CH_4 and TMS generally agree with those at 15 atm, with CH_4 inhibiting and TMS promoting ignition, but the magnitudes of the impact differ. It is apparent that the addition of CH_4 has minimal impact below 1050 K, though at higher temperatures the auto-ignition delay time is increased by up to a factor of 3. While the apparent activation energy (the slope of the auto-ignition delay time as a function of the inverse temperature) decreases as temperature decreases for all other mixtures, the apparent activation energy for the syngas with CH_4 mixture does not change as a function of

temperature. For 10 ppm TMS addition, there is no significant effect on the auto-ignition delay time; whereas for 100 ppm TMS addition, there is a consistent 20-30% decrease in the auto-ignition delay time. Interestingly, as the temperature increases to ~ 1070 K, the auto-ignition delay time appears to be increasingly less sensitive to addition of 100 ppm of TMS or CH_4, suggesting that the effects of these impurities at these mole fraction levels are negligible at temperatures above this value. This is may be the result of reductions in the magnitude of the auto-ignition delay times at these conditions, as compared to lower temperatures and higher pressures.

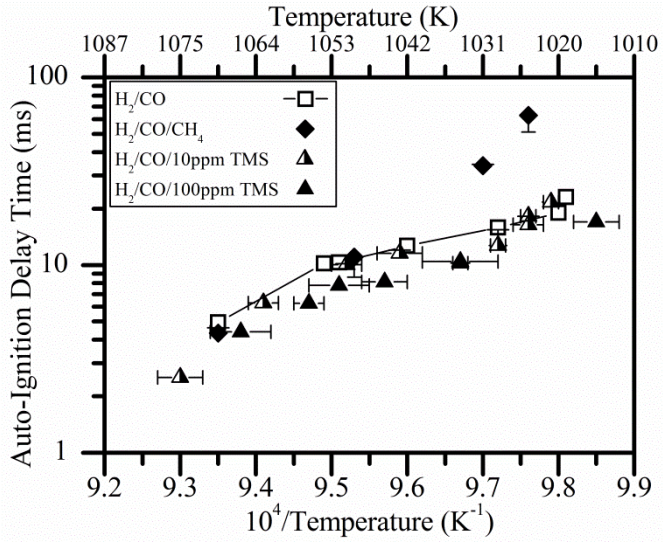

Fig.5-5. Measured auto-ignition delay time ($\tau_{i,2}$) as a function of inverse temperature for P = 5 atm. Uncertainty bounds of the auto-ignition measurements and temperatures are the limits of the post-processing algorithm filtering parameters. The solid line is provided for visual reference to the pure syngas data.

2.3 Pressure dependence

As demonstrated in the figures above, the effect of TMS addition on the auto-ignition delay time is highly pressure dependent, with significantly larger magnitude impact at 15 atm. Fig. 5-6 illustrates the auto-ignition delay time measurements for the second step of the ignition process ($\tau_{i,2}$) at both 5 and 15 atm for the pure syngas and syngas with TMS mixtures. Regarding the pressure dependence of the auto-ignition delay time, there is a clear dependence for the pure

syngas mixture illustrated in Fig. 5-6, with increases in ignition delay time of up to 100% as the pressure is increased from 5 to 15 atm at the same temperature. This behavior is indeed expected as the increase in pressure corresponds to a shift to slower HO_2 and H_2O_2 dominated chemical kinetic pathways [11]. While 10 ppm TMS addition has minimal impact on this pressure dependence, it is clear that 100 ppm TMS addition reduces the pressure dependence of the auto-ignition delay time to nearly zero. As this pressure dependence is likely closely related to HO_2 and H_2O_2 dominant chemistry, this suggests that the promoting effect of TMS is related to interaction with these species.

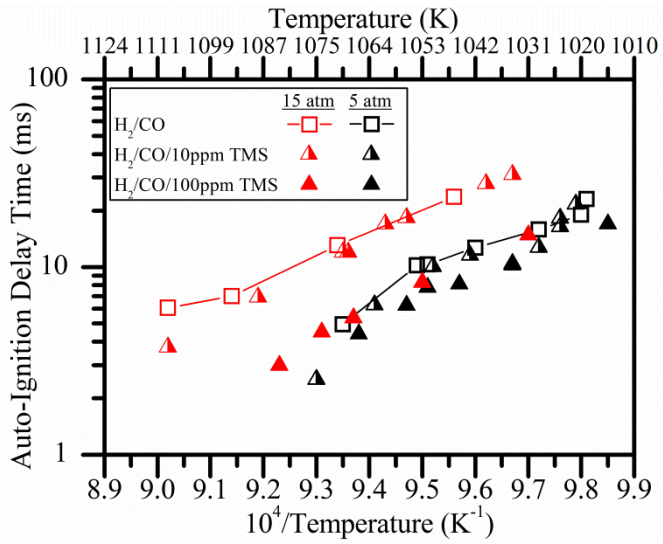

Fig.5-6. Measured auto-ignition delay time of the second step of ignition ($\tau_{i,2}$) as a function of inverse temperature for P = 5 and 15 atm for pure syngas and syngas with TMS mixtures. The solid lines are provided for visual reference to the pure syngas data. Uncertainty bounds of the auto-ignition measurements and temperatures are the limits of the post-processing algorithm filtering parameters, and are not visible on this scale.

Remarkably, similar significant reduction in both auto-ignition delay times and the pressure dependence of the auto-ignition delay time was reported by both Petersen et al. [12] and McLain et al. [13] for SiH_4 addition to pure H_2 mixtures. Jachimowski and McLain [14] postulated that this decrease in pressure dependence was due to HO_2 radical scavenging by SiH_4, promoting H_2O_2 and subsequently OH formation, though these claims have not been evaluated experimentally.

2.4 Comparison with kinetic model predictions

As previously mentioned, predictions for auto-ignition delay times of pure syngas and syngas with CH_4 were made using the Li 2007 mechanism and the homogeneous reactor model in CHEMKIN. For all 15 atm experiments, the kinetic model accurately predicted the existence of a two-step ignition process; whereas, for 5 atm the kinetic model predicted single step ignition in most cases, though two-step ignition in rapid succession (< 1 ms separation) was predicted for some conditions. This is not in disagreement with the measurements at 5 atm however, as the resolution of the experiment, due to the data smoothing process, is insufficient to accurately observe two ignition steps in such immediate occurrence. Typical pressure time history results (normalized by the initial pressure for clarity in the comparison) from simulations with initial conditions P = 5 and 15 atm, T = 1066 K, using the pure syngas mixture are seen in Fig. 5-7. These results demonstrate the relationship between the initial pressure and the time between first and second ignition steps; where for 15 atm the ignition steps are separated by ~ 4 ms, and for 5 atm, the separation is < 1 ms.

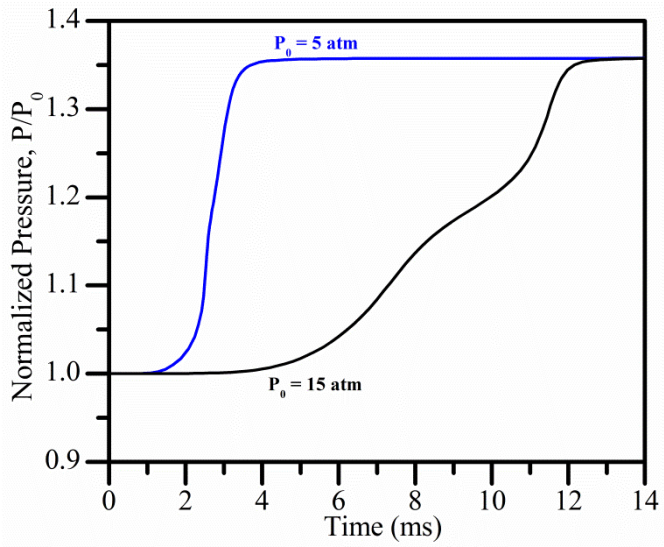

Fig.5-7. Typical predicted pressure time histories, normalized by the initial pressure, for P = 5 atm and 15 atm, T = 1066 K, and the pure syngas mixture.

Fig. 5-8 and 5-9 illustrate the measured and predicted auto-ignition delay times for 15 and 5 atm, respectively. Recall the uncertainty bounds of the predictions are the effect of the uncertainty in the rate coefficient of reactions R21, R10, R1, and R9. As seen in Fig. 5-8, predictions for all temperatures, both mixtures, and both $\tau_{i,1}$ and $\tau_{i,2,}$ are in excellent agreement with the measurements at 15 atm. Likewise, as illustrated in Fig. 5-9, predictions for both mixtures for all temperatures at 5 atm are in close agreement with the experimental data except for the syngas with CH_4 mixture. Predictions for this mixture at temperatures below ~ 1040 K are faster than the measurements and outside the uncertainty bounds. While this may suggest error in the Li 2007 kinetic mechanism, these data correspond to the lowest temperatures and longest auto-ignition delay times, therefore it is possible that the slight disagreement is the result of more pronounced heat transfer effects not sufficiently captured by the model. Overall the evidence in Figs. 5-7 through 5-9 show the system is well represented by the Li 2007 chemical kinetic reaction mechanism and a homogeneous reactor physical model, importantly allowing for more detailed chemical kinetic analysis.

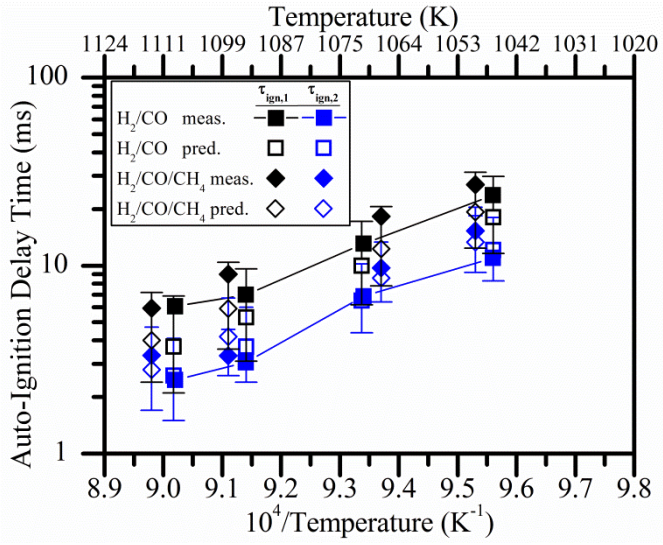

Fig.5-8. Measured and predicted auto-ignition delay times ($\tau_{i,1}$ and $\tau_{i,2}$) as a function of inverse temperature for P = 15 atm, for pure syngas and syngas with CH_4. Uncertainty bounds of the predictions are the effect of the uncertainty in the rate coefficient of reactions R1, R9, R10, and R21.

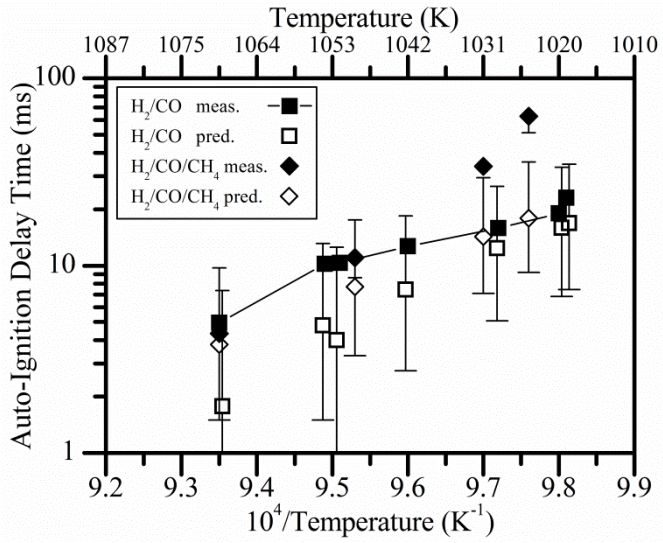

Fig.5-9. Measured and predicted auto-ignition delay time ($\tau_{i,2}$) as a function of inverse temperature for P = 5 atm, for pure syngas and syngas with CH_4. Uncertainty bounds of the predictions are the effect of the uncertainty in the rate coefficient of reactions R1, R9, R10, and R21.

3. DISCUSSION

3.1 Two-step Ignition Behavior

The experimental results of the present work clearly illustrate the existence of a two-step ignition process for experiments with 15 atm initial pressure, embodied by two distinct regions of rapid heat release and corresponding pressure rise. Furthermore, model predictions indicate that near 5 atm, two-step ignition is likely occurring though the steps are in such rapid succession that it is not possible to observe a separation in time experimentally. The existence of this two-step ignition behavior for syngas fuel mixtures has not been previously reported, although similar behavior is evident in the pressure time history results of Keromnes et al. [15] and Kalitan et al. [16]. As the auto-ignition delay time is often defined as the time where dP/dt is maximized, it is possible that in these and other previous studies multi-step ignition behavior was observed but only a single auto-ignition delay time was reported. Additionally, given that historical combustion experiments were conducted primarily near atmospheric pressures, according to Chaos and Dryer [7] and the references therein, it is possible that significant two-step ignition was not exhibited for a majority of these lower pressure studies.

As demonstrated above, the two-step nature of the ignition process was well predicted by the Li 2007 kinetic mechanism in the CHEMKIN reactor model. It was therefore possible to use this model in more detail, to probe trends in two-step behavior across various conditions as well as its chemical kinetic foundations. Of particular interest was the dependence of this behavior on initial pressure. Additionally, given the highly variable nature of syngas mixture composition, understanding how this two-step ignition behavior is affected by constituent variation, e.g. the ratio of H_2:CO, is also important. In order to evaluate the effects of these factors, simulations were conducted for a range of initial thermodynamic state and mixture conditions. Illustrated in Fig. 5-10 are predicted pressure time histories for syngas mixtures with P = 5 and 15 atm, T = 1066 K, for air-dilute mixtures with φ = 0.1, and variable H_2:CO (molar ratio) of 1:3, 1:1, 3:1, 1:0. Note that the pressure values are normalized by the initial unburned value for comparative clarity. Considering these predictions, it is clear that the occurrence of two-step ignition behavior is strongly dependent on both the initial pressure and the molar ratio of H_2 to CO. Noticeably, significant two-step ignition behavior is not apparent at 5 atm for these conditions; however, the addition of CO does impact the rate of pressure rise during the ignition event, with increasing amounts of CO yielding lower pressure rise rates. This is in excellent agreement with the experimental findings of the present work, and indeed supports the notion that previous studies of syngas near atmospheric conditions would likely not yield observations of two-step ignition behavior. In contrast, at 15 atm two-step ignition behavior, indicated by two distinct regions of differing rate of pressure rise, is clearly apparent for all mixtures except pure H_2. At this higher pressure both the relative magnitude of pressure rise from the second step and the time separation between first and second steps of the ignition process are increased with CO. Remarkably, at 15 atm and the highest CO concentration there is a marked increase in the time of energy release during both first and second steps of the ignition process as compared to the other conditions evaluated. For example, at 5 atm and H_2:CO = 1:1, the heat release and corresponding pressure rise from initial

to final states occurs over < 1 ms; whereas, for 15 atm and H_2:CO = 1:3 the same relative pressure rise occurs over more than 10 ms. In a practical application, two-step heat release and ignition behavior of this significance could have a marked impact on system performance if not appropriately considered.

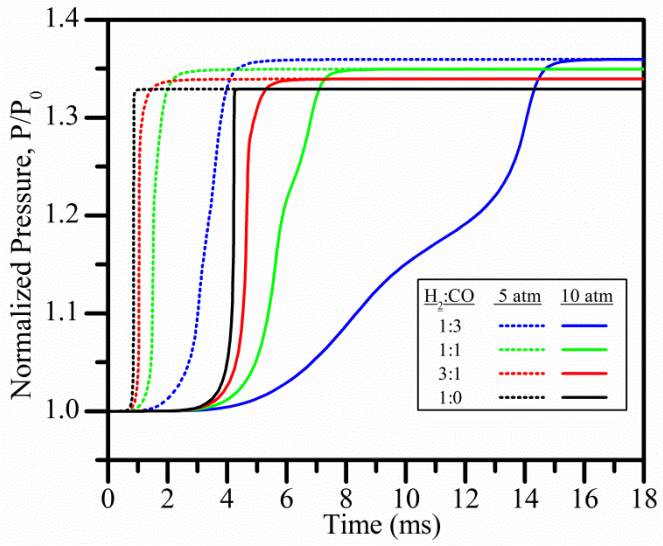

Fig.5-10. Predicted pressure time histories, for P = 5 and 15 atm, T = 1066 K, and syngas at φ = 1.0, H_2:CO (molar ratio) = 0:1, 1:3, 1:1, 3:1, 1:0, air-dilute with N_2.

The clear relationship between two-step ignition behavior and both the initial pressure and molar ratio of H_2:CO for syngas mixtures implies that these factors are important to the chemical kinetic foundations of this behavior. Regarding these foundations, it was desirable to develop an understanding of the root causes of two-step ignition behavior in syngas fuels. To accomplish this, the kinetic model was once more utilized to predict mole fraction time histories for both major and radical species during the ignition process. This simulation was conducted for the pure syngas mixture used in the present experimental work at P = 15 atm, T = 1066 K; a condition which exhibits significant two-step ignition. Illustrated in Fig. 5-11a & b are predicted mole fraction time histories at this condition, which reveal the stepped behavior in the pressure time history is reflected in the mole fraction time histories of both major and radical species. As evidenced in Fig. 5-11a, during the first step

of the ignition process both H_2 and CO are consumed, correspondingly forming H_2O and CO_2. When the H_2 supply is essentially exhausted, the rate of pressure rise decreases and the rate of CO consumption remains nearly constant. This reduction in pressure rise rate is expected, as the total rate of fuel consumption decreases when H_2 is no longer significantly available. The rate of pressure rise continues at this reduced magnitude until after some time the remaining CO is rapidly consumed and a significantly larger rate of pressure rise occurs. This second rapid rise in pressure forms the second step in the pressure time history. Shown in Fig. 5-11b are the major radical species (including HO_2 and H_2O_2) formed during the two-step ignition process. The simulation indicates H_2O_2 and HO_2 radicals dominate the first step of the ignition process, as predicted by Chaos et al. [11] and mentioned earlier; however, OH and O radicals clearly dominate the second step of the ignition process.

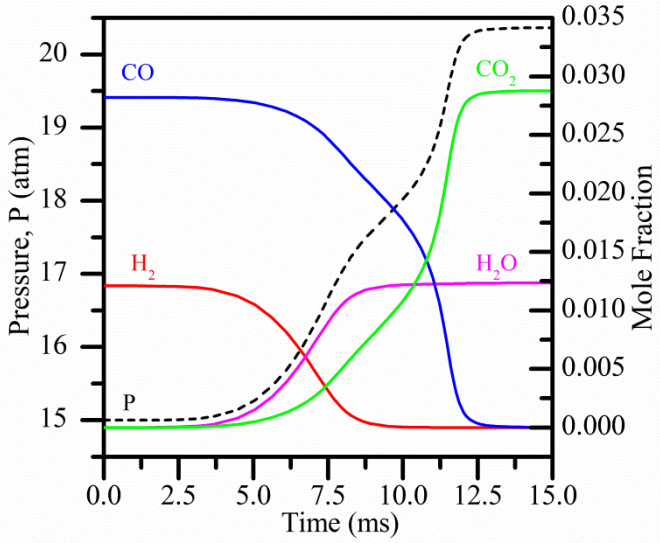

Fig.5-11a. Predicted pressure and major species mole fraction time histories for P = 15 atm, T = 1066 K, and the pure syngas mixture.

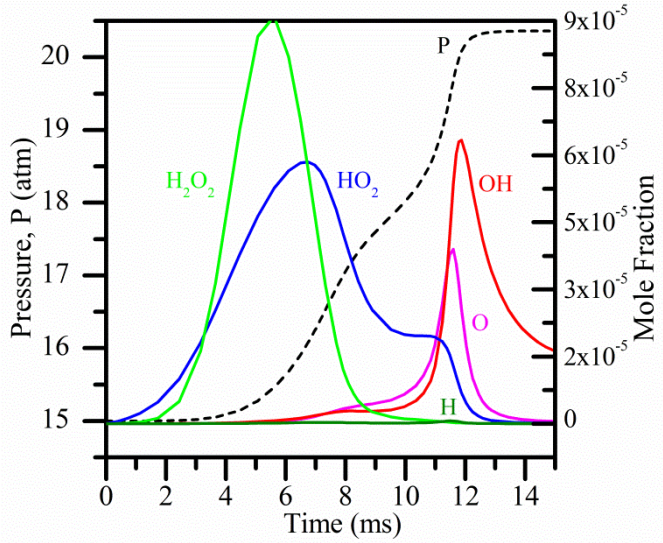

Fig.5-11b. Predicted pressure and radical species mole fraction time histories for P = 15 atm, T = 1066 K, and the pure syngas mixture.

As to the chemical kinetic foundation for two-stepped ignition behavior, the question is therefore what causes the delay in rapid CO oxidation characteristic of the second step of the ignition process? Rate-of-production analysis for CO at this condition, shown in the Supplemental Material, importantly indicates that nearly all CO is consumed via the reaction CO + OH = CO_2 + H (R23). This finding, in addition to the radical mole fraction time history results in Fig. 5-11b, suggests that the delay in rapid CO oxidation is likely related to a corresponding delay in the formation of OH. Rate-of-production analysis was therefore performed for OH, which is also shown in the Supplemental Material. Results of that analysis indicate that H_2O_2 (+M) = OH + OH (+M) (R15) dominates the formation of OH during the first step of the ignition process. Once the H_2 supply is nearly exhausted at the end of the first step of the ignition, the dominant formation reactions then change to primarily H + O_2 = OH + O (R1) and O + H_2O = OH + OH (R4). As discussed in detail by Chaos et al. [11] and Mansfield and Wooldridge [4], H + O_2 = OH + O (R1) is in direct competition with H + O_2 (+M) = HO_2(+M) (R9), and the corresponding formation rate of OH is highly dependent on both pressure and temperature. Considering the competition of these reactions, as pressure is increased and/or

temperature decreased the rate of OH production diminishes significantly. It is therefore likely that the pressure dependence of OH production from reactions R1 and R13 during the time after the first step of the ignition is the underlying foundation for the dependence of two-step ignition behavior on pressure. In other words, when pressure is increased, the rate of OH production after the first step of the ignition process is slowed and more time is required to build the OH radical pool to a sufficient level for rapid CO oxidation. This results in a more pronounced two-step ignition behavior as the first and second steps are separated by more time. Competition between reactions R1 and R13 can also explain the dependence of two-step ignition behavior on the H_2:CO molar ratio. This ratio will affect the temperature at the end of the first step of the ignition process, with more H_2 yielding a higher temperature. The increased temperature will lead to an increased rate of OH formation and correspondingly will decrease the time between first and second steps of the ignition.

Overall the results of both the experimental investigation and chemical kinetic analysis of the present work illustrate an important yet often overlooked characteristic of syngas mixtures - features of multi-stage heat release. With this in mind, the method of reporting a single auto-ignition delay time, as traditionally done for syngas mixtures, omits information important to understanding the combustion kinetics of these fuels. The approach of reporting both the first and second auto-ignition delay times is an important improvement in capturing multi-stage behavior. Other methods for reporting could include more characteristics such as magnitude and rates of pressure rise, which may further increase the value and accuracy of similar experimental data. Note that the magnitude of the effects of multi-stage heat release are convolved with the volume and heat transfer characteristics of the test section of the experimental apparatus. The amount of energy transferred to the test gases during the combustion process is balanced by the amount of energy lost to the cool test section walls and/or expended in compressing the cool boundary layer gas volume. Consequently, care should be used when comparing data from different facilities.

3.2 Inhibiting effect of CH_4

The experimental results of the present work illustrate a pressure dependent inhibiting effect of CH_4 on the auto-ignition of syngas, which is well predicted by the Li 2007 kinetic mechanism and the CHEMKIN reactor model. The inhibition effect and the trend in pressure dependence are both in excellent agreement with the findings by Mathieu et al. [10], who suggested that $CH_4 + OH = CH_3 + H_2O$ (R49) was the primary reaction through which CH_4 inhibits syngas auto-ignition (identified using sensitivity analysis). Uniquely, experimental results in the present work indicate that while $\tau_{i,1}$ and $\tau_{i,2}$ are increased by the addition of CH_4, the magnitude of their difference is consistent with that for pure syngas. This suggests that the CH_4 acts primarily on the kinetics during the first step of the ignition at the present concentration. In order to evaluate this hypothesis, the CHEMKIN reactor model was once more utilized. Illustrated in Fig. 5-12 are predicted mole fraction time histories for the syngas with CH_4 mixture at P = 15 atm, T = 1066 K for the major species. Additionally, the predicted pressure traces for both the pure syngas and syngas with CH_4 are included for comparison. As seen in the figure, the ignition proceeds in a very similar manner as predicted for pure syngas. Interestingly though, CH_4 is consumed completely along with H_2 during the first step of the ignition. Furthermore, OH rate-of-production analysis for this mixture, shown in the Supplemental Material, indicates that CH_4 scavenges OH during the first step of the ignition process via $CH_4 + OH = CH_3 + H_2O$ (R49) and $CH_2O + OH = CHO + H_2O$ (R38). After the first step of ignition, however, there is no major consumption of OH by CH_4 or related intermediates. The predicted pressure time history results also indeed illustrate a lengthening in the time of the first step of the ignition process by ~ 2 ms for the mixture with CH_4, though the time from the end of the first step to the second step remains approximately constant at ~ 3 ms. Therefore, the modeling results strongly support the notion that the effect of CH_4 impurity addition at this concentration is to directly increase $\tau_{i,1}$ through OH scavenging while minimally affecting the kinetics of the second step of the ignition

process. The experimentally observed effect on $\tau_{i,2}$ is therefore likely the result of delayed heat release from the first step of the ignition process. Important to note is that the preferential inhibition effect of CH_4 would not have been detected had only a single auto-ignition delay time been reported. This result highlights the importance of using thorough metrics to describe auto-ignition measurements at these multi-stage ignition conditions.

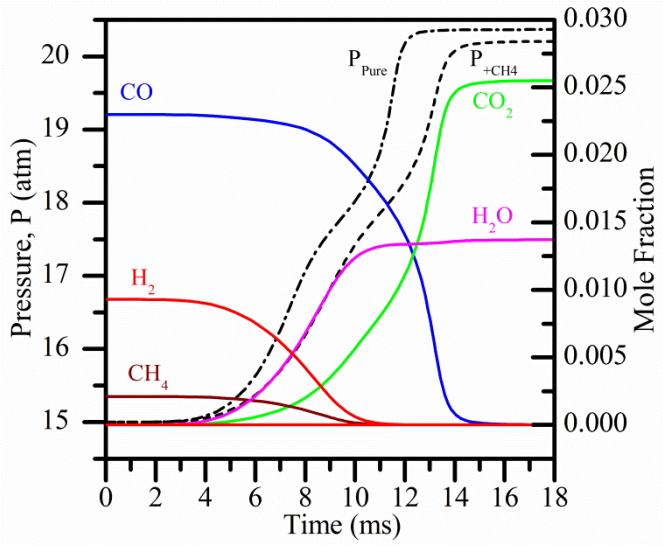

Fig.5-12. Predicted pressure and major species mole fraction time histories, for P = 15 atm, T = 1066 K, and the syngas with CH_4 mixture. The predicted pressure time history for the pure syngas mixture is also included, to illustrate the predicted effect of CH_4 addition.

Comparison of predicted pressure time history results for each mixture, seen in Fig. 5-12, illustrates a decrease in the maximum post-combustion pressure by ~ 0.15 atm for the mixture with CH_4. This can be explained by a reduction in the total heat of reaction (H_R) from 2.61 to 2.38 kcal/mol total mixture when changing from the pure syngas to the with CH_4 mixture. The specific heat capacity values are not significantly different between the two mixtures.

3.3 Promoting effect of TMS

As previously mentioned, no chemical kinetic mechanism currently exists which includes trimethylsilanol and the expected intermediate species. In order to

evaluate the possible chemical kinetic foundations of the observed effects of TMS addition, a perturbation study was conducted using the CHEMKIN reactor model with a pure syngas fuel mixture. The perturbations were designed to explore the potential effects of the TMS impurity on the high pressure formation pathways of OH. Both Jachimowski and McLain [14] and Petersen et al. [12] suggested that SiH_4 disrupts the formation and/or enhances the consumption of HO_2 thus boosting OH production rates at high pressures. Given the effects of TMS closely resemble those of SiH_4 addition, it is possible that the kinetic foundations of the ignition promoting effect for TMS are related to changes in the same reaction pathways.

In the current work, two perturbations to the computational model were considered, which were conducted at P = 5 and 15 atm, T = 1066 K, for the pure syngas mixture. In the first, HO_2 consumption was boosted by increasing the A-factor of the reaction $HO_2 + HO_2 = H_2O_2 + O_2$ (R14) by up to 10^2 times, and in the second perturbation, HO_2 formation was inhibited by decreasing the A-factor of $H + O_2$ (+ M) = HO_2 (+ M) (R9) by up to 10^{-3} times. The ranges were chosen to encompass limiting behaviors in the predicted trends of the auto-ignition delay times. Results of the model analysis, shown in the Supplemental Material, indicate that indeed reductions in both auto-ignition delay time ($\tau_{i,2}$) and in the pressure dependence of the auto-ignition delay time can be achieved by modifying these reactions in the manner described. However, the magnitude of the decrease in the pressure dependence and the precise trends in the auto-ignition delay times observed experimentally are not well captured. This is expected because replicating the precise trends would likely require accurate inclusion of TMS and several additional Si-based intermediate species in the chemical kinetic mechanism. While the creation of such a mechanism may improve quantitative accuracy of the prediction of auto-ignition delay time, mechanism development was beyond the scope of the present work. Regardless, the modeling results presented here are important in that they support the notion that the effect of TMS is indeed likely related to HO_2 kinetic pathways, in good qualitative agreement with previous assertions for the similar Si-based impurity, SiH_4.

4. CONCLUSIONS

This work represents a unique investigation on the effects of common yet understudied impurities on the combustion of syngas fuel at practical combustor conditions, providing not only the first direct observations of these sometimes drastic effects, but also highlighting trends in behavior that may extend beyond the specific compounds evaluated in the present work. Studies such as this are vital to the safe and effective application of real syngas or other high-hydrogen content fuels, especially when used in modern high-pressure low-temperature combustion strategies like dry low-NO_x.

The results of the present experimental work uniquely illustrate the occurrence of two-step ignition behavior at higher pressures, with two distinct regions of heat release and pressure rise. First and second auto-ignition delay times ($\tau_{i,1}$ and $\tau_{i,2}$) were therefore defined and interestingly the times were affected differently by the addition of CH_4 and TMS impurities. Modeling results suggest the occurrence and magnitude of two-step ignition behavior can be explained by highly pressure and temperature dependent OH kinetics, which can cause a delay between H_2 and CO oxidation thus creating two distinct steps in the ignition process. Trends identified using this model illustrate that two-step ignition behavior becomes more prominent with increasing pressure and decreasing molar ratio of H_2:CO.

The addition of CH_4 consistently increased both $\tau_{i,1}$ and $\tau_{i,2}$ up to 40% at 15 atm, while increasing delay times at 5 atm by a factor of 3 only for $T < \sim 1050$ K. Model analysis suggests this inhibiting effect is due to OH scavenging primarily via the $CH_4 + OH = CH_3 + H_2O$ (R49) reaction, which acts to slow the first step of the ignition process. Conversely, the addition of TMS consistently decreased the auto-ignition delay times, with the magnitude of the effect related to the TMS concentration and the initial pressure. 10 ppm TMS impurity addition caused a minimal effect on $\tau_{i,2}$ at both 5 and 15 atm and a consistent decrease of ~ 10-30% in $\tau_{i,1}$ at 15 atm. The effect of 100 ppm TMS impurity addition was much more drastic,

with consistent decreases of 50-70% in $\tau_{i,2}$ and 45-50% in $\tau_{i,1}$ at 15 atm and 20-30% reduction in $\tau_{i,2}$ at 5 atm. Furthermore, the pressure dependence of the auto-ignition delay time, typically causing up to 100% increase as pressure increased from 5 to 15 atm, was virtually eliminated for the 100 ppm TMS mixture. Kinetic modeling suggests that these ignition promoting effects are related to enhanced consumption and/or reduced production of HO_2, though the precise chemical kinetic effects cannot be resolved with existing kinetic mechanisms. The drastic effects of TMS have significant safety implications, as pronounced early ignition can lead to catastrophic failures. Furthermore, the upward trend in organic Si content in syngas mixtures and the current movement toward higher pressure combustion systems means consideration of these effects is of increasing importance.

The impact of TMS addition observed here is remarkably similar to that for SiH_4 in pure H_2 made in previous investigations. This suggests a possible trend for Si-based species to promote auto-ignition in syngas and hydrogen mixtures. Such a trend may facilitate an extension of the findings in the present results beyond SiH_4 and TMS, to other Si-based species commonly present in syngas fuel. Important to note, however, is that this extension is limited by the lack of understanding as to the exact mechanism for ignition promotion. Because of this, it is not immediately apparent if siloxane compounds, for instance, will necessarily have a promoting effect due to their Si content alone, or whether their alternative structure will lead to other effects.

REFERENCES

[1] Jones R, Shilling N. IGCC gas turbines for refinery applications. GE Power Syst Schenectady, NY 2003.

[2] United States Department of Energy. Hydrogen from Coal Program - Research, Development, and Demonstration Plan. 2009.

[3] Rasi S, Lehtinen J, Rintala J. Determination of organic silicon compounds in biogas from wastewater treatments plants, landfills, and co-digestion plants. Renew Energy 2010;35:2666–73.

[4] Mansfield AB, Wooldridge MS. High-pressure low-temperature ignition behavior of syngas mixtures. Combust Flame 2014;161:2242–51.

[5] Reaction Design. CHEMKIN 10101 2010.

[6] Li J, Zhao Z, Kazakov A, Chaos M, Dryer FL, Scire JJ. Mechanism for CO, CH2O, and CH3OH Combustion. Int J Chem Kinet 2007.

[7] Chaos M, Dryer FL. Syngas Combustion Kinetics and Applications. Combust Sci Technol 2008;180:1053–96.

[8] Mansfield a. B, Wooldridge MS, Di H, He X. Low-temperature ignition behavior of iso-octane. Fuel 2015;139:79–86.

[9] Gersen S, Darmeveil H, Levinsky H. The effects of CO addition on the autoignition of H2, CH4 and CH4/H2 fuels at high pressure in an RCM. Combust Flame 2012:2–5.

[10] Mathieu O, Kopp MM, Petersen EL. Shock-tube study of the ignition of multi-component syngas mixtures with and without ammonia impurities. Proc Combust Inst 2012;34:3211–8.

[11] Lieuwen T, Yang V, Yetter R. Gas Synthesis Combustion: Fundamentals and Applications. CRC; 2009.

[12] Petersen E, Kalitan D, Rickard MA. Reflected Shock Ignition of SiH4/H2/O2/Ar andSiH4/CH4/O2/Ar Mixtures. J Propuls Power 2004;20:665–74.

[13] Mclain AG. Ignition of Behind Reflected Shock Waves Ignition of SiH4-H2-02-N ~ Behind Reflected Shock Waves 1983.

[14] Jachimowski C, McLain A. A chemical kinetic mechanism for the ignition of silane/hydrogen mixtures. 1983.

[15] Kéromnès A, Metcalfe WK, Heufer K a., Donohoe N, Das AK, Sung C-J, et al. An experimental and detailed chemical kinetic modeling study of hydrogen and syngas mixture oxidation at elevated pressures. Combust Flame 2013;160:995–1011.

[16] Kalitan DM, Mertens JD, Crofton MW, Petersen EL. Ignition and Oxidation of Lean CO / H 2 Fuel Blends in Air. J Propuls Power 2007;23:1291–303.

SUPPLEMENTAL MATERIAL

OH Sensitivity & Rate-of-Production Analysis – Pure syngas mixture, 15 atm, 1066 K

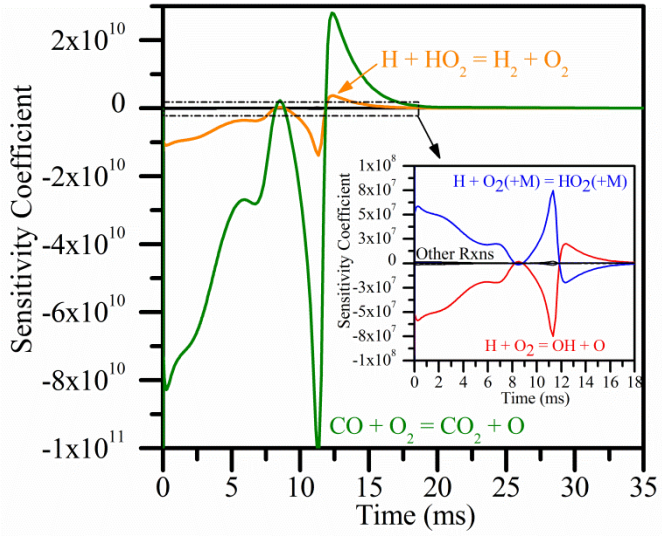

Fig.5-A. OH sensitivity analysis, using the Li 2007 mechanism [6]. Inset: Close-up view of boxed area.

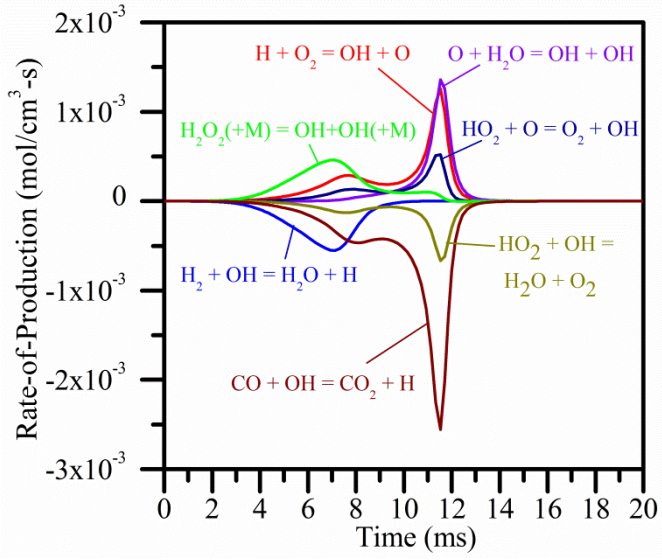

Fig.5-B. OH rate-of-production analysis, using the Li 2007 mechanism [6]. Insignificant reactions omitted for clarity.

CO Rate-of-Production Analysis – Pure syngas mixture, 15 atm, 1066 K

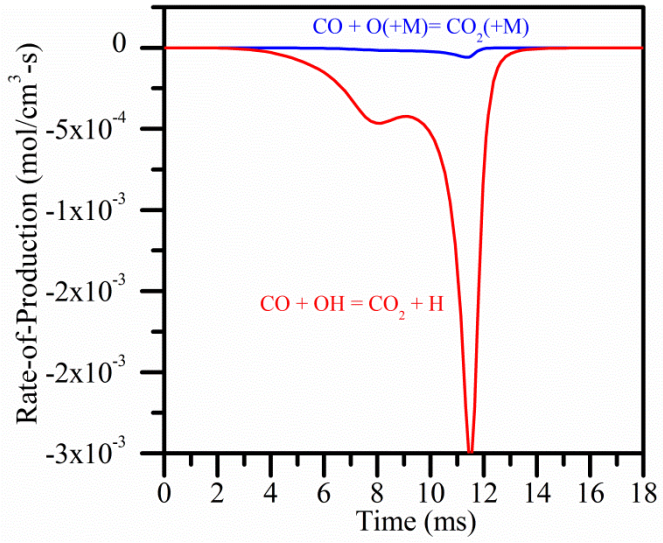

Fig.5-C. CO rate-of-production analysis, using the Li 2007 mechanism [6]. Insignificant reactions omitted for clarity.

OH Rate-of-Production Analysis – Syngas with CH_4 mixture, 15 atm, 1066 K

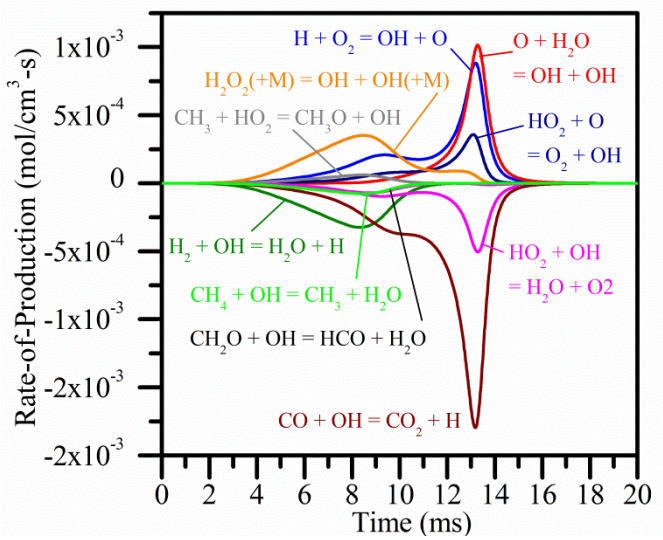

Fig.5-D. OH rate-of-production analysis, using the Li 2007 mechanism. Insignificant reactions omitted for clarity.

TMS Perturbation Modeling

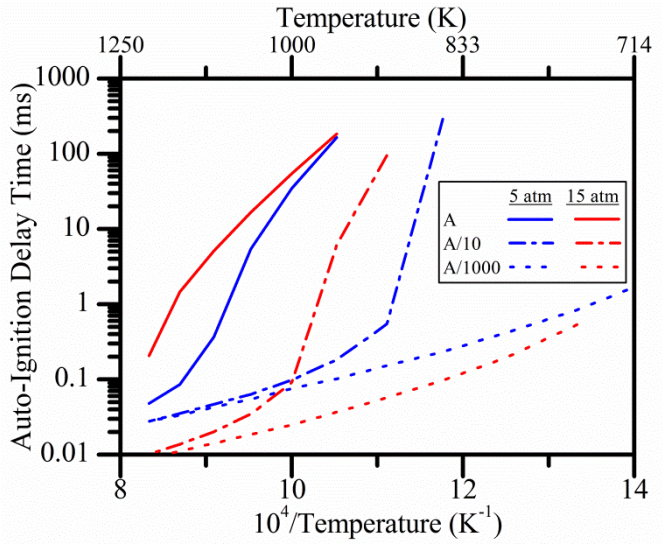

Fig.5-E. Predicted auto-ignition delay times for pure syngas mixture at 5 and 15 atm. A-factor of reaction H + O2 (+M) = HO2 (+M) (R9) multiplied by factor of 1, 1/10 and 1/1000 respectively.

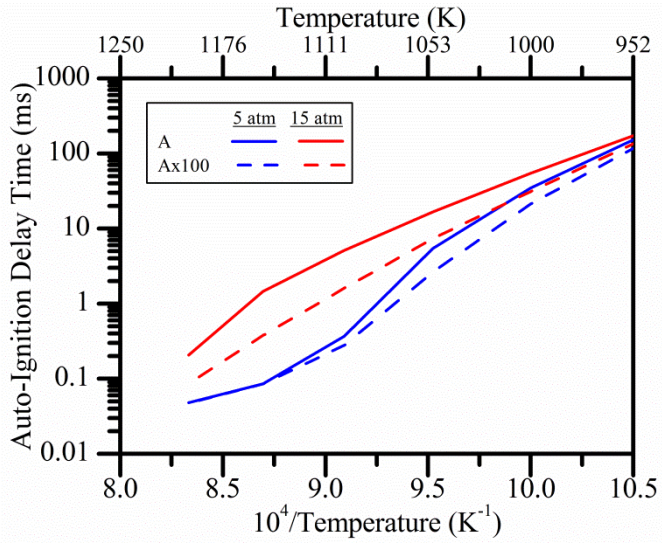

Fig.5-F. Predicted auto-ignition delay times for pure syngas mixture at 5 and 15 atm. A-factor of reaction $HO_2 + HO_2 = H_2O_2$ (R14) multiplied by factor of 1 and 100 respectively.

Table 5-A. Summary of experimental conditions and results

Test gas composition [a] (% Vol.)							Assigned Thermo. State [b]			Auto-ignition delay time [e] (ms)					
H_2	CO	CH_4	O_2	N_2	Ar	TMS (ppm)	*P* (atm)	*T* (K)	δT (+,-)	$\tau_{i,1}$	$\delta\tau_{i,1+}$	$\delta\tau_{i,1-}$	$\tau_{i,2}$	$\delta\tau_{i,1+}$	$\delta\tau_{i,1-}$
1.2	2.8	0	20.2	65.9	9.9	0	14.7	1094		3.1	0.1	0	7.0	0	0.1
1.2	2.8	0	20.2	75.2	0.6	0	14.8	1046		11.0	0.7	0	23.7	0.4	0.1
1.2	2.8	0	20.2	72.3	3.5	0	15.4	1071		6.9	0.5	0	13.1	0.1	0
1.2	2.8	0	20.2	65.4	10.5	0	15.0	1109		2.5	0	0.2	6.1	0	0.1
1.2	2.8	0	20.2	75.2	0.6	0	4.6	1019		x	x	x	23.0	0.3	0.4
1.2	2.8	0	20.2	72.3	3.5	0	4.6	1052	0,3	x	x	x	10.3	0	0.7
1.2	2.8	0	20.2	68.6	7.2	0	4.8	1069		x	x	x	5.0	0	0.4
1.2	2.8	0	20.2	75.1	0.8	0	4.5	1020	0,6	x	x	x	17.9	0	1
1.2	2.8	0	20.2	71.7	4.1	0	5.1	1054		x	x	x	10.2	0	0.5
1.2	2.8	0	20.2	73.9	1.9	0	4.8	1029		x	x	x	15.9	0	0.3
1.2	2.8	0	20.2	73.9	1.9	0	4.9	1042		x	x	x	12.7	0.5	0.3
0.9	2.3	0.2	20.3	75.1	1.2	0	14.9	1049		15.3	3.1	0	27.0	0.6	0
0.9	2.3	0.2	20.3	71.3	5.0	0	14.9	1067		9.7	0.3	0.2	18.3	0.3	0.2
0.9	2.3	0.2	20.3	67.6	8.7	0	15.5	1098		3.3	1.3	0	9.0	0.2	0
0.9	2.3	0.2	20.3	64.1	12.2	0	15.3	1114		3.3	0	0.3	5.9	0	0.2
0.9	2.3	0.2	20.3	75.1	1.2	0	4.7	1031		x	x	x	33.9	0.2	0.5
0.9	2.3	0.2	20.3	71.3	5.0	0	4.7	1049		x	x	x	11.0	2.4	0
0.9	2.3	0.2	20.3	67.6	8.6	0	4.9	1070	3,4	x	x	x	4.3	0.1	0.3
0.9	2.3	0.2	20.3	76.3	0	0	4.8	1025		x	x	x	62.6	0	11.4
1.2	2.8	0	20.2	67.4	0.4	10	14.8	1088		3.0	0	0.2	6.7	0.4	0.4
1.2	2.8	0	20.2	75.3	0	10	15.2	1040		11.5	0.1	0.3	27.8	0	0.1
1.2	2.8	0	20.	71.5	4.3	10	15.5	1069		4.7	0.5	0	12.0	0	0.4
1.2	2.8	0	20.2	71.5	4.3	10	15.3	1068		5.0	0	0.1	12.0	0.1	0.4
1.2	2.8	0	20.2	73.5	2.3	10	15.5	1060		7	0	0.3	17	0	0.3
1.2	2.8	0	20.2	74.0	1.8	10	14.9	1056		7.0	0.2	0	18.4	0.2	0.1
1.2	2.8	0	20.2	74.0	1.8	10	14.3	1034		14.3	0.3	0.2	31.1	0.3	0.3
1.2	2.8	0	65.1	65.1	10.7	10	14.9	1109		1.8	0	0.11	3.8	0.2	0
1.2	2.8	0	20.2	75.3	0	10	4.9	1021		x	x	x	21.7	0	4.3
1.2	2.8	0	20.2	75.6	4.3	10	4.8	1050		x	x	x	10.1	0.1	0.1
1.2	2.8	0	20.2	73.6	2.3	10	4.7	1025		x	x	x	16.4	0	0.8
1.2	2.8	0	20.2	73.6	2.3	10	5.1	1043	3,0	x	x	x	11.5	0.5	0
1.2	2.8	0	20.2	74.0	1.8	10	4.8	1029		x	x	x	12.7	2.7	0.2
1.2	2.8	0	20.2	74.0	1.8	10	4.7	1025		x	x	x	18.2	0	3
1.2	2.8	0	20.2	67.2	8.6	10	5.1	1075	3,0	x	x	x	2.5	0	0.2
1.2	2.8	0	20.2	70.2	5.6	10	5.0	1063		x	x	x	6.3	0	1
1.2	2.8	0	20.2	74.8	1	100	14.7	1053		5.7	0.2	0.2	8.3	0.2	0.3
1.2	2.8	0	20.2	74.8	1	100	14.6	1084		2.3	0.2	0	3	0.35	0.1
1.2	2.8	0	20.2	70.3	5.5	100	14.9	1074		3.2	0.3	0	4.5	0.3	0.3
1.2	2.8	0	20.2	71.4	4.4	100	14.9	1067		4.2	0	0.3	5.4	0.3	0.3
1.2	2.8	0	20.2	75.3	0	100	14.6	1031		9.9	0	0.2	14.8	0.2	0.1
1.2	2.8	0	20.2	74.8	1	100	4.7	1034		x	x	x	10.3	0	0.2
1.2	2.8	0	20.2	75.1	0.7	100	4.8	1034		x	x	x	10.5	0.3	0.3
1.2	2.8	0	20.2	73.2	2.6	100	4.8	1045	0,5	x	x	x	8.1	0	1.3
1.2	2.8	0	20.2	71.4	4.4	100	4.7	1051	1,3	x	x	x	7.8	0.1	0.2
1.2	2.8	0	20.2	71.5	4.4	100	4.8	1056	4,0	x	x	x	6.3	0	0.3
1.2	2.8	0	20.2	75.3	0	100	4.8	1015	3,0	x	x	x	17.0	0.1	0.1
1.2	2.8	0	20.2	70.3	0	100	5.0	1066	1,5	x	x	x	4.4	0	0.4

[a] Balance CO_2.

[b] Pressure uncertainty ~ 0.1 atm and temperature uncertainty ± ~ 2.5 K unless reported otherwise, δT+/- = upper and lower uncertainty bound of T assignment

[c] $\tau_{i,1}$ & $\tau_{i,2}$ = measured, $\delta\tau_i$ +/-=upper and lower uncertainty bound of measurement

\

Table 5-B. Summary of experimental conditions and modeling results

Test gas composition [a] (% Vol.)							Assigned Thermo. State [b]			Predicted auto-ignition delay time [e] (ms)					
H_2	CO	CH_4	O_2	N_2	Ar	TMS (ppm)	*P* (atm)	*T* (K)	δT (+,-)	$\tau_{i,1}$	$\delta\tau_{i,1+}$	$\delta\tau_{i,1-}$	$\tau_{i,2}$	$\delta\tau_{i,1+}$	$\delta\tau_{i,1-}$
1.2	2.8	0	20.2	65.9	9.9	0	14.7	1094		3.7	2.3	1.3	5.3	4.3	2.2
1.2	2.8	0	20.2	75.2	0.6	0	14.8	1046		12.1	5.9	3.8	18.1	11.7	6.5
1.2	2.8	0	20.2	72.3	3.5	0	15.4	1071		6.5	3.7	2.1	10.0	7.2	3.8
1.2	2.8	0	20.2	65.4	10.5	0	15.0	1109		2.6	1.5	1.1	3.7	3.2	1.6
1.2	2.8	0	20.2	75.2	0.6	0	4.6	1019		x	x	x	16.8	17.9	9.4
1.2	2.8	0	20.2	72.3	3.5	0	4.6	1052	0,3	x	x	x	4.0	8.5	3.0
1.2	2.8	0	20.2	68.6	7.2	0	4.8	1069		x	x	x	1.8	5.6	1.3
1.2	2.8	0	20.2	75.1	0.8	0	4.5	1020	0,6	x	x	x	15.9	17.5	9.1
1.2	2.8	0	20.2	71.7	4.1	0	5.1	1054		x	x	x	4.8	8.3	3.3
1.2	2.8	0	20.2	73.9	1.9	0	4.8	1029		x	x	x	12.4	14.1	7.3
1.2	2.8	0	20.2	73.9	1.9	0	4.9	1042		x	x	x	7.4	11.0	4.7
0.9	2.3	0.2	20.3	75.1	1.2	0	14.9	1049		13.3	7.1	4.1	19.3	12.0	6.9
0.9	2.3	0.2	20.3	71.3	5.0	0	14.9	1067		8.6	4.7	0	12.3	8.3	4.5
0.9	2.3	0.2	20.3	67.6	8.7	0	15.5	1098		4.2	2.5	1.6	5.9	4.5	2.3
0.9	2.3	0.2	20.3	64.1	12.2	0	15.3	1114		2.8	1.9	1.1	4.0	3.2	1.6
0.9	2.3	0.2	20.3	75.1	1.2	0	4.7	1031		x	x	x	14.3	15.2	7.2
0.9	2.3	0.2	20.3	71.3	5.0	0	4.7	1049		x	x	x	7.7	9.8	4.4
0.9	2.3	0.2	20.3	67.6	8.6	0	4.9	1070	3,4	x	x	x	3.8	5.9	2.3
0.9	2.3	0.2	20.3	76.3	0	0	4.8	1025		x	x	x	17.9	17.9	8.7

[a] Balance CO_2.

[b] Pressure uncertainty ~ 0.1 atm and temperature uncertainty ± ~ 2.5 K unless reported otherwise, δT+/- = upper and lower uncertainty bound of T assignment

[c] $\tau_{i,1}$ & $\tau_{i,2}$ = measured, $\delta\tau_i$ +/-=upper and lower uncertainty bound of prediction

Table 5-C. Reaction rate parameter with uncertainty

#	Reaction [a]	A_{min}	A_0	A_{max}	n	E_a
1	$H + O_2 = OH + O$ [b]	$2.789(10)^{15}$	$3.5458(10)^{15}$	$4.508(10)^{15}$	-0.4	$16.6(10)^3$
9	$H + O_2 (+M) = HO_2 (+M)$, k_∞ [c]	$1.11(10)^{12}$	$1.48(10)^{12}$	$1.85(10)^{12}$	0.6	0.0
9	$H + O_2 (+M) = HO_2 (+M)$, k_o [d]	$6.31(10)^{20}$	$6.37(10)^{20}$	$7.00(10)^{20}$	-1.72	$5.25(10)^2$
10	$HO_2 + H = H_2 + O_2$ [e]	$5.53(10)^{12}$	$1.66(10)^{13}$	$4.98(10)^{13}$	0	$8.23(10)^2$
21	$CO + O_2 = CO_2 + O$ [e]	$8.43(10)^{11}$	$2.53(10)^{12}$	$7.59(10)^{12}$	0	$4.77(10)^4$

Units are cm^3, s, cal, K; $k = AT^n \exp\left(-\frac{E_a}{RT}\right)$

[a] Nominal parameters from J. Li, Z. Zhao, A. Kazakov, M. Chaos, F.L. Dryer, and J.J. Scire, Int. J. Chem. Kinet. 39 (2007) 109-136.

[b] A-factor uncertainty from J.P. Hessler, J. Phys. Chem. A 102 (1998) 4517- 4526.

[c] A-factor uncertainty from C.J. Cobos, H. Hippler, J. Troe, J. Phys. Chem. 89 (1985) 342-349.

[d] A-factor uncertainty approximated as ±10%, from J.V. Michael, M.C. Su, J.W. Sutherland, J.J. Carroll, A.F. Wagner, J. Phys. Chem. A 106 (2002) 5297-5313.

[e] A-factor uncertainty approximated from W. Tsang, R.F. Hanson, J. Phys. Chem. Ref. 15 (1986) 1141

Chapter 6

Experimental study of OH time histories during syngas auto-ignition

Given the high value of OH mole fraction (χ_{OH}) measurements during syngas combustion at conditions and mixtures relevant to industry, the objective of this project was to provide transient χ_{OH} data corresponding to the auto-ignition process for syngas fuel and further to use this data to validate two commonly used chemical kinetic mechanisms for syngas oxidation. This was accomplished through an experimental investigation of auto-ignition delay times and maximum χ_{OH} values at engine relevant conditions, using a new ultra violet laser spectroscopy system in the UM-RCF. Considering known uncertainties in the two kinetic mechanisms of interest, experimental measurements and computational predictions of χ_{OH} and auto-ignition delay times were compared. In addition to these objectives, this project represents an important validation of the OH absorption system for future investigations.

1. METHODS

1.1 Experimental Methods

Auto-ignition experiments were conducted in the UM-RCF for realistic syngas mixtures with fuel to oxygen equivalence ratio of $\varphi = 0.1$ and were air-dilute with N_2, i.e. molar O_2 to inert gas ratio of 1:3.76. In some cases, small amounts of the N_2 diluent gas were replaced by Ar to modify the test temperature. The fuel mixture used was syngas with 30% H_2 and 70% CO by fuel volume, designed to represent lean syngas mixtures used in the power industry [1,2]. This is the identical mixture formulation as the "pure syngas" used in the project discussed in Chapter 5. Ignition experiments were conducted at 5 atm for the broadest range of

temperatures allowable in the UM-RCF for these mixtures (~ 1000-1100 K, based on experimental test times and associated uncertainties). A complete tabulation of all mixture and thermodynamic conditions for each experiment is given in the Supplemental Material.

The laser system consisted of an intra-cavity frequency-doubled ring dye laser (Coherent 899-05) using Rhodamine 6G dye and a potassium deuterated phosphorus (KDP) doubling crystal. The ring dye laser was pumped with a Coherent Verdi G7 solid state laser (~7 W @ 532nm). Fig. 6-1 presents a complete schematic of the system, with a detailed description of each component included in the Supplemental Material. This laser system was used to generate a beam with specific wavelength corresponding to the $R_1(5)$ line of the $A^2\Sigma^+ \leftarrow X^2\Pi_i$ (0,0) band of the OH spectrum (v_0 = 32606.556 cm^{-1} or ~ 306.687nm). As illustrated in Fig. 6-1, once generated this beam was split into a reference and probe beam, using various optics and fiber optic components. The probe beam was passed through the UM-RCF Test Section then both reference and probe beams were targeted on a pair of well-matched large area photodetectors (contained in one assembly) for continuous monitoring of the power. In order to ensure the system was tuned to the proper resonant wavelength, upon initialization the probe beam was passed through a stable flame using a Bunsen burner and the wavelength was modulated near v_0 = 32606.556 cm^{-1} until maximum power absorption was achieved. The laser frequency was then set at the value corresponding to maximum absorption. Any pressure shift of the resonant frequency from the atmospheric pressure flame to the pressure in the test section of the RCF is considered a negligible impact on the OH measurement uncertainty. The window ports though which the probe beam passes are heated for ~ 20 min prior to each experiment using integrated resistance heaters, in order to avoid water condensation on the windows during the experiment.

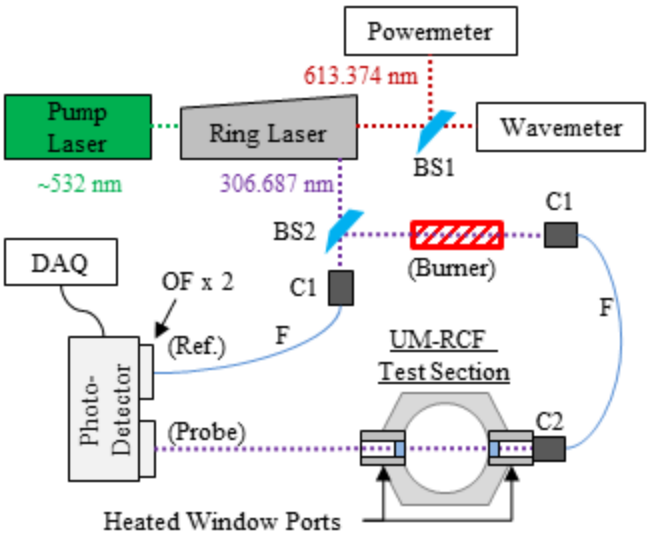

Fig. 6-1. Schematic of the OH laser absorption system. All components are described in detail in the Supplemental Material. BS = beam splitter, C = collimator, F = fiber optic cable, OF = optical filter, DAQ = data acquisition system.

Using this system, it was possible to measure the fractional absorption of the test beam in the Test Section during auto-ignition and then calculate the corresponding concentration of OH molecules. Assuming a basic Beer-Lambert relation for a non-saturating linearly absorbing medium with homogeneous conditions along the path length, the fractional absorption of the test beam power can be related to a wavelength dependent absorption coefficient, k_ν, via:

$$-\ln\left(\frac{I}{I_0}\right) = k_\nu L \tag{6-1}$$

Where, I_0 is the probe beam intensity before passing through the Test Section, I is the probe beam intensity after passing through the Test Section, and L is the path length of the beam through the absorbing medium. As explained in detail in He et al. [3] and Donovan et al. [4], k_ν can be expanded and the relationship in 6-1 can be rewritten as:

$$-ln\left(\frac{I}{I_0}\right)_\nu = S\,\varphi(\nu-\nu_0)\,P\,\chi_{OH}\,L \tag{6-2}$$

Where, S is the transition strength of the $R_1(5)$ line, $\varphi(v\text{-}v_0)$ is the line shape function, P is the bulk pressure, and χ_{OH} is the mole fraction of OH. It is therefore possible to directly relate the mole fraction of OH to the time (t) dependent fractional absorption of the probe beam intensity, via:

$$\chi_{OH}(t) = \frac{-1}{S\,\varphi(\nu-\nu_0)\,P\,L} ln\left(\frac{I}{I_0}\right)_{\nu}(t) \tag{6-3}$$

The line strength, S, is a function of temperature and the calculation of S as well as the various spectroscopic parameters used are described in detail in Donovan et al. [4] and found in the Matlab code in Appendix A of the present work. The line shape, $\varphi(v\text{-}v_0)$, is a function of temperature, pressure, and mixture composition. Both Doppler and collisional broadening were considered in the present work and the effects of these factors were convolved using a Voight profile. A detailed description of the method for calculating the line shape along with the broadening parameters used can be found in Donovan et al. [4] and Rea et al. [5] as well as in the Matlab code in Appendix A.

As noted previously by He et al. [3], it is vital to consider the uncertainty associated with the calculation of χ_{OH} using Eq. 6-3, which is primarily the result of uncertainty in: absorption path length, thermodynamic state, actual beam wavelength, mixture composition during combustion, and measured fractional absorption value. The path length L is approximated as 3.5 cm, as done by Donovan et al. [4] for similar UM-RCF experiments to compensate for the cool boundary layer region in the Test Section. The uncertainty of L is ± 0.5 cm, a conservative estimate based on in situ measurements of the boundary layer position within the Test Section by Donovan et al. [6] using a thermocouple. Uncertainty in the thermodynamic state is discussed in Chapter 2 and is ~ 1% for both P and T. Uncertainty in the beam wavelength is approximated as ± 0.05 cm^{-1} based on the precision of the wavemeter used in the laser apparatus. Uncertainty in the

assignment of the value of fractional absorption measurement is associated with the selection of specific smoothing algorithm parameters used in the data conditioning. The parameters of the smoothing algorithm were therefore varied by ± 50% and bounding values of χ_{OH} were calculated, in order to capture the uncertainty associated with this operation. The specific application of this algorithm is discussed in detail in a later section.

The mixture composition is used in the calculation of the collisional broadening effects mentioned above. Given that the gas mixture in the Test Section gradually changes composition between the unburned and burned states, each composition (burned and unburned) was used to calculate two values of χ_{OH} respectively, thus bounding the uncertainty associated with the exact mixture composition. The unburned mixture was assumed to include only O_2, N_2, and Ar (if included), given the small quantity of H_2 and CO. The burned mixture was assumed to include O_2, N_2, H_2O, CO_2, and Ar (if included). For both mixtures O_2 was assumed to have the same OH broadening parameters as N_2 due to limited OH broadening parameter data. For the burned mixture, CO_2 was assumed to have the same OH broadening parameters as H_2O due to lack of broadening parameters for CO_2 and the similar tri-atomic nature of the species. All broadening parameters used are from Rea et al [5] and Donovan et al. [4], and are shown in the Matlab code in Appendix A.

1.2 Computational Methods

Auto-ignition ignition delay time and OH mole fraction time history predictions were made using the constant volume adiabatic zero-dimensional homogeneous reactor model in the CHEMKIN software suite, described in Chapter 2, with both the Li et al. [7] (Li 2007) and the Keromnes et al. [8] (NUIG 2013) chemical kinetic mechanisms. The Li 2007 mechanism was selected given its previous success in predicting syngas ignition behavior [7,9], [10] and the NUIG 2013 mechanism was selected as it is the most recently made for syngas fuel and was comprehensively evaluated with recent experimental data [8]. Using the

CHEMKIN model, two corresponding auto-ignition delay time predictions were calculated for each ignition experiment in this study using the initial thermodynamic condition and mixture composition of the experiments. One auto-ignition delay time was defined as the time from the start of the calculation to the time when dT(t)/dt was maximized, the other was defined as the time from the start of the calculation to the time when the OH mole fraction (χ_{OH}) reached a maximum. Furthermore, the maximum value of χ_{OH} during ignition was recorded for comparison with the experimental measurements. For each delay time and OH prediction, quantified uncertainty bounds were calculated using the known uncertainty in the "A-factor" of the Arrhenius reaction rates for the most sensitive reactions, identified using OH sensitivity analysis for each kinetic mechanism. For the Li 2007 mechanism: $CO + O_2 = CO_2 + O$ (R21), $HO_2 + H = H_2 + O_2$ (R10), $H + O_2 = H + OH$ (R1) and $H + O_2 (+M) = HO_2 (+M)$ (R9) were used, and for the NUIG 2013 mechanism: $H + O_2 = OH + O$ (R1) and $H + O_2(+M) = HO_2(+M)$ (R9/10) were used. The results of the OH sensitivity analysis and the rate coefficients used for the NUIG 2013 mechanism are listed in Supplemental Material. Sensitivity analysis and rate coefficients for the Li 2007 mechanism are given in Chapter 5.

2. RESULTS

For each experiment in the UM-RCF, a pressure time history, high-speed imaging video, and two laser signals (probe and reference) were recorded. This facilitated the determination of two auto-ignition delay times (one at maximum dP/dt, one at maximum χ_{OH}) and the peak value of χ_{OH} during the auto-ignition event, as well as a direct observation of the auto-ignition behavior. A typical pressure time history during an experiment is presented in Fig. 6-2a. The pressure time history follows a profile similar to the observations in the UM-RCF of the other syngas studies of this body of work with a distinct and rapid rise in pressure during the ignition event. As was done in Chapter 5, the pressure data between P_{min} and P_{max} was filtered with a 100-point smoothing algorithm to reduce signal noise, and the numerical derivative of the pressure time history (dP(t)/dt) was calculated using

a center differencing scheme. Probe input and output laser signals are seen in Fig. 6-2a clearly indicating the existence of an absorption feature, i.e. some fraction of probe signal input intensity (I_0) is absorbed by the gas in the Test Section. Note the probe input signal is derived from the reference beam signal using a known beam splitting ratio.

For each experiment an auto-ignition delay time was determined ($\tau_{ign,dP/dt}$), defined as the time from EOC to the peak in the dP/dt time history, as done in Chapter 5. Also similar to the work detailed in Chapter 5, uncertainty bounds for this value as well as the other assigned values (t_{EOC}, P,T) were calculated by varying the smoothing algorithm parameters by ± 50%. For each experiment the fractional absorption (I/I_0) time history was calculated by dividing the probe output laser signal by the probe input then smoothing the result using a 50-point smoothing algorithm to reduce noise. A typical result can be seen in Fig. 6-2b, which corresponds to the measured laser signals in Fig. 6-2a. A clear minimum in the value of fractional absorption is apparent, corresponding directly to the maximum mole fraction of OH, and an alternate auto-ignition delay time ($\tau_{ign,\ OH}$) was defined as the time from EOC to this minimum. The fractional absorption time history determined for each experiment was then used directly in Eq. 6-3 to calculate the OH mole fraction time history and thereby the maximum value of χ_{OH}. As previously discussed, there is uncertainty associated with the selection of the smoothing algorithm parameters for the fractional absorption and those were therefore varied by ± 50% to calculate bounding values of χ_{OH}. Importantly, an "offline" auto-ignition experiment was conducted, where the laser was tuned to a wavelength off the resonant peak at the $R_1(5)$ transition and otherwise conducted in the same manner as normal experiments. No significant absorption or emission was detected in the offline experiment, indicating the fractional absorption measurements made at the conditions in the present work are directly representative of interactions of the probe beam with OH molecules in the Test Section gas only.

Fig. 6-2c presents a typical OH mole fraction time history result corresponding to the data presented in Fig. 6-2a & b, with uncertainty bounds indicated as dashed lines. The data illustrate minimal OH present prior to the ignition event (~0 – 2.5 ms), followed by a rapid rise in χ_{OH} to a maximum during the ignition event (~2.5 – 4.8 ms), and then a more gradual decline subsequent to the ignition event (~4.8 – 10 ms). During this decline, the rate of decrease lowers near ~ 6 ms forming a slight knee. Overall the measurements have excellent signal-to-noise ratio, and exhibit reasonable behaviors and quantities. Also included in Fig. 6-2c is a specific prediction of the χ_{OH} time history, calculated using the NUIG 2013 mechanism. As evidenced, this prediction has excellent qualitative and quantitative agreement with the measurement. The occurrence of a rapid rise, peak, and gradual decrease in OH mole fraction is well represented. Further, the maximum predicted value of OH mole fraction is in agreement with the measurement within the uncertainty bounds. The predicted and measured rates of increase and decrease in χ_{OH} before and after the maximum are in excellent agreement, respectively. However, the predicted rate of decrease after the knee at ~ 6ms is less than the measurement. This difference is likely the result of gas dynamic interactions that occur after ignition in the experiment. Such effects can lead to changes in the absorption path length and/or thermodynamic conditions affecting the accurate translation of fractional absorption to OH mole fraction. Note the A-factor values of the key reaction rates identified above were specifically modified within the accepted uncertainty bounds to optimize the predicted value for $\tau_{ign,OH}$ to the measurement in Fig. 6-2c.

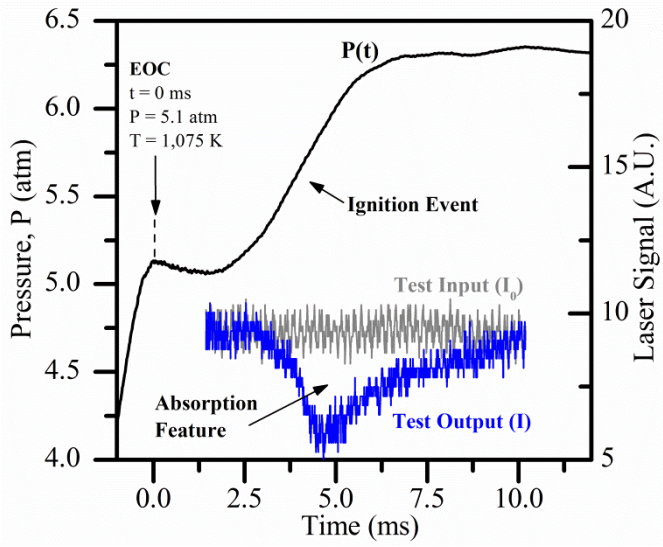

Fig.6-2a. Typical pressure time history, P(t), and laser signal intensity before and after passing through the Test Section (I_0 and I, respectively) showing the OH absorption feature during ignition, for experimental conditions P = 5.1 atm, T = 1,075 K.

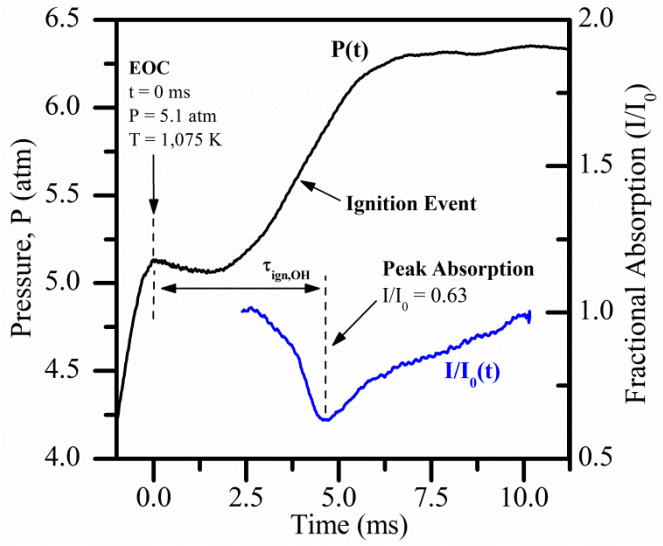

Fig.6-2b. Typical pressure time history, P(t), and fractional absorption (I/I_0) for experimental conditions P = 5.1 atm, T = 1,075 K; where, $\tau_{ign,OH}$ is the auto-ignition delay time corresponding to peak fractional absorption and therefore peak χ_{OH}.

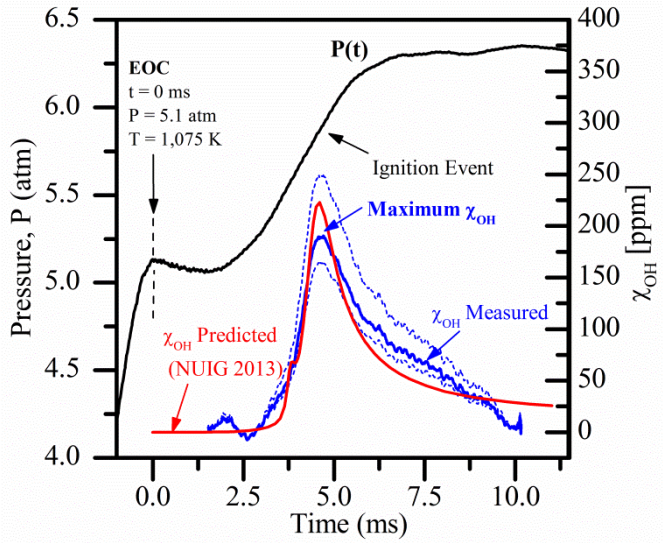

Fig.6-2c. Typical pressure time history, P(t), along with measured and predicted OH mole fraction time history, $\chi_{OH}(t)$ for experimental conditions P = 5.1 atm, T = 1,075 K. Nominal measurement is bold with uncertainty bounds, defined in the text, shown as dashed lines. Uncertainty in the prediction is omitted for clarity.

For each auto-ignition experiment a thermodynamic state was assigned representing the unburned isothermal isobaric condition at which the experiment was conducted, described in Chapter 2. A tabulated list of all experimental results, including calculated uncertainty bounds for the auto-ignition delay time measurements and assigned temperatures, is provided in the Supplemental Material. High-speed imaging results of chemilluminescence during syngas auto-ignition are in close agreement with the results seen in Chapter 5 and those indicate spatial uniformity of the chemilluminescence emission. This was an important validation for each experiment that the ignition behavior was homogeneous, a requirement when applying Eq. 6-3 to the system. As the imaging was nearly identical to that shown in Chapter 5, imaging results are not presented here.

2.1 Measured and predicted auto-ignition delay times

Figures 6-3 & 6-4 illustrate the measured and predicted auto-ignition delay time results for the $\tau_{ign,P}$ and $\tau_{ign,OH}$ as a function of inverse temperature

respectively. Overall the results for both times illustrate good repeatability and a consistent trend throughout the temperature range evaluated. For each experiment, nominal values of $\tau_{ign,OH}$ and $\tau_{ign,P}$ are generally very consistent, indicating OH production tracks with the increase in radical pool growth associated with the pressure rise at ignition, although values for $\tau_{ign,OH}$ are typically greater by ~ 15%. There is excellent agreement between the experimental measurements and predictions using both the Li 2007 and the NUIG 2013 mechanisms across all initial conditions. This agreement is not only an indication of the accuracy of the Li 2007 and NUIG 2013 chemical mechanisms in predicting auto-ignition delay times at these conditions, but also importantly suggests that the newly consturcted laser spectroscopy system is yielding reasonable results. There is no significant difference in predictions of either form of the auto-ignition delay time between each mechanism; though it appears that nominal predictions at the highest temperatures are consistently closer to measurements for the NUIG 2013 mechanism.

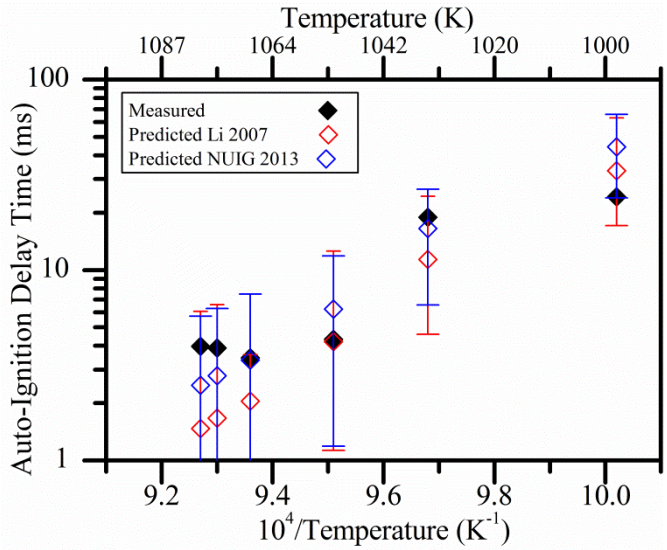

Fig.6-3. Measured and predicted auto-ignition delay times corresponding to peak dP/dt ($\tau_{ign,P}$) as a function of inverse temperature; where uncertainty bounds of the predictions are the result of known uncertainties in the A-factors of key reactions (see text). Uncertainty in the measurements and assigned temperature values, due to parameters used in the post-processing, is less than the symbol size on this scale.

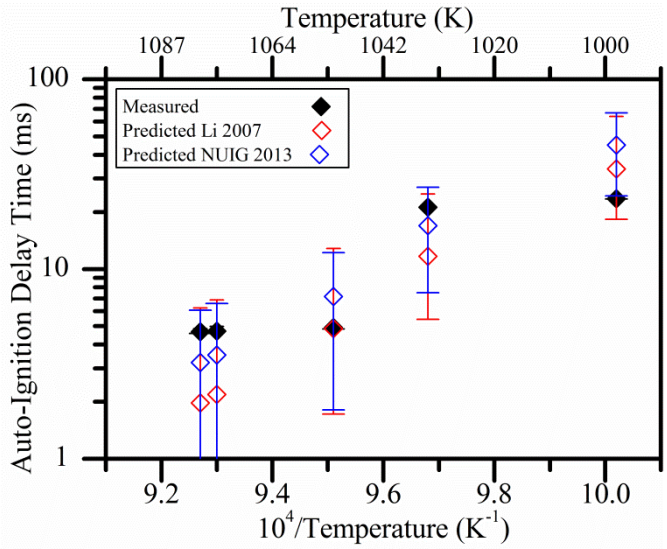

Fig.6-4. Measured and predicted auto-ignition delay times corresponding to peak χ_{OH} ($\tau_{ign,OH}$) as a function of inverse temperature; where uncertainty bounds of the predictions are the result of known uncertainties in the A-factors of key reactions (see text). Uncertainty in the measurements and assigned temperature values, due to parameters used in the post-processing, is less than the symbol size on this scale.

2.2 Peak OH mole fraction

Fig. 6-5 illustrates the measured and predicted values for peak χ_{OH} as a function of inverse temperature. As evidenced the measurement results range between ~ 100 and 225 ppm. There is excellent agreement between measurements and predictions for T < ~ 1050 K using both the Li 2007 and NUIG 2013 mechanisms, with nearly identical nominal values and largely overlapping uncertainty bounds; whereas, for T > ~ 1050 K the nominal measurement values are significantly less than predictions with partial agreement within the uncertainty bounds for predictions using the NUIG 2013 mechanism only. Predictions for the Li 2007 mechanism are above the upper uncertainty bounds of the measurements at these higher temperatures. Overall these results are an excellent indication that the present laser spectroscopy system yields reasonable results and that the NUIG 2013 mechanism applied to a homogeneous reactor physical model can accurately predict peak values of χ_{OH} during the auto-ignition process at the conditions studied here. Consideration of uncertainty in the kinetic mechanism and the calculation of χ_{OH} was critical to this evaluation. The reduced

agreement between measurements and predictions at higher temperatures is likely related to the fast nature of the auto-ignition experiments at those conditions (τ_{ign} < ~ 4 ms) which may increase the relative effects of mixing and/or reaction during the nosecone seating process on the interpretation of the data. More experimentation at the higher T conditions would help to evaluate these potential effects in more detail.

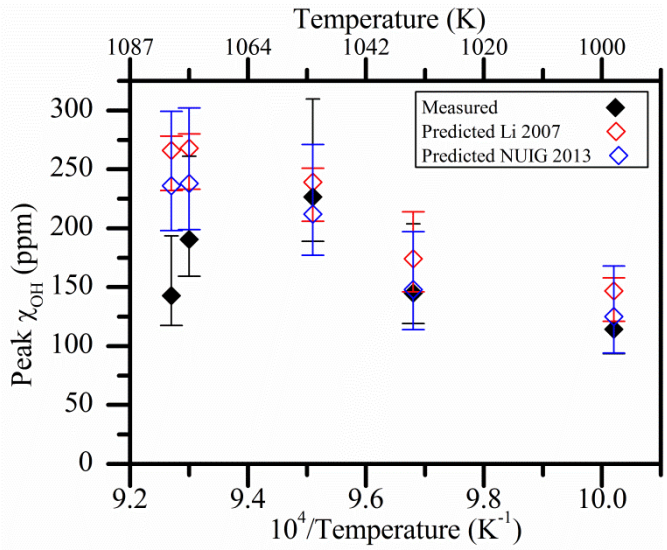

Fig.6-5. Measured and predicted maximum values of χ_{OH} as a function of inverse temperature; where uncertainties in the measurements are the result of various parameters (see text), and uncertainty of the predictions are the result of known uncertainties in the A-factors of key reactions (see text). Uncertainty in the assigned temperature values is less than the symbol size.

3. CONCLUSIONS

This work represents a unique and important investigation of the OH mole fraction throughout the auto-ignition process of syngas fuel at practical combustor conditions, providing the first data of its kind for this fuel at any conditions. Studies such as this are vital to the effective development and application of syngas and other high-hydrogen content fuels, considering that the accuracy of chemical kinetic mechanisms directly corresponds to the accuracy of any reacting system models to which it is applied. Furthermore, the results of this work are an important validation of the new laser absorption system applied to the UM-RCF.

The results of the present work illustrate excellent agreement between the characteristics of measured and predicted χ_{OH} time histories, from both qualitative and quantitative perspectives. Auto-ignition delay time measurements and predictions from two syngas chemical kinetic mechanisms (Li 2007 and NUIG 2013) were in excellent agreement, for auto-ignition delay times determined using both maximum dP/dt and peak OH mole fraction. Furthermore, measurements of maximum values of χ_{OH} were compared to predictions from these mechanisms, indicating excellent agreement for the NUIG 2013 mechanism at T < 1050 K and good agreement at higher T. This is an important validation of this mechanism, as no changes to reaction rates were not required to achieve this agreement. On the other hand, the Li 2007 mechanism accurately predicted χ_{OH} for T < 1050K but over-predicted concentrations at higher T, indicating that modification of the reaction rates could be necessary to improve the accuracy of this mechanism. In future studies, additional features of the χ_{OH} time histories could be interrogated, to more directly probe and refine the reaction rates involved in the auto-ignition process.

Overall, the results are an important illustration that the laser absorption system and post-processing techniques applied here indeed yield accurate quantifications of χ_{OH} in real time. This validation allows for the expansion of the spectroscopy techniques used here to other fuels and conditions in the UM-RCF.

REFERENCES

[1] Jones R, Shilling N. IGCC gas turbines for refinery applications. GE Power Syst Schenectady, NY 2003.

[2] United States Department of Energy. Hydrogen from Coal Program - Research, Development, and Demonstration Plan. 2009.

[3] He X, Zigler BT, Walton SM, Wooldridge MS, Atreya a. A rapid compression facility study of OH time histories during iso-octane ignition. Combust Flame 2006;145:552–70.

[4] Donovan MT. Experimental study of the role of OH in SiO2 particle nucleation in SiH4 combustion using UV absorption spectroscopy. University of Michigan, 2003.

[5] Rea C. Rapid-tuning laser wavelength modulation spectroscopy with applications in combusiton diagnostics and OH line shape studies. 1991.

[6] Donovan MT, He X, Zigler BT, Palmer TR, Wooldridge MS, Atreya A. Demonstration of a free-piston rapid compression facility for the study of high temperature combustion phenomena. Combust Flame 2004;137:351–65.

[7] Li J, Zhao Z, Kazakov A, Chaos M, Dryer FL, Scire JJ. Mechanism for CO, CH2O, and CH3OH Combustion. Int J Chem Kinet 2007.

[8] Kéromnès A, Metcalfe WK, Heufer K a., Donohoe N, Das AK, Sung C-J, et al. An experimental and detailed chemical kinetic modeling study of hydrogen and syngas mixture oxidation at elevated pressures. Combust Flame 2013;160:995–1011.

[9] Chaos M, Dryer FL. Syngas Combustion Kinetics and Applications. Combust Sci Technol 2008;180:1053–96.

[10] Mansfield AB, Wooldridge MS. High-pressure low-temperature ignition behavior of syngas mixtures. Combust Flame 2014;161:2242–51.

SUPPLEMENTARY MATERIAL

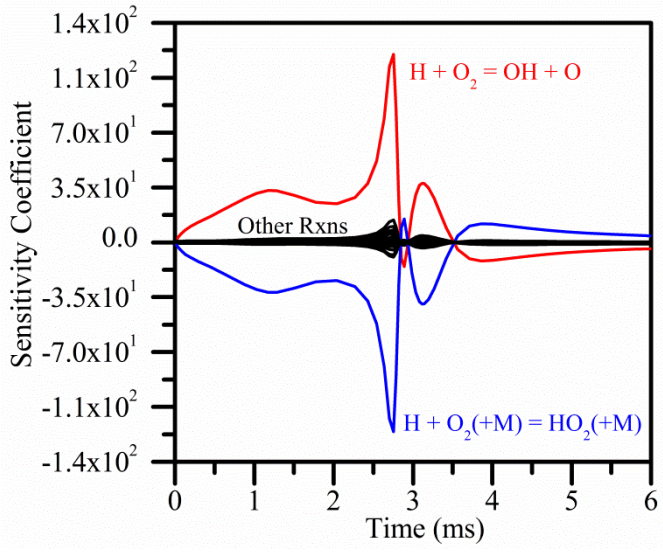

Fig. 6-A. OH sensitivity analysis, using the NUIG 13 mechanism, P = 5 atm, T = 1066 K [8].

Table 6-A. Summary of experimental conditions and auto-ignition delay time results

Mixture (% by vol) [a]				Assigned Thermo. State [b]		Measured (ms) [c]		Predicted Li 2007 (ms) [c]		Predicted NUIG 2013 (ms) [c]	
H_2	CO	O_2	N_2	P (atm)	T (K)	$\tau_{ign,P} \pm \Delta$	$\tau_{ign,OH} \pm \Delta$	$\tau_{ign,P} \pm \Delta$	$\tau_{ign,OH} \pm \Delta$	$\tau_{ign,P} \pm \Delta$	$\tau_{ign,OH} \pm \Delta$
1.2	2.8	20.2	67.9	5.3	1079	4.0 (-0.2)	4.7 (+0.1,-0.2)	1.5 (+4.6,-1.1)	2.0 (+4.3,-1.2)	2.5 (+3.9,-2.1)	3.1 (+3.6,-2.2)
1.2	2.8	20.2	75.8	5.0	1033	18.9 (-0.2)	21.2 (-0.5)	11.4 (+13.1,-6.8)	11.7 (+13.2,-6.3)	16.5 (+10.0,-10.4)	16.9 (+10.2,-9.9)
1.2	2.8	20.2	75.8	4.3	998	24.2 (+0.2,-0.2)	23.5 (+0.2)	33.2 (+29.8,-16.1)	33.7 (+29.9,-15.4)	44.6 (+21.1,-21.6)	44.9 (+21.6,-21.6)
1.2	2.8	20.2	67.9	4.9	1068	3.5 (-0.2)	n/a [d]	2.1 (+5.8,-1.6)	n/a	3.4 (+4.8,2.8)	n/a
1.2	2.8	20.2	67.9	4.7	1052	4.3 (-0.1)	4.9 (+0.1)	4.2 (+8.4,-3.1)	4.9 (+7.9,-3.1)	6.2 (+6.4,-5.1)	7.2 (+5.6,-5.4)
1.2	2.8	20.2	67.9	5.1	1075	3.9 (-0.4)	4.7 (-0.3)	1.7 (+4.9,-1.3)	2.2 (+4.7,-1.3)	2.8 (+4.0,-2.4)	3.5 (+3.7,-2.6)

[a] Balance Ar
[b] Pressure uncertainty ~ 0.1 atm and temperature uncertainty ± ~ 2.5 K
[c] Nominal value (+ uncertainty, - uncertainty). If no value listed, uncertainty is negligible.
[d] Off-line experiment, no spectroscopy measurements made

Table 6-B. Summary of experimental conditions and OH mole fraction results

Mixture (% by vol) [a]				Assigned Thermo. State [b]		max(χ_{OH}) ± Δ (ppm)		
H_2	CO	O_2	N_2	P (atm)	T (K)	Measured [c]	Pred. Li 2007[c]	Pred. NUIG 2013 [c]
1.2	2.8	20.2	67.9	5.3	1079	143 (+51,-25)	266 (+12,-34)	234 (+62,-45)
1.2	2.8	20.2	75.8	5.0	1033	145 (+59,-26)	174 (+40,-28)	148 (+52,-34)
1.2	2.8	20.2	75.8	4.3	998	114 (+44,-21)	147 (+11,-26)	124 (+46,-30)
1.2	2.8	20.2	67.9	4.9	1068	n/a [d]	n/a [d]	n/a [d]
1.2	2.8	20.2	67.9	4.7	1052	227 (+83,-38)	239 (+12,-33)	212 (+59,-43)
1.2	2.8	20.2	67.9	5.1	1075	190 (+71,-31)	268 (+12,35)	238 (+65,-45)

[a] Balance Ar
[b] Pressure uncertainty ~ 0.1 atm and temperature uncertainty ± ~ 2.5 K
[c] Nominal value (+ uncertainty, - uncertainty).
[d] Off-line experiment, no spectroscopy measurements made

Table 6-C. Reaction rate parameter with uncertainty – Li 2007 mechanism

#	Reaction [a]	A_{min}	A_0	A_{max}	n	E_a
1	$H + O_2 = OH + O$ [b]	$2.789(10)^{15}$	$3.5458(10)^{15}$	$4.508(10)^{15}$	-0.4	$16.6(10)^3$
9	$H + O_2 (+M) = HO_2 (+M)$, k_∞ [c]	$1.11(10)^{12}$	$1.48(10)^{12}$	$1.85(10)^{12}$	0.6	0.0
9	$H + O_2 (+M) = HO_2 (+M)$, k_o [d]	$6.31(10)^{20}$	$6.37(10)^{20}$	$7.00(10)^{20}$	-1.72	$5.25(10)^2$
10	$HO_2 + H = H_2 + O_2$ [e]	$5.53(10)^{12}$	$1.66(10)^{13}$	$4.98(10)^{13}$	0	$8.23(10)^2$
21	$CO + O_2 = CO_2 + O$ [e]	$8.43(10)^{11}$	$2.53(10)^{12}$	$7.59(10)^{12}$	0	$4.77(10)^4$

Units are cm^3, s, cal, K; $k = AT^n \exp\left(-\frac{E_a}{RT}\right)$

[a] Nominal parameters from J. Li, Z. Zhao, A. Kazakov, M. Chaos, F.L. Dryer, and J.J. Scire, Int. J. Chem. Kinet. 39 (2007) 109-136.
[b] A-factor uncertainty from J.P. Hessler, J. Phys. Chem. A 102 (1998) 4517- 4526.
[c] A-factor uncertainty from C.J. Cobos, H. Hippler, J. Troe, J. Phys. Chem. 89 (1985) 342-349.
[d] A-factor uncertainty approximated as ±10%, from J.V. Michael, M.C. Su, J.W. Sutherland, J.J. Carroll, A.F. Wagner, J. Phys. Chem. A 106 (2002) 5297-5313.
[e] A-factor uncertainty approximated from W. Tsang, R.F. Hanson, J. Phys. Chem. Ref. 15 (1986) 1141

Table 6-D. Reaction rate parameter with uncertainty – NUIG 2013 mechanism

#	Reaction [a]	A_{min}	A_0	A_{max}	n	E_a
1	$H + O_2 = OH + O$ [b]	$1.01\ (10)^{14}$	$1.04(10)^{14}$	$1.07(10)^{14}$	0	$1.529(10)^4$
9	$H + O_2(+M) = HO_2(+M), k_\infty$ [c]	$3.49\ (10)^{12}$	$4.65(10)^{12}$	$5.81(10)^{12}$	0.44	0.0
9	$H + O_2(+M) = HO_2(+M), k_o$ [c]	$1.30(10)^{19}$	$1.74(10)^{19}$	$2.17(10)^{19}$	-1.23	0.0
9	$H + O_2(+Ar) = HO_2(+Ar), k_o$ [c]	$5.11(10)^{18}$	$6.81(10)^1$	$8.51(10)^{18}$	-1.23	0.0

Units are cm^3, s, cal, K; $k = AT^n \exp\left(-\frac{E_a}{RT}\right)$

[a] Nominal parameters from A. Kéromnès, W.K. Wetcalfe, K.A. Heufer, N. Donohoe, A.K. Das, C.J. Sung, J. Herzler, C. Naumann, P. Griebel, O. Mathieu, M.C. Krejci, E.L. Petersen, W.J. Pitz, H.J. Curran, Comb. Flame 160 (2013) 995-1011.
[b] A-factor uncertainty from Z. Hong, D.F. Davidson, E.A. Barbour, R.K. Hanson, Proc. Comb. Inst. 33 (2011) 309-316.
[c] A-factor uncertainty from R.X. Fernandes, K. Luther, J. Troe, V.G. Ushakov, Phys. Chem. Chem. Phys. 10 (2008) 4313-4321.

Table 6-E. Laser spectroscopy system components

Name in Fig. 6-1 / Component	Make, Model, Description
Pump Laser	Verdi G7, High-Power Optically Pumped Semiconductor Laser
Ring Laser	Coherent 899-05 Ring Dye Laser
Powermeter	Coherent, Lasermate-Q, 33-0324
Wavemeter	Advantest, Wavelength meter, TQ8325
Photodetector	Thorlabs, PDB220A2, Large Area Balanced Amplified Photodetector
BS1/Beam splitter	Esco, V610250, Precision wedge window, S1-UV Grade Fused Silica
BS2/Beam splitter	Thorlabs, BSW20, 50:50 beamsplitter, UV Fused Silica, 250-450nm
C1/Collimator	Multimode Fiber Optics, Inc., LC-4U, 4mm aperature, UV-Vis silica lens broadband UV coating, SMA
OF/Optical Filter	Thorlabs, FSR-UG11, UV Bandpass color glass filter
C3/Adjustable Length Collimator Refocusing Assy	Custom Assembly. Multimode Fiber Optics, Inc. LC-4U collimator (FC) + Thorlabs, LA4936-UV, ½"Diameter UV Fused Silica Plano-Convex Lens, AR coated + ½" Diameter Al housing
F-Fiber Optic Cable	Multimode Fiber Optics, Inc., PCU600-10-SF, 10m length, UV-Vis 600um silica core, 0.22na, SMA to FC, PVC monocoil sheath
Mirrors	(Not shown in Fig. 6-1) Newport Optics, 10D20AL.2, Broadband metallic mirror, AL.2 coated, UV enhanced
Heated Mirror Ports	Custom Assembly. ESCO ZGC105197 sapphire window + Al port + Kapton flexible heater, Omega, KHLV-0504/10

Chapter 7
Summary, Conclusions, and Future work

1. Summary

The development and implementation of syngas fuel is of great interest, as it can enable a gradual transition from fossil to renewable fuel sources while simultaneously reducing the emissions associated with both. While it is a seemingly simple mixture composed primarily of H_2 and CO, there are fundamental issues preventing the successful application of syngas fuels to commercially viable combustion systems. These issues arise largely within the context of increasing NO_x emission standards, which are driving the development of combustors toward lean pre-mixed, low-temperature, and high-pressure conditions often outside the scope of historical syngas and H_2 combustion research. While understanding of syngas fuels has indeed expanded in recent decades to include these conditions in some respects, research has focused largely on the combustion of pure mixtures of H_2 and CO in highly homogeneous environments. As discussed previously, this is far from reality for actual syngas mixtures burned in practical gas turbine or reciprocating engine systems. Indeed recent research and experiences by those in industry have revealed that the effects of both chemical and physical disturbances in syngas fueled combustors can be dramatic and are not well-understood. These effects are manifested quite visibly as uncontrolled auto-ignition in homogeneous environments like those in shocktubes and rapid compression machines. Furthermore, drastic changes in reactivity have been observed for syngas fuels with the addition of even very small quantities of various chemical impurities.

This body of work represents an important investigation of syngas fuel combustion, aimed specifically at comprehensively understanding the effects of specific chemical and physical disturbances. The findings here will help to facilitate a more predictable and controllable application of this fuel to practical devices. This investigation was completed in the UM-RCF, a well characterized, quiescent, and constant volume combustion system, which eliminates turbulence, flow field, and fuel/air mixing effects and thus allows for a focus on the underlying chemical kinetics.

First, the auto-ignition behavior of syngas fuel at practical combustor conditions was investigated. These behaviors were mapped over a wide range of thermodynamic and mixture conditions for numerous experimental facilities, revealing consistent and well grouped behaviors strongly related to the initial thermodynamic and mixture state. This unique mapping, intrinsically valuable to combustor designers and other investigators, was then used to investigate predictive models and the fundamental source of inhomogeneous behaviors in these experimental systems. It was discovered that the Sankaran Criterion, a previously proposed relationship between dominant chemical kinetics, transport properties, and thermal characteristics of the system, could predict the occurrence (albeit not the magnitude) of inhomogeneous auto-ignition behavior with remarkable accuracy. The success of the Sankaran Criterion is a strong indication that minor thermal disturbances distributed throughout the test volume can be the underlying source of inhomogeneous auto-ignition behavior in syngas mixtures. This predictive capability and newfound fundamental description of inhomogeneous behaviors exhibited by syngas mixtures is an important contribution to both the scientific and industrial communities, which until now have either ignored categorizing the behavior or avoided low-temperature high-pressure conditions entirely.

This work represents the first attempt to integrate results from diverse experimental platforms to describe common auto-ignition behaviors in high-hydrogen content fuels, and further to provide a quantitative basis for predicting and interpreting data of other ignition studies, beyond syngas and the conditions

studied here. To this end, auto-ignition behaviors were also investigated and mapped for iso-octane fuel in the present work, an important primary reference fuel for gasoline. Results indicate that the Sankaran Criterion was again successful in predicting the conditions at which inhomogeneous auto-ignition will occur – providing an important tool potentially useful to the successful implementation of modern boosted direct injection combustion strategies in automotive engines.

Regarding the impact of inhomogeneous auto-ignition for both syngas and iso-octane fuels, the effect of these behaviors on the accuracy of basic auto-ignition delay time predictions was also investigated. For both fuels these behaviors indeed impacted the accuracy of predictions at certain mixture conditions, leading to global auto-ignition up to several orders of magnitude faster than predictions. This is an important indication that while inhomogeneous behaviors are localized in nature, they can impact global phenomena significantly and their consideration is therefore critical. This is especially true at low-temperature conditions where inhomogeneous ignition behaviors are far more prominent.

After exploring ignition behaviors, the effects of impurities on the combustion of syngas were then investigated. This work focused on CH_4, a common component of syngas, and trimethylsilanol (TMS), an impurity related to those commonly found in landfill-based syngas. Interestingly, through the course of this study multi-stage auto-ignition behaviors were observed; where the pressure rise associated with ignition had two distinct regions of rapid heat release. This behavior has not been reported prior to the present work and was found to depend strongly on pressure and the relative concentration of CO in the mixture. The impact of CH_4 impurity was to inhibit ignition, evidenced by auto-ignition delay time increases by up to a factor of 3. This effect is likely through OH scavenging early in the ignition process. Alternatively, the impact of TMS impurity was to promote ignition, causing drastic reductions in auto-ignition delay time of up to 70%. This is likely related to enhanced consumption and/or reduced production of HO_2, though the precise chemical kinetic effects cannot be resolved with existing kinetic mechanisms.

The drastic effects of TMS have significant safety implications, as pronounced early auto-ignition can lead to catastrophic failures. Furthermore, the upward trend in organic Si content in syngas mixtures and the current movement toward higher pressure combustion systems means consideration of these effects is of increasing importance. The impact of TMS addition observed here is remarkably similar to that for SiH_4 in pure H_2 made in previous investigations. This suggests a possible trend for Si-based species to promote auto-ignition in syngas and hydrogen mixtures. Overall, this work represents a unique investigation on the effects of common yet understudied impurities on the combustion of syngas fuel at practical combustor conditions, providing not only the first direct observations of these sometimes drastic effects, but also highlighting trends in behavior that may extend beyond the specific compounds evaluated in the present work.

3. Major Conclusions

- Trimethylsilanol impurity significantly increases reactivity of syngas at ~ 100ppm concentrations. Similarity to the effect of SiH_4 may indicate dangerous trend for organic Si impurities. This is the first combustion data on these important compounds.
- Syngas can exhibit multi-stage heat release for high-P, high CO conditions, which has never before reported. This is an important validation of heat release for high-P syngas combustion.
- First OH data for syngas auto-ignition provided here for any condition, validating two common syngas kinetic mechanisms.
- Auto-ignition behaviors of syngas are repeatable and consistent across many devices in thermodynamic state space, which allowed for mapping and development of predictive capabilities.
- The methods and approach for characterizing syngas ignition behaviors is applicable to other fuels, demonstrated by its extension to iso-octane fuel.
- Inhomogeneous auto-ignition strongly correlates to error in typical auto-ignition delay modeling, with magnitude highly correlated to φ.

2. Recommendations for future work

While the mapping of auto-ignition behaviors and establishment of the Sankaran Criterion mark an important step towards the safe and effective application of syngas fuels to combustion systems, the reach of the present work is potentially limited to quiescent and nominally homogeneous environments with minimal fluid motion. At the present time it is unclear how this predictive capability will translate to more practical engine systems which include, for example, turbulence, large magnitude thermal gradients, active ignition sources, and significant fluid motions. Logical future work therefore should include a thoughtful investigation of the effects of these factors on the ignition behaviors of syngas fuels at high-pressure low-temperature conditions. Of particular interest would be the evaluation of auto-ignition behaviors and flame stability in a flow reactor or actual combustor, where temporal and spatial dimensions are no longer independent. It is possible that through such a study the Sankaran Criterion could be modified to include spatial dimensions and velocities, which would add greatly to its usefulness in the design of practical engine systems using syngas or other fuels. Furthermore, by varying flow field characteristics it may also be possible to investigate turbulence effects in such an experiment. Considering previous investigations it is likely that future computational modeling could be used to understand the potential impact of turbulence on auto-ignition behaviors and the effectiveness of the Sankaran Criterion as well. In such a study, the ability to precisely control the magnitude and distribution of disturbances is a key advantage over experimentation. With this in mind, the optimal future approach is likely to combine experimental and computational methods to study syngas behaviors in a flow reactor or combustor at practical engine conditions.

Regarding the impact of chemical impurities on the combustion of syngas, future work should include an effort to assess the effect of species more broadly. Given the vast fluctuation of impurity species and concentrations in real syngas mixtures it is simply impractical to study all possible combinations. Therefore, it is

imperative to establish a method of categorizing impurities and their impact which may eliminate the need for extensive testing of each compound. This would require a more detailed assessment of certain important compounds initially, to determine the precise mechanism for their impact. Considering the successful development of a laser spectroscopy system for the UM-RCF in the present work, it is now possible to make some of these assessments using this apparatus. It is likely however, that corresponding advanced chemical modeling would be required to identify the precise mechanisms through which certain impurities act. From a practical perspective, the development of categories and the identification of key impurity species could have significant impact on the design of syngas manufacturing processes, as purification efforts could be tailored to the most important species rather than broadly to all impurities. Furthermore, the usefulness of this categorization of species may also translate to hydrocarbon fuels, given that H_2/CO chemistry is the basis for its oxidation.

Appendix A

Laser spectroscopy analysis code

1. Program OH_CALC

Note that the complete reference for "Donovan thesis 1991" is:

M. T. Donovan, "Experimental study of the role of OH in SiO2 particle nucleation in SiH4 combustion using UV absorption spectroscopy," PhD Thesis, University of Michigan, 2003.

```
%%%%%%%%%%%%%%%%%%%%%%%%PROGRAM OH_CALC%%%%%%%%%%%%%%%%%%%%%%%%%%%%%%%%%%%%%%%%

%Author: A.B. Mansfield
%Last edited: 10-9-2014

%This program calculates X_OH (OH mole fraction), given the mixture
%composition,P, T, and I/I_0 (laser fractional absorption) as input.

%Note that this is a function file, which is run in conjunction with the
%University of Michigan- Rapid Compression Machine analysis software common
%to all experiments in this body of work.

%P_cut = pressure (atm), T_cut = temperature (K), laser_ratio_smooth =
%fractional absorption, mix = mixture composition (mole fractions)

%mix = [X_H2 X_CO X_CH4 X_O2 X_N2 X_CO2 X_Ar X_H2O X_iC8H18];


function [X_OH, X_OH_min, X_OH_max] =
OH_calc(P_cut,T_cut,laser_ratio_smooth,mix);

%%%%%%%%%%%%Set analysis parameters


for i = 1:3

    v_0 = 32606.555735;    %[cm-1],  resonant freq. target, R1(5) line

    %Cycles through three scenarios which represent the min, max, and nominal
    %OH value

    signal = 0;

    if i == 1                   %nominal scenario
        T = T_cut;
        P = P_cut;
        L = 3.5;                %path length, [cm], from Donovan Thesis 2003
        L0 = L;
        v = 32606.555735;       %[cm-1],  resonant freq. target
```

```
end
if i == 2                    %minimum scenario
    T = T_cut*0.99;
    P = P_cut*0.99;
    L = L0+0.5;
    v = 32606.555735;
end
if i == 3                    %maximum scenario
    T = T_cut*1.01;
    P = P_cut*1.01;
    L = L0 - 0.5;
    v = 32606.555735+0.06;
    signal = 1;
end

%%%%%%%%%%BASIC CALCULATION

% -ln(I(v)/I_0) = -k(v)*L    Beer's Law
% S = int (k(v)dv, freq. range)
% k(v) = S*phi(v-v_0)   v_0 = resonant transition freq., phi(v) = line
%   shape function
%S_lu = S/P_OH --> S_lu*P_OH = int(k(v)dv)

%ln(I(v)/I_0)=-S_lu*phi(v-v_0)*P*X_OH*L    L = pathlength

%Therefore, need to define S_lu, phi

%X_OH = ln(I/I_0)/(-S_lu*phi(v-v_0)*P*L);

%%%%%%%%LINE SHAPE FUNCTION, phi(v-v_0)%%%%%%%%%%

%Ideally, all absorption is at resonance, but in reality, broadening
%Assume no line shifing

%Assume natural broadening is negligible

%%%%%%%COLLISIONAL BROADENING

%%%Collisional broadening, due to collisions between absorbing molec.
%%%and other species

%del_v_coll = P*sum(X_a*2*gamma_A*(T/T_ref)^n_a);

%%%Use N2, H2O, Ar parameters only
%%%Assumed broadening parameter for O2 = that for N2
%%%Assume broadening for CO2 = that for H2O

%%Uncertainty -->
%%#1 Assume all at initial mixture
%%#2 Assume all at final mixture

%Set revised mixture given grouped broadening parameters

%Initial mixture (mixx = [N2, Ar, H2O])
```

```
    mixxT = mix(4)+mix(5)+mix(7)+mix(8);

    mixx = [(mix(4)+mix(5))/mixxT,mix(7)/mixxT,mix(8)/mixxT];

    if signal ==1;  %Final mixture (mixx = [N2+O2, Ar, H2O+CO2])

        mixxT = (mix(5) + (2*mix(4)-mix(1)-
mix(2))/2)+mix(7)+(mix(1)+mix(2)+mix(8));
        mixx = [(mix(5) + (2*mix(4)-mix(1)-
mix(2))/2)/mixxT,mix(7)/mixxT,(mix(1)+mix(2)+mix(8))/mixxT];

    end

    T_ref = [2000,2000,1620];%[K], Rea Thesis 1991 [N2,Ar,H2O]

    gamma_0_2 = [0.043,0.032,0.16];%[cm-1atm-1],Rea thesis 1991 [N2,Ar,O2]

    n = [-0.83,-0.8,-0.66];%Rea thesis 1991 [N2,Ar,H2O]

    del_v_coll = P_cut*sum(mixx.*gamma_0_2.*(T./T_ref).^n);  %[cm-1]

    %%%%%%%%%DOPPLER BROADENING

    %%%Doppler Broadening, due to molecules moving toward/away from incid.
    %%%radiation

    %del_v_dopp = (8*k*T*ln(2)/(M*c^2))^0.5*v_0    M = molecular weight

    del_v_dopp = v_0*7.1623E-7*(T/17.007)^0.5;


    %%%%%%%%VOIGHT CONVOLUTION

    %%%Combine two effects with Voight profile
    %Voight profile is convolution of Gaussian and Lorenzian profiles

    %Need to use numerical approximation to solve for V

    w = 2*log(2)^0.5*(v-v_0)/del_v_dopp;%  = 0 if only at line center
    a = (log(2))^0.5*(del_v_coll/del_v_dopp);

    phi = (log(2)/3.1415)^0.5*2/del_v_dopp*Voight(w,a); %See Voight m-file
    %Voight m-file coded, but copied directly from Donovan thesis 2003

    %%%%%%%%%%%%%%%%%%%LINE INTENSITY (S_lu)%%%%%%%%%%%

    % S_lu =
    % 1/(8*pi*c*v_0^2)*N_OH/P_OH*exp(-h*c*E/(k*T))/Q_int*A_ul*(2J+1)*...
    %...(1-exp(-hcv_0/(k*T))
    % N_OH/P = 1/(k*T)
```

```
    c = 29979245800;     %speed of light [cm/s]
    k = 1.380658e-23;    %Boltzman constant [J/K]
    h = 6.626076e-34;    %Planck constant [J-s]

    E = 543.5949;        %[cm-1], Donovan thesis 1991

    A_ul = 235500;       %[s-1], Donovan thesis 1991

    we = 3737.7341;      %[cm^-1] Vibrational constant

    Qv = 1/(1-exp(-h*c/k * we/T));

    QeQr = -4.0913399+1.436522e-1*T+3.3773243e-6*T^2-6.3316152e-
10*T^3+7.1957228e-14*T^4;

    Q_int = Qv*QeQr;

    S_lu = 1/(8*3.1415*c*v_0^2)*1/(k*T)*exp(-
h*c*E/(k*T))/Q_int*A_ul*(2*5+4)*(1-exp(-h*c*v_0/(k*T)));

    S_lu = S_lu/1000000/9.8692e-6;   %[cm^-1/cm-atm]  Integrated line
intensity, S = int(k_v,dv)


    %%%%%%%%%%CALCULATE ABSORPTION%%%%%%%%%%%%%%%%%%%%

    %ln(I(v)/I_0)=-S_lu*phi(v-v_0)*P*X_OH*L    L = pathlength

    % for j = 1:length(v)
    %     ABS(K,j,I) = S_lu*phi(j)*P*X_OH*L;
    % end


    if i == 1
        X_OH = log(laser_ratio_smooth)/(-S_lu*phi*P_cut*L)*10^6;
    end
    if i == 2
        X_OH_min = log(laser_ratio_smooth)/(-S_lu*phi*P_cut*L)*10^6;
    end
    if i == 3
        X_OH_max = log(laser_ratio_smooth)/(-S_lu*phi*P_cut*L)*10^6;
    end

end
```